Physicochemical Understanding of Solubility and Supersaturation for the Enhancement of the Oral Absorbability of Poorly Soluble Drugs

Shunsuke Ozaki

2015

Contents

General Introduction

Many new chemical entities are developed as oral solid form drugs such as tablets and capsules due to their patient-friendliness.[1,2] An oral medication must be absorbed from the intestine in order to be effective, and high intrinsic activity against a target molecule would be useless if a large fraction of the administered drug is excreted without absorption.[2–6] The rate and extent of oral absorption of a drug are predominantly controlled by its physicochemical properties.[2,4,5] Poorly water-soluble drugs cannot dissolve completely in the intestinal tract within normal transit time and thus show poor oral bioavailability.[5,6] Insufficient drug absorption results in decreased drug efficacy and incomplete evaluation of safety profiles in preclinical and clinical studies.[4,6] In recent years, the number of poorly soluble drug candidates has been increasing.[1,7–10] Therefore, improving their aqueous solubility is currently one of the major challenges in drug discovery and development.[11,12]

The absorption problem occurs when the amount of drug absorbable from the intestine, the absorbable dose (AD), is lower than the target dose level necessary for a drug to exhibit efficacy. AD of a drug is generally expressed as Eq. (I)[13]:

$$\mathrm{AD} = C_{\mathrm{intestine}} \times P_{\mathrm{eff}} \times A_{\mathrm{intestine}} \times T_{\mathrm{intestine}} \qquad \text{(I)}$$

where $C_{\mathrm{intestine}}$ is the average drug concentration in the intestinal tract, P_{eff} is the effective intestinal membrane permeability, and $A_{\mathrm{intestine}}$ and $T_{\mathrm{intestine}}$ are the effective surface area of and transit time in the intestine, respectively. The ratio of AD to administered dose is the fraction absorbed.[13] Incomplete oral absorption due to low solubility can be attributed to either dissolution rate-limited absorption or thermodynamic solubility-limited absorption.[14] This distinction is based on the balance between solubility, dissolution rate and membrane permeation rate (= the rate of disappearance from the intestinal tract) of a drug.[4,13]

When the dissolution of a drug is the rate-limiting step in its oral absorption, $C_{\mathrm{intestine}}$ is lower than its thermodynamic solubility and proportional to the rate of drug release from

the formulation [Figure I(a)].[14] Therefore, AD can be easily enhanced by micronizing active pharmaceutical ingredients (API) and increasing their surface area.[14,15] In addition, dose-linearity of oral absorption is maintained under the dissolution rate-limited condition [Figure I(b)].[4,5,13] AD can reach the target dose level simply by administering a higher dose to the patient. Therefore, improving dissolution rate-limited absorption is less of a challenge to drug development than is thermodynamic solubility-limited absorption.

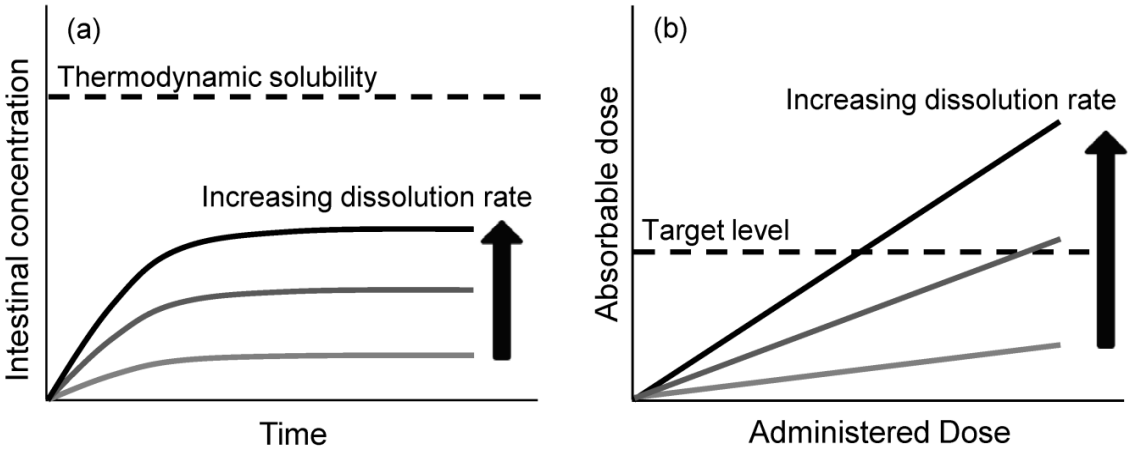

Figure I. Schematic diagrams of (a) time-drug concentration curves in the intestine, and (b) the relationship between administered dose and absorbable dose for dissolution rate-limited oral absorption.

The upper limits of $C_{intestine}$ and AD are controlled by the thermodynamic solubility of a drug. Solubility-limited absorption is observed when the drug's thermodynamic solubility is relatively low and the target dose level exceeds the maximum absorbable dose (MAD) (Figure II).[4,13,14] Under solubility-limited conditions, the drug exposure for the patient no longer increases with an increase in dose, and micronization of API is not effective since the intestinal fluid is already drug-saturated.[14] Evaluation of the efficacy and safety profile of the drug becomes difficult due to inability to measure dose-response.

In order to avoid this problematic nonlinear absorption, MAD of drug candidates

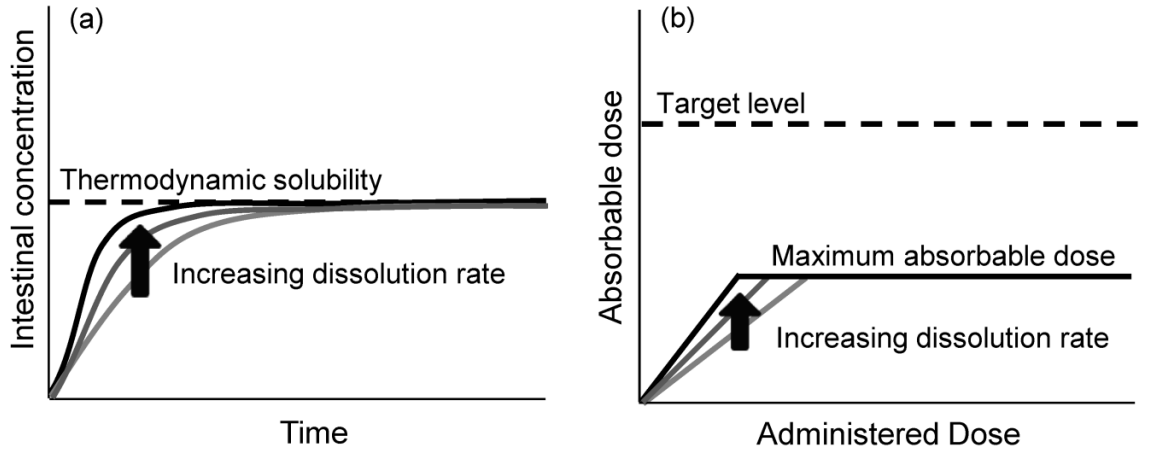

Figure II. Schematic diagrams of (a) time-drug concentration curves in the intestine, and (b) the relationship between administered dose and absorbable dose for thermodynamic solubility-limited oral absorption.

should be enhanced and exceed the target dose level. Equation (I) indicates that improvement of membrane permeability (P_{eff}) as well as that of solubility can increase MAD. However, most of the poorly soluble compounds are highly hydrophobic and their membrane permeation rate is predominantly limited by their rate of diffusion to the surface of intestinal membrane.[5,16] The diffusion rate of a compound in an aqueous phase is mainly determined by its molecular size.[17] Therefore, it is difficult to dramatically improve membrane permeability of poorly soluble compounds, and enhancement of their solubility is a practical way to increase the upper limit of $C_{intestine}$ and MAD.

The solubility of drug candidates can be improved by the following approaches; (i) improvement of thermodynamic solubility by structural optimization, (ii) induction of supersaturation using metastable solid forms, and (iii) stabilization of the supersaturated state using a crystallization inhibitor (Figure III). These three approaches to increasing solubility have been extensively studied.[11,12,18–32] However, they have been understood only empirically and qualitatively to date. In this study, solubility and supersaturation, which are the basis of the approaches to enhance oral drug absorbability, are investigated in a more

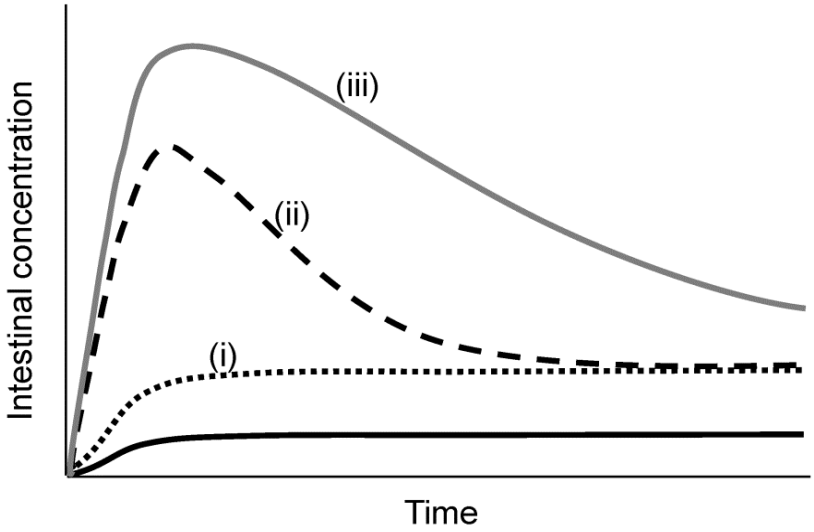

Figure III. Schematic diagrams of time-intestinal drug concentration curves for a poorly soluble drug candidate (black solid curve). (i) Improving thermodynamic solubility by structural modification is the simplest approach to increase average intestinal concentration ($C_{intestine}$). (ii) Metastable forms such as amorphous forms, salts and cocrystals induce supersaturation and show higher apparent solubility than thermodynamic solubility. (iii) Crystallization inhibitors can further improve supersaturation profiles of the metastable forms.

quantitative manner from the viewpoint of physical chemistry.

The structural optimization of a drug candidate [approach (i)] is a classic and fundamental strategy for improving thermodynamic solubility in the drug discovery stage.[2,11] Thermodynamic solubility can be improved by promoting drug hydration and/or decreasing intermolecular interaction in crystal packing.[2,11] Understanding structure-property relationships enables medicinal chemists to design soluble molecules efficiently. On the other hand, it is difficult to evaluate the impacts of structural modifications on drug hydration and crystal packing separately. In Chapter 1, the quantitative relationship between hydration, crystal packing and solubility is investigated by thermodynamic analysis of model structural analogs.

However, even ambitious synthetic approaches for improving solubility can be

unsuccessful. When the thermodynamic solubility of a drug candidate does not reach the target level, $C_{intestine}$ can be also improved by preformulation [approach (ii)].[18–25] In this approach, apparent solubility of a drug candidate is enhanced by using thermodynamically high-energy forms such as salts, amorphous solids and cocrystals. These solid forms are also called metastable forms and show higher apparent solubility than thermodynamic solubility. Over time, crystallization of the stable form occurs and the drug concentration decreases to its thermodynamic solubility (Figure III). This phenomenon, supersaturation, has been extensively studied and shown to improve solubility without structural modification of the candidate compound.[23,25–28] On the other hand, supersaturable solid forms are not always effective in enhancing oral absorption.[23,25,28] In order to increase $C_{intestine}$ and MAD, a high degree of supersaturation should be generated and maintained during the intestinal transit time ($T_{intestine}$) without crystallization of the stable forms. Although supersaturation characteristics are dependent on the drug species,[28] it is still unknown how they are controlled. In Chapter 2, we focus on the rate of crystal nucleation, a key step in crystallization, to explain drug-specific supersaturation behavior. Simple and practical methods to evaluate nucleation kinetics and stability of supersaturation are proposed.

For salts and cocrystals, their solubility product values are generally high in aqueous media and would not be a limiting factor for drug supersaturation.[5,20] Therefore, it is reasonable to assume that crystal nucleation kinetics is a single factor that can control degree of supersaturation for drugs in salt and cocrystals. On the other hand, the degree of supersaturation of an amorphous solid might be thermodynamically controlled when the solid does not have high chemical potential.[26–28] It is important to understand the roles of nucleation kinetics and thermodynamic potential of solids in determining the degree of supersaturation of amorphous forms. In Chapter 3, the supersaturation behavior of amorphous solids is evaluated in detail by a thermodynamic approach to supplement the kinetic approach proposed in Chapter 2.

The $C_{intestine}$ and MAD values of a drug in a high-energy form can be further enhanced by utilizing crystallization inhibitors [approach (iii)],[28–31] when the supersaturation ratio of the drug is controlled by its crystallization kinetics. It has been suggested that several water-soluble polymers inhibit crystal nucleation and/or growth and enhance the degree of supersaturation.[12,23,25,28–31] However, the role of polymers in improving the supersaturation ratio has not been clarified in detail. In Chapter 4 the inhibitory efficiency of polymers against crystal nucleation and growth is separately evaluated and the relationship between the inhibitory efficiency and the supersaturation behavior of drugs is clarified.

In the Conclusion chapter, a science-based strategy to improve solubility and absorbability of drug candidates is discussed based on current quantitative understanding of thermodynamic solubility and supersaturation.

1. Substituent Effect on the Thermodynamic Solubility of Structural Analogs: Relative Contribution of Crystal Packing and Hydration

1.1 INTRODUCTION

Improving the thermodynamic solubility of drug candidates by structural modification is the most important approach to increase maximum absorbable dose and avoid solubility-limited nonlinear absorption.[2,11,12] The thermodynamic solubility of a drug candidate corresponds to the equilibrium solubility of its stable crystalline form. A stable crystalline form is often preferable for drug development since it tends to have good chemical and physical stability.[33–35]

It has been reported that hydrophobicity and crystal packing energy are the major factors which determine thermodynamic solubility.[11,36] The reduction of hydrophobicity is a classic and general strategy for improving aqueous solubility.[4,11,36] The octanol-water partition coefficient (log P_{oct}) is a useful hydrophobicity index since it is often a good predictor variable for intrinsic activity, membrane permeability and metabolic stability, as well as solubility.[37–40] A reduction in hydrophobicity would help enhance aqueous solubility by promoting drug hydration. Using a different strategy, the disruption of crystal packing has been shown effective for improving the aqueous solubility of crystalline materials.[11,41–43] An increase in molecular flexibility can interfere with rigid crystal packing and increase solubility.[44–46] On the contrary, planar structures comprising fused aromatic rings and biaryls tend to form strong intermolecular π–stacking interactions and have a negative impact on solubility.[41–43]

The simultaneous contribution of these two factors, crystal packing and hydration, may complicate structure-solubility relationships in drug discovery, where many structural analogs are synthesized to find the best clinical candidate. Medicinal chemists can easily predict the substituent effect on log P_{oct} values before synthesis by using packaged

software,[36,39,40,44] and they expect a negative correlation between solubility and log P_{oct}. However, the introduction of a substituent sometimes causes unexpected results. For example, the addition of a hydrophobic substituent does not always decreases solubility, and the addition of a hydrophilic substituent occasionally decreases solubility.[41–43, 46] In these cases, an alteration in the crystal packing pattern, induced by the substituents, likely plays an important role in determining drug solubility.

Yalkowsky *et al*. have proposed a general solubility equation for estimating the impact of crystal packing and hydration on solubility from the melting point and log P_{oct} values of the compound.[47,48] The equation can roughly predict the solubility of structurally diverse compounds.[48] However, the relative importance of crystal packing and hydration on the solubility of structural analogs has not been investigated in detail. A better understanding of the quantitative relationship between crystal packing, hydration and solubility will allow the efficient design of soluble molecules and allow complete evaluation of their physicochemical properties. If the impact of crystal packing on solubility is comparable to that of hydration, we should pay as much attention to the substituent effect on crystal structure as on log P_{oct} to address solubility problems during the molecular optimization process. Exploration of the stable crystal form earlier in the discovery stage will become important for evaluating thermodynamic solubility and prioritizing drug candidates.[49]

In this chapter, the aqueous thermodynamic solubility of a family of drug-like model compounds, benzoylphenylurea derivatives, was measured. These derivatives have been studied as anticancer, anti-diabetic and anti-inflammatory agents.[50–52] In agricultural chemistry, a variety of analogs have been synthesized for the quantitative structure-activity studies of their larvicidal potency.[53] The substituent effect on hydration was estimated from log P_{oct} values and a linear free-energy relationship, and that on crystal packing was evaluated by thermal analysis. A thermodynamic model which considers both crystal packing and hydration was constructed to explain the relative solubility of the model

compounds. The relative importance of crystal packing and hydration in determining thermodynamic solubility was estimated and strategies for improving solubility during drug discovery are discussed.

1.2 MATERIALS AND METHODS

1.2.1 Chemicals

Benzoylphenylurea derivatives (BPUs) listed in Table 1.1 were synthesized as previously reported.[53] Antipyrine and caffeine were purchased from Wako Pure Chemical Industries, Ltd. (Osaka, Japan). Sodium nitrate, ethylbenzene, propylbenzene and butylbenzene were purchased from Tokyo Chemical Industry Co., Ltd. (Tokyo, Japan). All other reagents were of reagent grade and were used without further purification. The water used was filtered through a Milli-Q Water Purification System (Millipore, Bedford, Massachusetts, US) prior to use.

1.2.2 Measurement of thermodynamic solubility

The thermodynamic aqueous solubility of BPUs was determined at 25 °C using a shake flask method. Excess solid was added to glass tubes containing 5 mL of water. The test solutions were placed in a shaker incubator (Personal Lt-10, Taitec Co., Ltd., Saitama, Japan) for 24 h and then transferred to high performance liquid chromatography (HPLC) glass vials. The solutions were left for 48 h in a temperature-controlled autosampler (model G1329, Agilent Technologies, Inc., Santa Clara, California, US) at 25 °C to allow the solids to sediment. The concentration of each compound remaining in solution was determined by HPLC using UV detection (model 1100 series HPLC system, Agilent Technologies, Inc.) and an YMC-Triart C18 column (4.6 mm i.d., 100 mm length, 3 μm, YMC Co., Ltd., Kyoto, Japan). Mobile phase A consisted of 0.1% (v/v) $HClO_4$ and 1% (v/v) acetonitrile in water. Mobile phase B consisted of 0.1% (v/v) $HClO_4$ and 10% (v/v) water in acetonitrile. The

analytes were eluted with a linear gradient by ramping mobile phase B from 60% to 100% over 3 min at a flow rate of 1 mL min^{-1}. The sample injection volume was 50 μL and the detection wavelength was set at 254 nm. HPLC analysis of each vial was repeated 3 times periodically to confirm complete solid separation. All solubility measurements were performed in triplicate.

1.2.3 DSC measurement

The thermodynamic properties of BPUs were determined by differential scanning calorimetry (DSC, model Q2000, TA Instruments Inc., New Castle, Delaware, US). The instrument was calibrated for temperature and cell constant using high purity indium. Enthalpy of fusion and melting temperature were measured by placing crystalline samples in aluminum pans and heating at 1 °C min^{-1}. All experiments were performed in triplicate and the mean values were used for thermodynamic analysis of solubility.

1.2.4 Chromatographic determination of partition coefficient

The log P_{oct} values of BPUs were evaluated indirectly by a reverse phase isocratic HPLC method[54] since their extremely low aqueous solubility made it difficult to measure these values accurately by the shake flask method.[38] BPUs, sodium nitrate and calibration compounds were chromatographed on an Inertsil ODS-4 column (3.0 mm i.d., 30 mm length, 5 μm, GL Science Inc., Tokyo, Japan). The analytes were eluted with 13 mM phosphate buffer (pH 6.8) containing 40% acetonitrile at a flow rate of 0.8 mL min^{-1} and the capacity factor, k, was obtained according to Eq. (1.1):

$$k = \frac{t_R - t_0}{t_0} \qquad (1.1)$$

where t_R is the retention time of a test substance and t_0 is the retention time of sodium nitrate (dead-time marker). The logarithm of the obtained k values (log k) for the calibration compounds, antipyrine, caffeine ethylbenzene, propylbenzene and butylbenzene, were plotted against their known log P_{oct} values, –0.07, 0.38, 3.15, 3.72 and 4.38, respectively.[55] A calibration curve was obtained by linear regression in order to relate log k to log P_{oct}. The log P_{oct} value of each BPU was calculated using this linear relationship.

1.2.5 Thermodynamic model for solubility analysis

In this study, relative solubility was defined as the ratio of the thermodynamic solubility of BPU-i (i = 1 to 12) to that of BPU-1 (the reference compound) and was used for the thermodynamic analysis. The relationship between the observed relative solubility ($R_{s,\,obs\text{-}i}$) and the difference in the Gibbs energy change on dissolution between BPU-i and BPU-1 ($\Delta\Delta G°_{obs\text{-}i}$) at a given temperature is described as:

$$\Delta\Delta G^{\circ}_{obs-i} = -RT\ln\left(R_{s,obs-i}\right) \qquad (1.2)$$

where R is the gas constant and T is the temperature (=298 K). The relative contribution of crystal packing and hydration to solubility was estimated by constructing a thermodynamic model which can satisfactorily explain the $\Delta\Delta G°_{obs\text{-}i}$ value for each BPU.

The dissolution of a crystalline solid is composed of two steps: the break up of the crystalline solid into dissociated molecules followed by hydration by water molecules.[56] Therefore, the theoretical difference in the Gibbs energy change on dissolution between BPU-i and BPU-1 ($\Delta\Delta G°_{calc\text{-}i}$) at T is described using a crystal packing term ($\Delta\Delta G°_{crystal\text{-}i}$) and a hydration term ($\Delta\Delta G°_{hydration\text{-}i}$):

$$\Delta\Delta G^{\circ}_{calc-i} = \Delta\Delta G^{\circ}_{crystal-i} + \Delta\Delta G^{\circ}_{hydration-i} \qquad (1.3)$$

$\Delta\Delta G°_{\text{crystal-}i}$ is the difference in the Gibbs energy change on crystal dissociation between BPU-*i* and BPU-1 at *T*, and is derived from the difference in the Gibbs energy change upon sublimation as shown in Eq. (1.4):

$$\begin{aligned}\Delta\Delta G^{\circ}_{\text{crystal}-i} &= \left(\Delta G^{\circ}_{\text{CL}-i} - \Delta G^{\circ}_{\text{CL}-1}\right) + \left(\Delta G^{\circ}_{\text{LG}-i} - \Delta G^{\circ}_{\text{LG}-1}\right) \\ &\approx \Delta G^{\circ}_{\text{CL}-i} - \Delta G^{\circ}_{\text{CL}-1}\end{aligned} \tag{1.4}$$

where $\Delta G°_{\text{CL-}i}$ and $\Delta G°_{\text{LG-}i}$ are the changes in Gibbs energy on transition from crystalline to liquid state and liquid to gas state at *T* for BPU-*i*, respectively, and $\Delta G°_{\text{CL-1}}$ and $\Delta G°_{\text{LG-1}}$ are those for BPU-1. It was assumed that the difference between $\Delta G°_{\text{LG-}i}$ and $\Delta G°_{\text{LG-1}}$ is much smaller than the difference between $\Delta G°_{\text{CL-}i}$ and $\Delta G°_{\text{CL-1}}$ and was thus negligible, since the intermolecular interactions in the liquid and gas states would be similar between structural analogs. $\Delta G°_{\text{CL-}i}$ is composed of enthalpy and entropy terms as shown in Eq. (1.5):

$$\Delta G^{\circ}_{\text{CL}-i} = \Delta H^{\circ}_{\text{CL}-i} - T\Delta S^{\circ}_{\text{CL}-i} \tag{1.5}$$

where $\Delta H°_{\text{CL-}i}$ and $\Delta S°_{\text{CL-}i}$ are the irreversible changes in enthalpy and entropy on the transition from crystalline to liquid states at *T* for BPU-*i*. They can be obtained from Eqs. (1.6) and (1.7) by considering reversible processes: heating a crystalline material from *T* to melting temperature (T_{m}), melting the crystal at T_{m}, and cooling the supercooled liquid from T_{m} to *T*,

$$\Delta H^{\circ}_{\text{CL}-i} = \Delta H_{\text{f}} - \Delta C_{\text{p}}^{\text{C,L}}(T_{\text{m}} - T) \approx \frac{T}{T_{\text{m}}}\Delta H_{\text{f}} \tag{1.6}$$

$$\Delta S^{\circ}_{\text{CL}-i} = \frac{\Delta H_{\text{f}}}{T_{\text{m}}} - \Delta C_{\text{p}}^{\text{C,L}} \ln\left(\frac{T_{\text{m}}}{T}\right) \approx \frac{\Delta H_{\text{f}}}{T_{\text{m}}}\left[1 - \ln\left(\frac{T_{\text{m}}}{T}\right)\right] \tag{1.7}$$

where ΔH_f is the enthalpy of fusion, and $\Delta C_p^{C,L}$ is the difference in heat capacity between a crystal and a supercooled liquid. $\Delta C_p^{C,L}$ was approximated as the entropy of fusion, ΔS_f, (= $\Delta H_f/T_m$).[48] $\Delta\Delta G°_{crystal\text{-}i}$ was calculated for each BPU by using Eqs. (1.4–1.7) and their thermal properties (ΔH_f and T_m) were evaluated by DSC.

The hydration term, $\Delta\Delta G°_{hydration\text{-}i}$, can be described as Eq. (1.8):

$$\begin{aligned}\Delta\Delta G^{\circ}_{hydration\text{-}i} &= \Delta G^{\circ}_{hyd\text{-}i} - \Delta G^{\circ}_{hyd\text{-}1} \\ &= 2.303RT\left(\log P_{GW-i} - \log P_{GW-1}\right)\end{aligned} \tag{1.8}$$

where $\Delta G°_{hyd\text{-}i}$ and log $P_{GW\text{-}i}$ are the hydration Gibbs energy and the gas-water partition coefficient at T for BPU-i, respectively, and $\Delta G°_{hyd\text{-}1}$ and log $P_{GW\text{-}1}$ are those for BPU-1. Eq. (1.9) is obtained by assuming a linear free-energy relationship (LFER)[38,57] between partition coefficients in gas-water and octanol-water systems:

$$\log P_{GW-i} - \log P_{GW-1} = \alpha(\log P_{oct-i} - \log P_{oct-1}) \tag{1.9}$$

where log $P_{oct\text{-}i}$ and log $P_{oct\text{-}1}$ are log P_{oct} for BPU-i and BPU-1, respectively, and α is the constant of proportionality. Eqs. (1.10) and (1.11) are obtained by using Eqs. (1.3), (1.8), and (1.9):

$$\Delta\Delta G^{\circ}_{hydration\text{-}i} = 2.303RT\alpha\left(\log P_{oct-i} - \log P_{oct-1}\right) \tag{1.10}$$

$$\Delta\Delta G^{\circ}_{calc-i} = \Delta\Delta G^{\circ}_{crystal-i} + 2.303RT\alpha\left(\log P_{oct-i} - \log P_{oct-1}\right) \tag{1.11}$$

The α value is determined by linear least squares fitting between $\Delta\Delta G°_{calc\text{-}i}$ in Eq. (1.11) and $\Delta\Delta G°_{obs\text{-}i}$. Thus, $\Delta\Delta G°_{calc\text{-}i}$, $\Delta\Delta G°_{crystal\text{-}i}$ and $\Delta\Delta G°_{hydration\text{-}i}$ for each BPU have been obtained. The contribution of crystal packing and hydration to the theoretical relative solubility

($R_{\text{s, calc-}i}$) can be separately evaluated as:

$$\Delta\Delta G^{\circ}_{\text{crystal}-i} = -RT\ln\left(R_{\text{s, crystal}-i}\right) \tag{1.12}$$

$$\Delta\Delta G^{\circ}_{\text{hydration}-i} = -RT\ln\left(R_{\text{s, hydration}-i}\right) \tag{1.13}$$

$$\Delta\Delta G^{\circ}_{\text{calc}-i} = -RT\ln\left(R_{\text{s, calc}-i}\right) \tag{1.14}$$

$$R_{\text{s, calc}-i} = R_{\text{s, crystal}-i} \times R_{\text{s, hydration}-i} \tag{1.15}$$

where $R_{\text{s, crystal-}i}$ and $R_{\text{s, hydration-}i}$ are the potential fold changes in solubility which are attributable to the differences in crystal packing and hydration between BPU-*i* and BPU-1, respectively. Equation (1.15) was obtained by using Eqs. (1.3) and (1.12–1.14). The $R_{\text{s, crystal-}i}$, $R_{\text{s, hydration-}i}$ and $R_{\text{s, calc-}i}$ values for BPU-2 to BPU-11 show the X-ring substituent effects on crystal packing, hydration and solubility, respectively. The corresponding values for BPU-12 indicate the impact of removing the 4-Cl substituent on the Y-ring.

1.3 RESULTS

1.3.1 Thermodynamic aqueous solubility of BPUs

The thermodynamic solubilities of crystalline BPUs are shown in Table 1.1. All but BPU-12 exhibited solubilities below 1 μM, indicating extremely poor solubility. The HPLC method had a quantification limit of 0.003 μM and was thus applicable in this solubility range. Filtration and centrifugation caused a decrease in solubility, probably due to adsorption (data not shown) and thus were not suitable for separating undissolved solid. On the other hand, excess solid of each BPU was easily separated by sedimentation. The $R_{\text{s, obs-}i}$ and $\Delta\Delta G^{\circ}_{\text{obs-}i}$ values for each BPU were calculated using the solubility values (Table 1.1) and

ranged from 0.16 to 12.12 and from −6.18 to 4.57 kJ mol^{-1}, respectively. Six of the 11 compounds were more soluble than BPU-1 and the others showed lower solubility.

Table 1.1. Physicochemical Properties of the BPUs

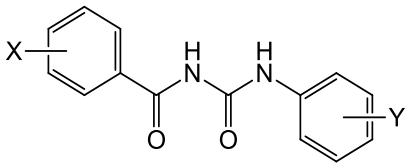

	Substituents		Solubility[a]	$R_{s,\,obs\text{-}i}$	$\Delta\Delta G°_{obs\text{-}i}$	log P_{oct}	T_m	ΔH_f
	X	Y	μM		kJ mol^{-1}		K	kJ mol^{-1}
BPU-1	H	4-Cl	0.19 (± 0.02)	1	0	3.32	510	39.1
BPU-2	2-F	4-Cl	0.59 (± 0.00)	3.13	–2.82	3.37	465	32.9
BPU-3	3-F	4-Cl	0.08 (± 0.01)	0.42	2.14	3.52	510	39.1
BPU-4	4-F	4-Cl	0.08 (± 0.02)	0.42	2.14	3.45	532	41.6
BPU-5	2-Me	4-Cl	0.32 (± 0.08)	1.68	–1.29	3.53	474	35.2
BPU-6	4-Me	4-Cl	0.03 (± 0.01)	0.16	4.57	3.77	511	38.9
BPU-7	2-Cl	4-Cl	0.37 (± 0.01)	1.95	–1.65	3.44	471	35.5
BPU-8	4-Cl	4-Cl	0.08 (± 0.01)	0.42	2.14	3.88	518	40.8
BPU-9	2-OMe	4-Cl	0.47 (± 0.03)	2.45	–2.22	3.88	438	26.0
BPU-10	2-OEt	4-Cl	0.15 (± 0.00)	0.79	0.59	4.39	420	27.0
BPU-11	2-Et	4-Cl	0.45 (± 0.03)	2.37	–2.14	3.94	436	23.9
BPU-12	H	H	2.30 (± 0.04)	12.12	–6.18	2.72	477	32.1

[a] Mean (± SD), n = 3; $R_{s,\,obs\text{-}i}$, observed relative solubility; $\Delta\Delta G°_{obs\text{-}i}$, observed difference in Gibbs energy change on dissolution; log P_{oct}, logarithm of octanol-water partition coefficient; T_m, melting temperature; ΔH_f, enthalpy of fusion.

1.3.2 Impact of crystal packing on solubility

The thermal properties determined by DSC are listed in Table 1.1. T_m of the 12 BPUs spanned the range 420 to 532 K, and ΔH_f ranged from 26.0 to 41.6 kJ mol^{-1}. A positive

correlation was observed between T_m and ΔH_f. A wide range of values indicates that the thermodynamic properties of crystalline BPUs are highly compound-specific, even though the compounds are structurally similar to each other. The $\Delta\Delta G°_{crystal\text{-}i}$ values, which were calculated using T_m and ΔH_f, ranged from −6.06 to 1.23 kJ mol^{-1} (Table 1.2). The corresponding $R_{s,\ crystal\text{-}i}$ values ranged from 0.61 to 11.54. A $R_{s,\ crystal\text{-}i}$ value larger than 1 indicates that a structural modification potentially enhances solubility by decreasing the thermodynamic stability of the crystalline phase. The substituent effect on crystal packing depended on the substituent position. It was apparent that substituents at the 2-position on the X-ring had positive impacts on $R_{s,\ crystal\text{-}i}$ (Table 1.2). The $R_{s,\ crystal\text{-}i}$ values for small substituents such as F, Cl and methyl groups (BPU-2, 5 and 7) ranged from 2.24 to 3.22. The positive effect was more prominent for larger substituents such as methoxy, ethoxy and ethyl groups (BPU-9, 10 and 11): their $R_{s,\ crystal\text{-}i}$ values reached approximately 10. On the other hand, the $R_{s,\ crystal\text{-}i}$ values ranged from 0.61 to 1.02 when substituents were introduced at the 3- or 4-position on the X-ring (BPU-3, 4, 6 and 8). These substituents were ineffective or even undesirable for thermodynamic solubility in terms of crystal packing. A similar result was also observed for the Y-ring: the $R_{s,\ crystal\text{-}i}$ value of BPU-12 indicated that the 4-Cl substituent stabilizes crystal packing, causing an approximately 3-fold decrease in solubility.

1.3.3 Estimation of $\Delta\Delta G°_{hydration\text{-}i}$ and thermodynamic solubility analysis

A good linear relationship (coefficient of determination, $R^2 = 0.998$) was observed between log k versus log P_{oct} for the calibration compounds. The log P_{oct} values of BPUs, obtained using the calibration curve, are shown in Table 1.1. For twelve BPUs, the log P_{oct} values ranged from 2.72 to 4.39, indicating high hydrophobicity, and are consistent with their poor aqueous solubility. Only BPU-12 showed a lower log P_{oct} value than BPU-1 (the reference compound), probably due to the absence of the hydrophobic 4-Cl substituent on the Y-ring. The other compounds had a hydrophobic substituent on the X-ring and were more hydrophobic than BPU-1. The proportionality constant of LFER between log $P_{GW\text{-}i}$ and

Table 1.2. Thermodynamic Solubility Analysis of the BPUs

	Substituents		$\Delta\Delta G°_{\text{crystal-}i}$	$\Delta\Delta G°_{\text{hydration-}i}$	$\Delta\Delta G°_{\text{calc-}i}$	$R_{\text{s, crystal-}i}$	$R_{\text{s, hydration-}i}$	$R_{\text{s, calc-}i}$
	X	Y	kJ mol^{-1}	kJ mol^{-1}	kJ mol^{-1}			
BPU-1	H	4-Cl	0	0	0	1	1	1
BPU-2	2-F	4-Cl	–2.90	0.29	–2.60	3.22	0.89	2.86
BPU-3	3-F	4-Cl	0.00	1.17	1.17	1.00	0.62	0.62
BPU-4	4-F	4-Cl	1.23	0.76	1.99	0.61	0.74	0.45
BPU-5	2-Me	4-Cl	–2.01	1.23	–0.78	2.25	0.61	1.37
BPU-6	4-Me	4-Cl	–0.04	2.63	2.59	1.02	0.35	0.35
BPU-7	2-Cl	4-Cl	–1.99	0.70	–1.29	2.24	0.75	1.68
BPU-8	4-Cl	4-Cl	0.70	3.28	3.98	0.75	0.27	0.20
BPU-9	2-OMe	4-Cl	–5.46	3.28	–2.19	9.07	0.27	2.41
BPU-10	2-OEt	4-Cl	–5.70	6.26	0.56	9.99	0.08	0.80
BPU-11	2-Et	4-Cl	–6.06	3.63	–2.43	11.54	0.23	2.67
BPU-12	H	H	–2.84	-3.51	–6.35	3.15	4.13	13.00

$\Delta\Delta G°_{\text{crystal-}i}$, difference in Gibbs energy change on crystal dissociation; $\Delta\Delta G°_{\text{hydration-}i}$, difference in Gibbs energy of hydration; $\Delta\Delta G°_{\text{calc-}i}$, theoretical difference in Gibbs energy change on dissolution; $R_{\text{s, crystal-}i}$, partial relative solubility attributable to crystal packing; $R_{\text{s, hydration-}i}$, partial relative solubility attributable to hydration; $R_{\text{s, calc-}i}$, theoretical relative solubility.

log $P_{\text{oct-}i}$, α, was 1.03 and was determined by linear least squares fitting between $\Delta\Delta G°_{\text{calc-}i}$ [Eq. (1.11)] and $\Delta\Delta G°_{\text{obs-}i}$. The $\Delta\Delta G°_{\text{hydration-}i}$ and $R_{\text{s, hydration-}i}$ values were calculated using this α value and ranged from −3.51 to 6.26 kJ mol^{-1} and from 0.08 to 4.13, respectively (Table 1.2). A $R_{\text{s, hydration-}i}$ value larger than 1 indicates that a structural modification potentially enhances solubility by promoting hydration. The substituent effect on $R_{\text{s, hydration-}i}$ was also dependent on the substituent position. The negative impacts on $R_{\text{s, hydration-}i}$ of the F, Cl, and methyl substituents on the X-ring (BPU-2 to BPU-8) were larger at the 3- and 4-

positions than at the 2-position. As shown in Figure 1.1, good agreement was observed between $\Delta\Delta G°_{\text{calc-}i}$ versus $\Delta\Delta G°_{\text{obs-}i}$. The regression line showed a slope close to unity, an intercept close to zero, and a good R^2 value (0.906). The $\Delta\Delta G°_{\text{calc-}i}$ values spanned the range –6.35 to 3.98 kJ mol^{-1}, and the corresponding $R_{\text{s, calc-}i}$ values ranged from 0.20 to 13.00 (Table 1.2). In contrast to the relationship between $\Delta\Delta G°_{\text{calc-}i}$ and $\Delta\Delta G°_{\text{obs-}i}$, no clear correlation was observed between $\Delta\Delta G°_{\text{crystal-}i}$ and $\Delta\Delta G°_{\text{obs-}i}$, or between $\Delta\Delta G°_{\text{hydration-}i}$ and $\Delta\Delta G°_{\text{obs-}i}$ (Figure 1.2).

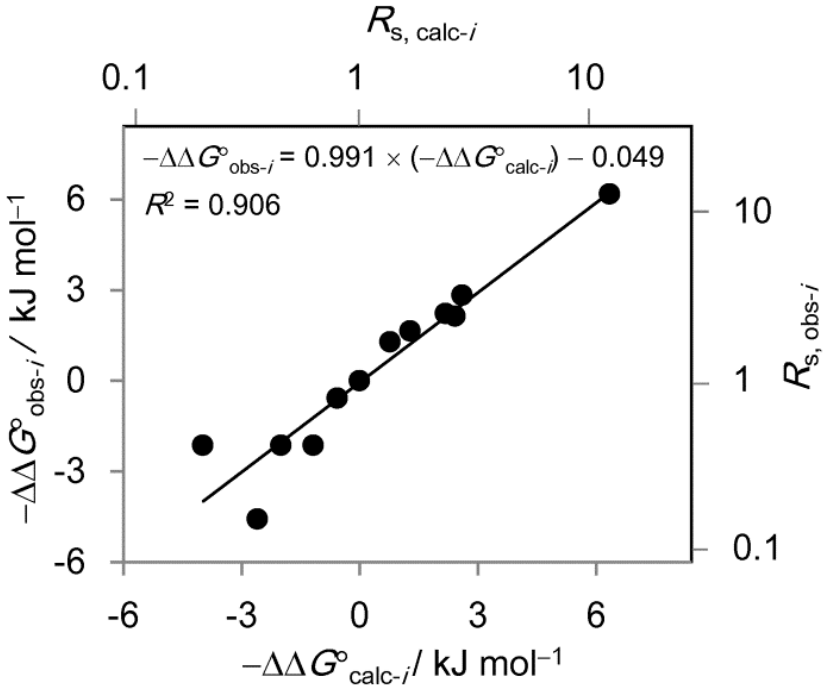

Figure 1.1. Plots of $-\Delta\Delta G°_{\text{obs-}i}$ versus $-\Delta\Delta G°_{\text{calc-}i}$ for BPUs. The top and right axes show the corresponding $R_{\text{s, calc-}i}$ and $R_{\text{s, obs-}i}$ values, respectively. The solid line represents the regression line.

1.4 DISCUSSION

1.4.1 Validity of thermodynamic solubility model

Twelve BPUs evaluated in the current study showed a wide range of thermodynamic solubility even though the compounds were structurally similar to each other (Table 1.1). Their solubility was not controlled by one single factor such as crystal packing ($\Delta\Delta G°_{\text{crystal-}i}$) or hydration ($\Delta\Delta G°_{\text{hydration-}i}$) (Figure 1.2). On the other hand, the relative solubility of this

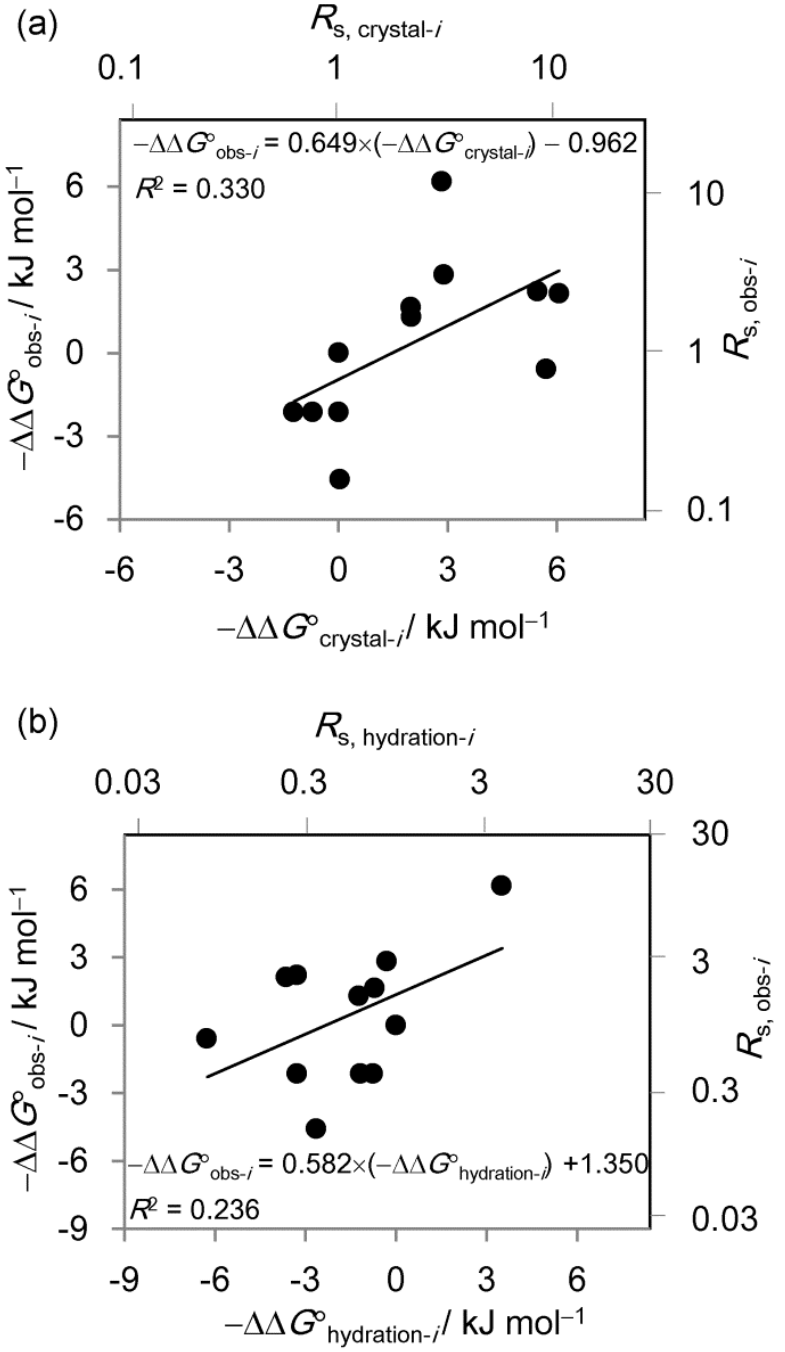

Figure 1.2. (a) Plots of $-\Delta\Delta G°_{obs\text{-}i}$ versus $-\Delta\Delta G°_{crystal\text{-}i}$ for BPUs. The top and right axes show the corresponding $R_{s,\ crystal\text{-}i}$ and $R_{s,\ obs\text{-}i}$ values, respectively. (b) Plots of $-\Delta\Delta G°_{obs\text{-}i}$ versus $-\Delta\Delta G°_{hydration\text{-}i}$ for BPUs. The top and right axes show the corresponding $R_{s,\ hydration\text{-}i}$ and $R_{s,\ obs\text{-}i}$ values, respectively. The solid lines represent the regression lines.

family of compounds was satisfactorily explained by a theoretical model which considers both crystal packing and hydration, as shown in Figure 1.1. These results indicate the

validity of the thermodynamic model described by Eqs. (1.1–1.15). In order to further verify the model, two major assumptions in these equations were examined.

In Eq. (1.4), it was assumed that the intermolecular interactions in the liquid and gas states would be similar between structural analogs and therefore the crystal packing term can be described only by the changes in Gibbs energy on transition from the crystalline to the liquid state. The intermolecular interactions of BPUs in the liquid and gas states would be less compound-specific than the interactions in the crystalline state. In addition, the interactions would be predominantly controlled by the core structure when the added substituent contains no hydrogen bond donor (since H-bond donors often contribute to strong intermolecular interactions).[58,59] These assumptions in Eq. (1.4) would be verified by applying our thermodynamic model to the solubility of liquid compounds. According to Eqs. (1.11) and (1.14), the negative logarithm of aqueous solubility (–log C_s) of liquids should be predominantly controlled by $\log P_{oct}$ ($\propto \Delta\Delta G°_{hydration\text{-}i}$; the validity of the relationship between $\Delta\Delta G°_{hydration\text{-}i}$ and $\log P_{oct}$ is discussed below) since the assumption indicates that $\Delta\Delta G°_{crystal\text{-}i}$ of a liquid is zero. Previous studies have shown a good linear correlation between –log C_s and $\log P_{oct}$ for liquids,[48,60] in contrast to the poor correlation for crystalline solids [Figure 1.2(b)].

In Eq. (1.9), a LFER between the partition coefficients in the gas-water system and those in the octanol-water system was assumed. LFERs between partition coefficients in various solvent-water systems such as octanol-water, hexane-water and chloroform-water systems have been reported,[58,59] even though these organic layers have different physicochemical properties. The dielectric constant (ε_r) is an important property for solvation behavior; the ε_r values for hexane, chloroform and octanol are 1.9, 4.8 and 10.3, respectively.[59,61] The proportionality constants of LFER between these systems, which were determined using several model compounds, ranged from 0.80 to 1.10,[59,61] and were close to the α value obtained in the current study (α = 1.03). These results suggest that the LFERs observed for the solvent-water systems are applicable to the gas (ε_r = 1)-water system. In

addition, the α values of liquid compounds are easily estimated as a coefficient of the log P_{oct} term in the linear regression analysis between log P_{oct} and –log C_s, as described in the verification of Eq. (1.4). The general solubility equation proposed by Yalkowsky *et al*. suggests that the average α value for structurally diverse compounds is close to unity.[24,25] On the other hand, Hansch *et al*. have reported that the α values for various compound classes range from 1.00 to 1.34.[60] Since the α value would be compound class-specific, it will be necessary to determine it for each series of analogs in order to estimate the contribution of the hydration term accurately.

Thus, the validity of the thermodynamic model has been shown. Good agreement was also observed between $R_{s,\ calc\text{-}i}$ and $R_{s,\ obs\text{-}i}$ (Table 1.1 and Table 1.2) and the differences between them were not more than 1.5-fold for nine BPUs. The relatively large (approximately 2-fold) deviation observed for BPU-6 and 8 might be attributable to the difficulty of accurately measuring the solubility of these extremely water-insoluble compounds. For simplicity, the theoretical values (the $R_{s,\ crystal\text{-}i}$, $R_{s,\ hydration\text{-}i}$, and $R_{s,\ calc\text{-}i}$ values and their corresponding $\Delta\Delta G°_{crystal\text{-}i}$ $\Delta\Delta G°_{hydration\text{-}i}$ and $\Delta\Delta G°_{calc\text{-}i}$ values) are used in the discussion below.

1.4.2 Relative contribution of crystal packing and hydration to solubility

Table 1.2 shows the structure-property relationship for these BPUs. Substituent effects on crystal packing, hydration and overall solubility were separately estimated from the $R_{s,\ crystal\text{-}i}$, $R_{s,\ hydration\text{-}i}$ and $R_{s,\ calc\text{-}i}$ values, respectively. For example, the results for BPU-2 indicate that a 2-F substituent on the X-ring potentially caused a 3.22-fold increase in solubility (= $R_{s,\ crystal\text{-}i}$) by decreasing the thermodynamic stability of crystal packing and a 0.89-fold decrease in solubility (= $R_{s,\ hydration\text{-}i}$) by inhibiting hydration. As a result, the solubility ($R_{s,\ calc\text{-}i}$) increased by 2.86-fold (= 3.22 × 0.89) in total. The relationship between $R_{s,\ crystal\text{-}i}$, $R_{s,\ hydration\text{-}i}$ and $R_{s,\ calc\text{-}i}$ for each BPU is shown in Figure 1.3 and clarifies the relative contribution of crystal packing and hydration to thermodynamic solubility. We

conclude that crystal packing and hydration equally contribute to the thermodynamic solubility of BPUs because the range of $R_{s,\ crystal\text{-}i}$ is on average comparable to that of $R_{s,\ hydration\text{-}i}$. This result is consistent with Figure 1.1 and Figure 1.2, which demonstrated that both factors are necessary to explain the relative thermodynamic solubility. The overall substituent effects on solubility ($R_{s,\ calc\text{-}i}$) resulted from the composite of $R_{s,\ crystal\text{-}i}$ and $R_{s,\ hydration\text{-}i}$ for each BPU (Figure 1.3).

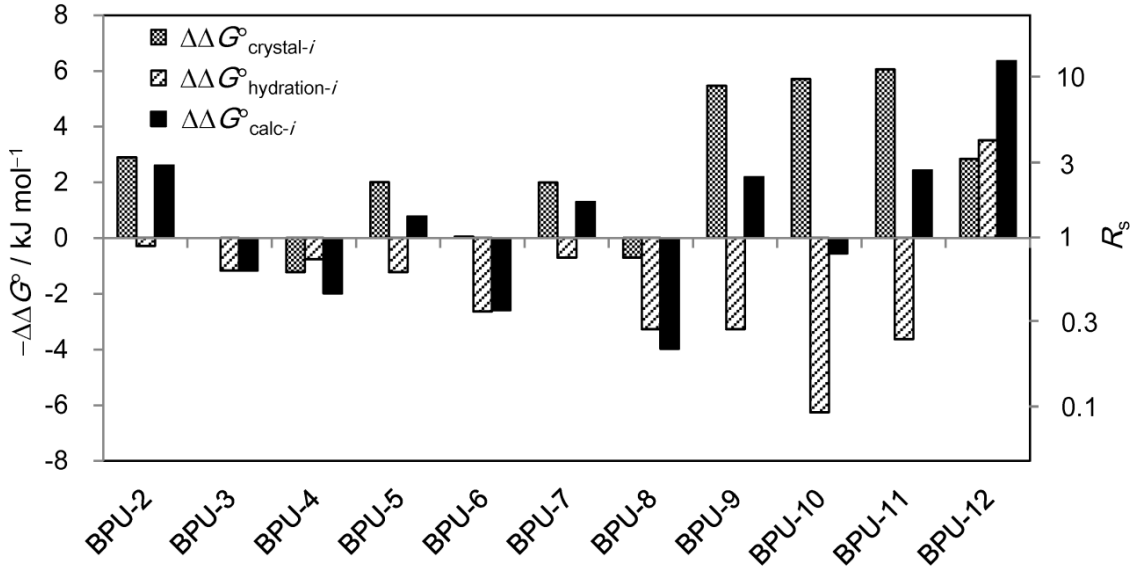

Figure 1.3. The relationships between $\Delta\Delta G°_{crystal\text{-}i}$, $\Delta\Delta G°_{hydration\text{-}i}$ and $\Delta\Delta G°_{calc\text{-}i}$ for each BPU. The right axis shows the corresponding R_s ($R_{s,\ crystal\text{-}i}$, $R_{s,\ hydration\text{-}i}$ and $R_{s,\ calc\text{-}i}$) values.

For the substituents examined, all substituents at the 3- or 4-position on the X- and Y-rings (BPU-3, 4, 6, 8 and 12) decreased the thermodynamic solubility due to their synergistic negative contribution to $R_{s,\ crystal\text{-}i}$ and $R_{s,\ hydration\text{-}i}$. On the other hand, the $R_{s,\ calc\text{-}i}$ value of a 2-substituted derivative was larger than 1 when its positive substituent effect on $R_{s,\ crystal\text{-}i}$ exceeded its offsetting effect on $R_{s,\ hydration\text{-}i}$. As a result, the thermodynamic solubility of several BPUs can be enhanced by introducing a hydrophobic substituent. Such substituents will be also preferable for the intrinsic activity of drug molecules, which often increases with an increase in the log P_{oct} value.[38] In order to improve solubility by utilizing

hydrophobic substituents, we must consider the substituent effects on both $R_{s,\ crystal\text{-}i}$ and $R_{s,\ hydration\text{-}i}$. Bulky substituents at the 2-position on the X-ring (BPU-9, 10 and 11) were desirable for $R_{s,\ crystal\text{-}i}$ but they significantly decreased the $R_{s,\ hydration\text{-}i}$ value due to their high hydrophobicity. For BPU-10, the large $R_{s,\ crystal\text{-}i}$ value was completely negated by the undesirable $R_{s,\ hydration\text{-}i}$. Conversely, simple reduction of the log P_{oct} value may decrease solubility when we ignore the substituent effect on $R_{s,\ crystal\text{-}i}$. The true substituent effects on crystal packing and hydration are usually unclear since only their composite effects ($R_{s,\ obs\text{-}i}$) are observed in solubility measurements. The separate evaluation of $R_{s,\ crystal\text{-}i}$ and $R_{s,\ hydration\text{-}i}$ by the present method will be useful for understanding the structure-solubility relationships of analogs in detail.

The ratio of $R_{s,\ calc\text{-}i}$ between BPU-2 and BPU-8, approximately 14-fold, was the maximum difference in overall solubility produced by changing a single substituent on the X-ring. This indicates that a more than 10-fold improvement in solubility may be achievable by a minor structural modification in a lead optimization step during drug discovery, without dramatic reduction of the log P_{oct} values. The degree of solubility enhancement was comparable to that observed in the development of amorphous formulations.[27] Murdande *et al*. reported that the solubility ratio between amorphous and crystalline forms is 10-fold or less for 8 out of the 9 model drugs studied.[27] Although amorphous formulations are a powerful tool for improving the solubility of poorly soluble drugs, this approach is generally time-consuming and may pose serious challenges to formulation developers.[23,35] It would be desirable to increase thermodynamic solubility by structural optimization in order to mitigate future risks during formulation development. However, advantageous substituent effects, and therefore a good drug candidate, might be overlooked if only kinetic solubility is evaluated. In the kinetic (or solution precipitation) method, compounds are dissolved in organic solvent and then added to aqueous medium.[4] The solubility value obtained by this method often corresponds to that of amorphous solids[4] and ignores the substituent effect on $R_{s,\ crystal\text{-}i}$. Therefore, it is necessary to characterize crystalline forms of drug candidates and

evaluate their thermodynamic solubility in drug discovery. A correct understanding of the physicochemical properties of drugs will allow us to prioritize drug candidates appropriately.

The range of $R_{s,\ crystal\text{-}i}$ (0.61 to 11.54) indicated that the alteration in the crystal packing pattern produced by small structural modifications were equivalent to a 19-fold change in solubility. This value was larger than the solubility ratio generally observed between polymorphs.[62] The solubility difference between polymorphs is typically less than 2-fold and is attributable to changes in crystal packing energy without a modification to the chemical structure. On the other hand, much larger (> 100-fold) increases in solubility have been observed when a modification to the chemical structure is accompanied by a significant conformational change in each molecule.[11,42,43] For example, a substituent on a biaryl moiety often increases a dihedral angle and inhibits intermolecular π-stacking interactions[11]. The substituents introduced onto the BPUs presumably promoted larger changes in the crystal packing pattern than those observed in polymorphs, but infrared spectroscopy demonstrated that a significant conformational change in each molecule was unlikely.[63] Therefore, the $R_{s,\ crystal\text{-}i}$ range observed in the current study is reasonable.

In order to enhance solubility by a small structural change, it is critical to explore suitable substituents. However, our knowledge base for predicting $R_{s,\ crystal\text{-}i}$ is limited compared to that for $R_{s,\ hydration\text{-}i}$, which can be estimated from knowledge of the structure-log P_{oct} relationships.[38,55,59] Although it is anticipated that the substituents at the 2-position in BPUs inhibit intermolecular hydrogen bonding at the urea moiety, the actual mechanism by which they decrease the stability of crystal packing remains unknown. In addition to the thermodynamic analysis presented in this study, crystallographic data may be helpful to elucidate the mechanism for improving $R_{s,\ crystal\text{-}i}$ and predict more effective substituents.[42] A better understanding of the substituent effect on solubility will allow us to design and synthesize promising clinical candidates efficiently.

1.5 CONCLUSION

Separate evaluation of the crystal packing and hydration demonstrated that both factors equally contribute to the thermodynamic solubility of BPUs. All hydrophobic substituents are undesirable for solubility in terms of hydration. However, they sometimes decrease the thermodynamic stability of crystalline phases and improve solubility when their desirable impacts on crystal packing exceed their counteracting effects on hydration. A more than 10-fold solubility enhancement was achieved by the optimization of a single substituent; the degree of improvement was comparable to that generally attained by utilizing amorphous formulations. The thermodynamic analysis presented in the current study will be helpful in understanding substituent effects and structure-solubility relationships quantitatively. Although the set of analogs is limited in the present study, additional studies for a wider range of compounds are in progress. A systematic investigation of the substituent effect on solubility will allow us to create drug-like candidates more efficiently.

2. Supersaturation-Nucleation Behavior of Poorly Soluble Drugs and its Impact on the Oral Absorption of Drugs in Thermodynamically High-Energy Forms

2.1 INTRODUCTION

Solubility of a drug candidate might be enhanced even after the medicinal chemistry approach is completed and the chemical structure is fixed. In the preformulation research, solid forms such as amorphous forms, salts, and cocrystals have been intensely studied to maximize the absorbability of a selected clinical candidate. These thermodynamically high-energy forms improve not only the dissolution rate, but also the apparent solubility of the drug in the intestine by inducing supersaturation. Therefore, these drug forms can also increase the maximum absorbable dose that is otherwise limited by solubility.[23,24] There have been many studies reporting efficient methods for screening excipients, counter ions, and cocrystal formers in order to explore high-energy forms.[32,64,65] These studies have focused mainly on formulation techniques; drug molecular properties have often been ignored. However, high-energy forms of poorly soluble drugs do not always satisfactorily improve their solubility and absorbability. This suggests that the ability of a high-energy form to enhance solubility and absorbability is highly dependent on the molecular properties of the drug itself, as well as on the selection of excipients, counter ions, and cocrystal formers.

When a drug in a high-energy form dissolves in the intestine, its concentration reaches a supersaturated value which is higher than the equilibrium solubility of the thermodynamically stable form. The concentration of the drug reaches a critical concentration where nucleation of the stable form is initiated. Once nucleation occurs, precipitation leads to a decrease in drug concentration to the thermodynamic solubility of a stable form.[5] Therefore, in a solubility-limited situation, the nucleation characteristics can

be the critical factors that control the effective drug concentration for absorption. If a drug maintains high degree of supersaturation without nucleation occurring, the effective concentration can benefit from high-energy forms. On the other hand, it is difficult to improve the oral absorption of a drug which rapidly nucleates even at a low degree of supersaturation.

Clearly, detailed characterization of supersaturation-nucleation behavior, including nucleation kinetics and the duration of supersaturation, is essential for understanding the oral absorption of drugs in high-energy forms. Recently, several studies on the kinetics and mechanisms of nucleation have been reported.[66–71] However, convenient and efficient characterization methods have not been reported to date, and the impact of supersaturation-nucleation behavior on oral absorption also remains poorly understood.

In the present work, the supersaturation-nucleation behavior of poorly water-soluble drugs in fasted state simulated intestinal fluid was characterized by measuring the induction time for nucleation. The model drugs used in this study were itraconazole, troglitazone, erlotinib and vemurafenib (Table 2.1), which are typical drugs developed as high-energy forms. The relationship between supersaturation-nucleation characteristics and oral absorption is also discussed.

Table 2.1. Chemical Structures of Model Drugs

Itraconazole	Erlotinib	Troglitazone	Vemurafenib
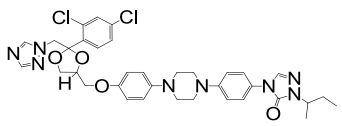	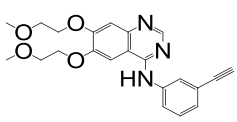	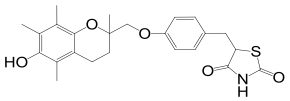	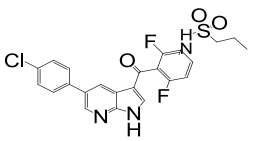

2.2 MATERIALS AND METHODS

2.2.1 Chemicals

Vemurafenib was synthesized in Eisai Tsukuba Research Laboratories (Ibaraki, Japan). Erlotinib free base was prepared from erlotinib hydrochloride (Cayman Chemical Company, Ann Arbor, Michigan, US) by suspending in 30 mM phosphate buffer pH 6.5 for 24 h and collecting the precipitated crystals. Lecithin (Coatsome-50) was purchased from Nippon Oil and Fat Co., Ltd. (Tokyo, Japan). Sodium taurocholate and itraconazole were purchased from Wako Pure Chemical Industries, Ltd. (Osaka, Japan). Troglitazone was provided from LKT Laboratories, Inc. (St Paul, Minnesota, US). All other reagents were of reagent grade and were used without further purification. The water used was filtered through a Milli-Q Water Purification System (Millipore, Bedford, Massachusetts, US) prior to use.

2.2.2 Preparation of FaSSIF

Fasted state simulated intestinal fluid (FaSSIF) was prepared by the dilution method as described in Sugano *et al*.[4] Sodium taurocholate (30 mM) and lecithin (7.5 mM) were dispersed into 28.4 mM phosphate buffer (pH 6.5) containing 103.3 mM KCl to prepare concentrated sodium taurocholate/lecithin solution. FaSSIF was then obtained by diluting the concentrated solution by 10 times with the phosphate buffer.

Dynamic light scattering analysis (Zetasizer nano ZS, Malvern Instruments Ltd., Worcestershire, UK) showed that the size of the vesicles in FaSSIF gradually increased in the first few hours after dilution, as reported previously.[4] However, the vesicle size remained constant (ca. 100 nm) between 12 and 48 h following dilution at 25 °C (data not shown). In order to obtain FaSSIF with consistent characteristics, FaSSIF was incubated at 25 °C for 24 h prior to measurement of the nucleation induction time.

2.2.3 Measurement of thermodynamic solubility

The thermodynamic solubility (C_s) of model drugs in FaSSIF at 25 °C and 37 °C was determined using a shake flask method. Excess amount of drug was added to glass tubes containing 5 mL of FaSSIF. The test solutions were placed in a shaker incubator (Personal Lt-10, Taitec Co., Ltd., Saitama, Japan) for 24 h, and then filtered through a 0.45 μm filter (Chromatodisc 13A, GL Science Inc., Tokyo, Japan). The first 1 mL of filtrate was discarded to avoid concentration underestimation due to adsorption. The filtrate was immediately diluted twice with acetonitrile. The concentration of each drug was determined by HPLC analysis using UV detection (HPLC model Prominence, Shimadzu Co., Kyoto, Japan) and an X-Bridge column (2 mm i.d., 35 mm length, 3 μm, Waters, Milford, Massachusetts, US). Mobile phase A consisted of 0.1% (v/v) $HClO_4$ and 1% (v/v) acetonitrile in water. Mobile phase B consisted of 0.1% (v/v) $HClO_4$ and 10% (v/v) water in acetonitrile. The analytes were eluted with a linear gradient where the mobile phase B was ramped from 10% to 100% over 6 min with a flow rate of 0.3 mL min^{-1}. The detection wavelengths were set at 257 nm (itraconazole), 254 nm (erlotinib), 285 nm (troglitazone) and 254 nm (vemurafenib), respectively. All solubility measurements were performed in triplicate.

2.2.4 Measurement of induction time for nucleation

The induction time (t_{ind}) for nucleation, which is defined as the time lag for the observable crystals to appear, was measured for the model drugs. It is generally accepted that t_{ind} is inversely proportional to the nucleation rate.[72] The measurement of t_{ind} was performed in FaSSIF. Although it has been reported that supersaturation behavior of poorly soluble drugs depends on test medium composition,[67] the previous study reported by Takano *et al*. has suggested that FaSSIF is a suitable biorelevant medium for predicting *in vivo* performance of supersaturable drugs.[24] Supersaturated drug solutions were prepared in FaSSIF by the

solvent shift method[67] and stirred constantly. In brief, itraconazole, erlotinib, troglitazone and vemurafenib were dissolved in dimethyl sulfoxide (DMSO) to obtain 2, 10, 20, and 40 mg mL^{-1} stock solutions, respectively. A suitable volume (~10 μL) of the stock solution was added to 2 mL of FaSSIF in a quartz cuvette (10 mm × 10 mm × 45 mm) installed in a UV-Vis spectrophotometer (UV2400PC, Shimadzu Co., Kyoto, Japan). The DMSO concentration never exceeded 0.5% (v/v) in the supersaturated solution, and no significant influence of DMSO on t_{ind} was observed in this concentration range. Absorbance versus time curves were measured using a UV detector and t_{ind} was obtained by detecting precipitation as previously reported.[73]

The supersaturated solution was stirred with a magnetic micro stir bar (8.1 mm × ϕ3.2 mm) using a controller (CS-1, As One Co. Osaka, Japan) at 300 rpm. The solution UV absorptions were monitored at 275 nm (itraconazole), 335 nm (erlotinib), 284 nm (troglitazone) and 340 nm (vemurafenib), until a sharp change due to precipitation was observed. The precipitated solid was collected by filtration and analyzed with a powder X-ray diffractometer (model RINT-TTRIII, Rigaku Co. Tokyo, Japan). The measurements of t_{ind} were performed in triplicate at 25 ± 0.5 °C (thus avoiding temperature-related artifacts such as bubble formation and evaporation).

2.3 RESULTS

2.3.1 Thermodynamic solubility FaSSIF

The thermodynamic solubilities of the model drugs in FaSSIF are shown in Table 2.2 These were important base values for the study on supersaturation. The solubilities slightly increased with an increase in temperature. The solubilities of the model drugs were less than 10 μg mL^{-1}, each, indicating extremely poor solubility even in the presence of sodium taurocholate and lecithin.

Table 2.2. Thermodynamic Solubility of Model Drugs in FaSSIF (Mean ± SD, n = 3)

Solubility (μg mL^{-1})	Itraconazole	Erlotinib	Troglitazone	Vemurafenib
25 °C	0.3 ± 0.0	5.8 ± 0.3	3.5 ± 0.1	4.4 ± 0.3
37 °C	0.3 ± 0.0	7.4 ± 0.4	4.5 ± 0.1	4.7 ± 0.3

2.3.2 Induction time for nucleation in FaSSIF

Figure 2.1 shows absorbance versus time curves of 60, 80, 100 and 120 μg mL^{-1} troglitazone in FaSSIF. These initial concentrations (C_{init}) of troglitazone were higher than its thermodynamic solubility at 25 °C (Table 2.2), so troglitazone was considered to exist in a supersaturated state. When an aliquot of the stock solution of each model drug was added into FaSSIF, the solution was visually clear and no fluctuation in absorbance was observed at any tested concentrations. Therefore, supersaturated solutions of all the tested drugs can be created in FaSSIF even in the absence of precipitation inhibitors, as previously reported by Bevernage *et al*.[67] After a given period of time, a steep increase in absorbance occurred and the time it took for initiation to occur was dependent on C_{init}. The more concentrated the solution was, the sooner initiation took place.

The shapes of the time-absorbance curves of itraconazole, vemurafenib and troglitazone were similar, whereas a steep decrease was observed in the curve of erlotinib. Accordingly, it appears that the shapes of the time-absorbance curves depend on the nature of the precipitates such as size and dispersibility. For all four drugs, powder X-ray diffractometry demonstrated that the change in UV absorbance was due to precipitation of the crystalline free form of the investigated drug. The formation of critical nuclei may sometimes be overlooked by UV detection, but UV detection has often been utilized to measure t_{ind} because crystal growth rates are much faster than nucleation rates.[72,74,75] The time lag where critical nuclei grow into observable crystals will be negligible. t_{ind} at each C_{init} was determined by drawing regression lines through the two distinct linear regions and

taking the intersection of the two lines.

The relationships between t_{ind} and C_{init} for the four model drugs are shown in Figure 2.2. Regardless of the drug species examined, the observed t_{ind} decreased with an increase in C_{init}, but the C_{init} range where nucleation occurred was clearly compound-dependent. For example, nucleation was quickly induced at low C_{init} (~15 μg mL^{-1}) for itraconazole, but the t_{ind} of vemurafenib was longer than 1000 s at even a much higher C_{init} range. Since the term "apparent solubility" describes the ability to maintain a high supersaturated concentration, the compounds plotted on the right side in Figure 2.2 have higher apparent solubility than those on the left side. The approximate rank order of the apparent solubility of these drugs was vemurafenib ≥ troglitazone > erlotinib > itraconazole.

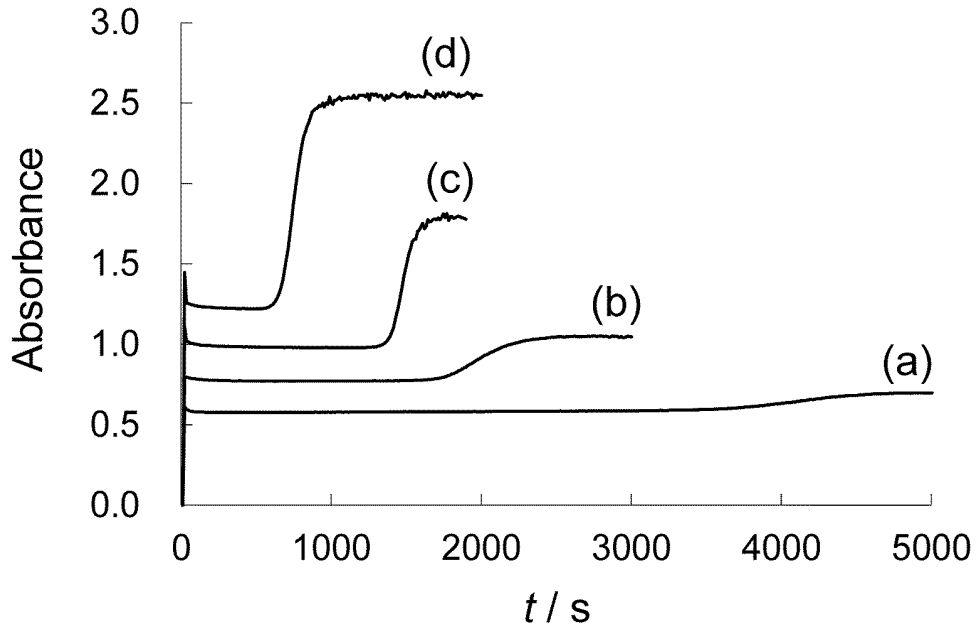

Figure 2.1. Time-absorbance curves of supersaturated solution in the presence of (a) 60, (b) 80, (c) 100 and (d) 120 μg mL^{-1} of troglitazone.

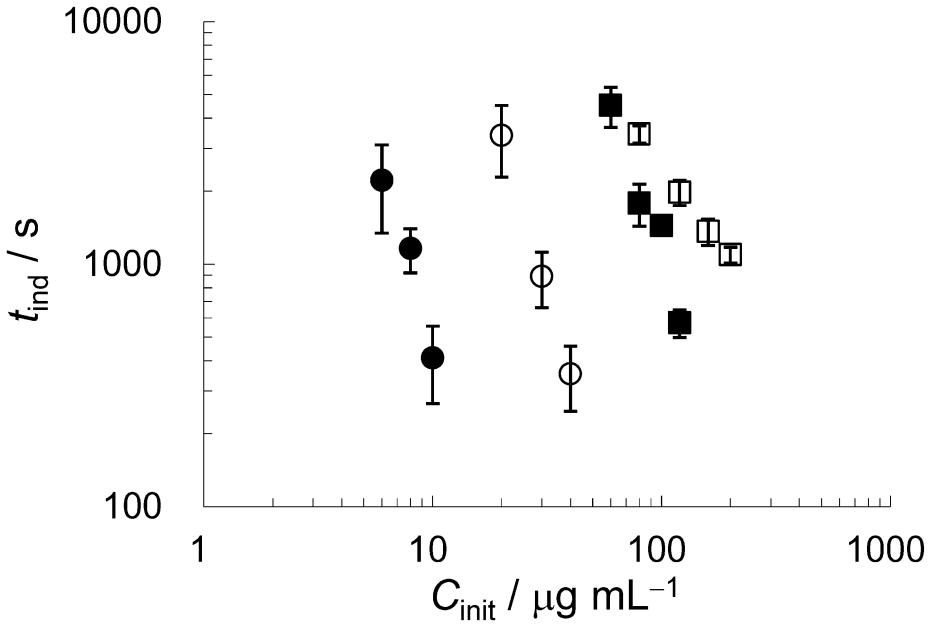

Figure 2.2. Plots of t_{ind} versus C_{init} for itraconazole (●), erlotinib (○), troglitazone (■) and vemurafenib (□). Each value represents the mean ± SD (n=3).

2.4 DISCUSSION

2.4.1 Interpretation of supersaturation stability based on classical nucleation theory

According to the classical nucleation theory,[5,72,74] nucleation rate increases with an increase in the degree of supersaturation, S (= C_{init}/C_s in this study). If the nucleation rate and t_{ind} are determined only by S, compounds with higher thermodynamic solubility should show higher apparent solubility. However, the rank order of the thermodynamic solubility of the model drugs in FaSSIF (erlotinib > vemurafenib > troglitazone >> itraconazole) is different from that of their apparent solubility. These results clearly demonstrate that: (i) the apparent solubility in FaSSIF is governed not only by the thermodynamic solubility, but also by the supersaturation stability of the drug, and (ii) the supersaturation stability is dependent on the drug species. High supersaturation stability means the ability to maintain a high S without nucleation for a long period of time, which corresponds to the magnitude of the activation

energy barrier to form nuclei.

To clarify the supersaturation-nucleation characteristics, the relationship between t_{ind} and S was analyzed in detail. In classical nucleation theory, the relationship between the nucleation rate (J) and the degree of supersaturation is expressed as shown in Eq. (2.1)[74]:

$$J = A\exp\left(-\frac{4f_s^3\pi\upsilon^2\gamma^3}{27f_v^3k^3T^3\ (\ln S)^2}\right) \tag{2.1}$$

where f_s and f_v are the surface and volume shape factors, υ is the molecular volume of the solute, γ is the interfacial energy per unit area, T is the absolute temperature and k is the Boltzmann constant. The pre-exponential factor A is mainly dependent on the concentration of the solute and the degree of agitation. Assuming that nucleation rate is inversely proportional to t_{ind}, the linear relationship between S and t_{ind} is obtained as:

$$\log t_{ind} = \alpha + \beta(\log S)^{-2} \tag{2.2}$$

where α is a dimensionless empirical constant and β consists of a number of variables dependent on the molecular properties of the solute and T. The linear relationship given by Eq. (2.2) has been experimentally observed for inorganic salts, organic compounds and proteins.[73–75]

As shown in Figure 2.3, the measured $\log t_{ind}$ of each drug followed a linear relationship with $(\log S)^{-2}$. In several previous studies, similar plots consist of two straight lines which have higher slope in the high S region and lower slope in the low S region. This change in slope is attributable to the change in nucleation mechanism, from homogenous nucleation in the high S region to heterogeneous nucleation in the low S region.[73–75] Such changes were not observed in this study. Thus, it is reasonably assumed that only

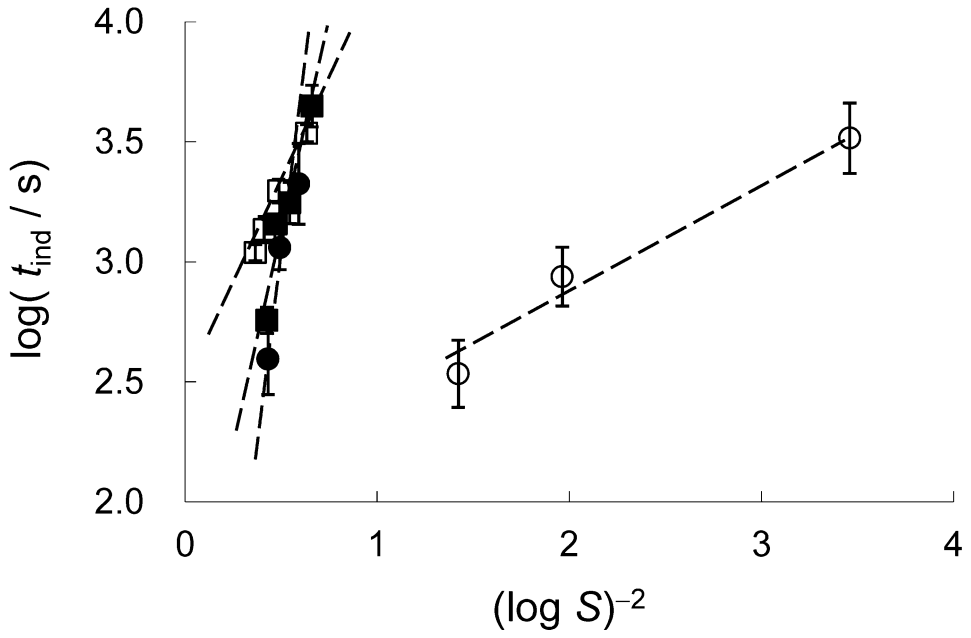

Figure 2.3. Plots of log t_{ind} versus (log S)$^{-2}$ for itraconazole (●), erlotinib (○), troglitazone (■) and vemurafenib (□). Each value represents the mean ± SD (n=3). The broken lines are the regression lines.

homogenous nucleation was predominant in the current study where S was relatively high. Under such conditions, the nucleation process is governed by the nucleation characteristics of the drug itself, rather than other experimental conditions such as the experimental scale and the volume-surface area ratio of the cuvette.

For vemurafenib, troglitazone and itraconazole, nucleation was observed only in the relatively high S [= low (log S)$^{-2}$] region. On the other hand, nucleation of erlotinib occurred even under relatively low S conditions. These results show that vemurafenib, troglitazone and itraconazole have higher supersaturation stability than erlotinib. We designated "log $S(t_{1000})$," the logarithm of the S value at t_{ind} = 1000 s, as an index of supersaturation stability. These values were calculated by linear regression analysis (Table 2.3). In an *in vitro* dissolution test for high-energy forms reported previously, precipitation of the stable form was often observed in the time range of 600 to 1200 s after its dissolution, and the dissolution-precipitation profiles were satisfactorily explained the relative *in vivo*

performance.[29,76] Also, it has been suggested that short-term stability of supersaturation under the high *S* condition is important in estimating intestinal absorption.[64] For example, Guzman *et al*. used the area under the drug concentration versus time curve for the first 600 s of *in vitro* dissolution to establish *in vitro-in vivo* correlations for various formulations of the high-energy form of celecoxib.[29] It was therefore reasonable to expect that nucleation would occur in the intestine on a similar time scale, and that t_{ind} = 1000 s would be an appropriate time period over which to investigate the relationship between *in vitro* supersaturation-nucleation behavior and *in vivo* absorption. A high $\log S(t_{1000})$ value corresponds to high supersaturation stability; the rank order of the model drugs was vemurafenib ≥ troglitazone ≅ itraconazole > erlotinib. The drug with the highest supersaturation stability, vemurafenib, attains an approximately 10 times higher *S* value than the drug with the lowest supersaturation stability, erlotinib.

As discussed above, nucleation kinetics is generally described in terms of *S*. On the other hand, the relationship between nucleation kinetics and drug level in intestinal fluid is meaningful for the consideration of oral absorbability. "$\log C(t_{1000})$", the logarithm of the C_{init} /μg mL^{-1} value at t_{ind} = 1000 s, was considered to be a useful index to discuss the relationship between nucleation and intestinal drug level of thermodynamically high energy forms. This value is calculated by summation of $\log S(t_{1000})$ and $\log C_s$ (/μg mL^{-1}) at 25 °C [because $C(t_{1000}) = C_s \times S(t_{1000})$, Table 2.3]. The rank order of $\log C(t_{1000})$ was consistent with that of apparent solubility in FaSSIF presented above (vemurafenib ≥ troglitazone > erlotinib > itraconazole, Figure 2.2). Thus, the drugs with higher $\log C(t_{1000})$ value maintain higher drug concentration and nucleates only at higher drug levels in FaSSIF. Both apparent solubility and $\log C(t_{1000})$ are considered to be composite parameters of thermodynamic solubility ($\log C_s$) and supersaturation stability [$\log S(t_{1000})$], because the rank orders of apparent solubility and $\log C(t_{1000})$ are fully explained by these two parameters. Vemurafenib and troglitazone showed higher $\log C(t_{1000})$ values than erlotinib which showed the highest thermodynamic solubility, with the aid of their supersaturation stability,

but the log $C(t_{1000})$ value of itraconazole did not exceed that of erlotinib due to its extremely low thermodynamic solubility.

Table 2.3. Indexes of Supersaturation Stability, Thermodynamic Solubility and Apparent Solubility

	Itraconazole	Erlotinib	Troglitazone	Vemurafenib
log $S(t_{1000})$	1.41	0.66	1.46	1.72
log C_s	-0.53	0.76	0.55	0.64
log $C(t_{1000})$	0.88	1.42	2.01	2.36

2.4.2 Oral absorption of poorly soluble drugs in high-energy forms

In this study, supersaturation-nucleation behavior has been characterized for several model drugs. This behavior is especially important when considering the oral absorption of drugs in thermodynamically high-energy forms such as amorphous forms, salts and cocrystals because these forms can create drug supersaturation in gastrointestinal fluid. The high-energy forms of a drug are often studied in order to improve oral absorption and achieve high exposure even at higher clinical doses. For example, solid dispersion techniques and microprecipitated bulk powder techniques have been applied to itraconazole, troglitazone and vemurafenib to obtain their amorphous forms,[64,77,78] and erlotinib has been developed as a hydrochloride salt. These methods allow solubility-limited nonlinear absorption of the poorly soluble drugs to be overcome, and enhance the maximum absorbable dose (MAD) by increasing the effective concentration for intestinal absorption.

A schematic diagram of time-drug concentration curves in the intestine is shown in Figure 2.4. When a drug in a high-energy form dissolves, its concentration exceeds the solubility of the thermodynamically stable form due to supersaturation. Following a certain period of supersaturation, crystal nucleation is initiated and the concentration of the drug falls to that of the stable form. In this chapter, it is assumed that the equilibrium solubility of the amorphous form[26,27] or the solubility product values[5,20] of salts are not limiting factors for intestinal drug concentration because nucleation of the stable form often occurs before

the concentration reaches to their values[5,26,79] (the thermodynamic limit of supersaturation is discussed in Chapter 3). Therefore, the nucleation of a stable form is a critical step to control the effective concentration for intestinal absorption, which corresponds to the area under the dissolution/precipitation-time curve. In this model, it is expected that absorbability of a drug in a high-energy form increases with an increase in the log $C(t_{1000})$ value, which indicates the concentration range where nucleation occurs (Figure 2.4). However, the relationship between the supersaturation-nucleation characteristics and the oral absorption of a drug still remains unclear.

In order to clarify the relationship between *in vitro* supersaturation-nucleation characteristics and *in vivo* absorption, four absorption-related parameters, MAD_{stable}, $F_{a,stable}$, MAD_{obs} and $F_{a,\,obs}$, were evaluated for itraconazole, erlotinib, troglitazone and vemurafenib. MAD_{stable} and $F_{a,\,stable}$ are the maximum absorbable dose limited by solubility and the absorbed fraction of thermodynamically stable forms, respectively. For the four model drugs, the crystalline free form was the thermodynamically stable form. MAD_{stable} was calculated by:

$$MAD_{stable} = P_{eff} \times C_s \times A_{intestine} \times T_{intestine} \tag{2.3}$$

$$P_{eff} = 10^{-3} \times \left(\frac{180}{MW} \right)^{1/3} \text{cm s}^{-1} \tag{2.4}$$

where P_{eff} is the effective intestinal membrane permeability, C_s is the thermodynamic solubility in FaSSIF at 37 °C, MW is the molecular weight, and $A_{intestine}$ and $T_{intestine}$ are the effective surface area (800 cm^2) of and transit time (4 h) in the human intestine, respectively.[3,6]

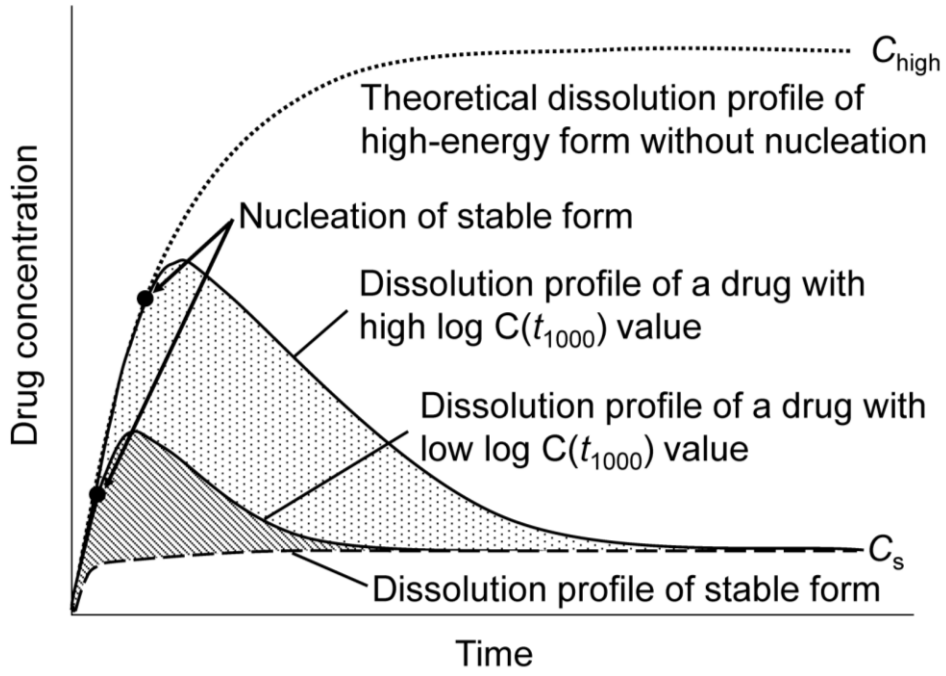

Figure 2.4. Schematic diagram of time-drug concentration curves in the intestine. Two solid lines are the time-drug concentration curves of high-energy forms with different nucleation kinetics, and the broken line is that of a stable form. The dotted line shows the time-drug concentration curves of a high-energy form under an imaginary situation in which nucleation never occurs. C_{high}: theoretical equilibrium solubility of an amorphous form or solubility of salts and cocrystals determined by the solubility product; C_s: thermodynamic solubility of a stable form.

Equation (2.4) is based on the assumption that P_{eff} of a lipophilic drug is equal to the permeability through an unstirred water layer, which is inversely proportional to the molecular radius.[6] In a solubility-limited situation, $F_{a,\ stable}$ is obtained by:

$$F_{a,\,stable} = \frac{\mathrm{MAD}_{stable}}{D} \qquad (2.5)$$

where D is the administered dose. Although MAD_{stable} and $F_{a,\ stable}$ are theoretical parameters, they are important base values for evaluating the effect of high-energy forms. The physicochemical properties of model drugs used in this study are listed in Table 2.4.

Table 2.4. Molecular Properties of Model Drugs

Compound	pK_a	clog P	MW	P_{eff} 10^{-4} cm s^{-1}
Itraconazole	3.7 (basic)[a]	5.99	705.6	6.3
Erlotinib	5.4 (basic)[b]	3.63	441.5	7.7
Troglitazone	7.6 (acidic)[c]	5.59	393.4	7.4
Vemurafenib	2.7 (basic), 5.7 (acidic)[c]	4.20	489.9	7.2

[a] From the Sporanox® (Janssen Pharmaceuticals Inc., Titusville, New Jersey, US) drug label.

[b] From the Tarceva® (Chugai Pharmaceutical Co., Ltd., Tokyo, Japan) drug label.

[c] Calculated using ADMET Predictor 5.0.0012 (Simulation Plus Inc., Lancaster, California, US).

$F_{a,\,obs}$ is the absorbed fraction of high-energy forms observed in clinical studies and was calculated based on relative bioavailability data reported on the drug label and in the literature.[78,80] For basic drugs, supersaturation can be created by the pH transition from the stomach to the intestine, but this study focuses on the effect of supersaturation generated by high-energy forms. Therefore, $F_{a,\,obs}$ at elevated gastric pH was calculated for itraconazole and erlotinib, in order to investigate the situation where both drug dissolution and nucleation occur predominantly in the intestine. The thermodynamic solubility of vemurafenib, which contains a basic group, was extremely low (<1 μg mL^{-1}) in the absence of bile acids, even at acidic pH (data not shown). Thus, the dissolution of vemurafenib in the stomach is negligible. Details of the methods and assumptions used for these calculations are summarized in Table 2.5.

The maximum absorbable dose observed in clinical studies (MAD_{obs}), which implies an index of drug absorbability under the solubility-limited conditions, was obtained by:

$$MAD_{obs} = D \times F_{a,\,obs} \quad (2.6)$$

$F_{a,\,obs}$ and MAD_{obs} of vemurafenib cannot be calculated directly due to insufficient clinical data. The MAD_{obs} of vemurafenib was obtained by Eq. (2.7) by assuming that the area under the plasma concentration-time curve at extremely high dose (1600 mg) of crystalline formulation (AUC_{stable}) was equivalent to MAD_{stable}:

$$MAD_{obs} = MAD_{stable} \times \frac{AUC_{amorphous}}{AUC_{stable}} \qquad (2.7)$$

where $AUC_{amorphous}$ was the AUC with an amorphous formulation. Then, the $F_{a,\,obs}$ of vemurafenib was calculated by Eq. (2.6).

Table 2.5. Method for the Calculation of Clinically Observed Fraction Absorbed.

Compound	Assumptions and calculation methods
Itraconazole	$F_{a,\,solution,\,fasted}$ = 100%, $AUC_{solid,\,fed}/AUC_{solution,\,fasted} \times AUC_{solid,\,fasted}/AUC_{solid,\,fed} \times rel.BA_{high\ pH}$ =59% × 61% × 39%[a]
Erlotinib	$F_{a,\,solid,\,fed}$ = 100%, $AUC_{solid,\,fasted}/AUC_{solid,\,fed} \times rel.BA_{high\ pH}$ = 51% × 54%[b]
Troglitazone	$F_{a,\,solid,\,fed}$ = 100%, $AUC_{solid,\,fasted}/AUC_{solid,\,fed}$ = 63%[c]
Vemurafenib	MAD_{stable}/Dose × $AUC_{amorphous}/AUC_{stable}$ = 39 mg/1120 mg × 14 fold[d] (see text.)

Subscripts express the dosage condition. AUC, area under the plasma concentration-time curve; solution, solution dosage; solid, solid dosage; fasted, in the fasted state; fed, in the fed state; $Rel.BA_{high\ pH}$, the relative bioavailability to the subject with high gastric pH against low gastric pH.

[a] From Sporanox® (Janssen Pharmaceuticals Inc.) drug label.

[b] From Tarceva® (Chugai Pharmaceutical Co, Ltd.) drug label.

[c] From Rezulin® (Warner-Lambert Co., Morris Plains, New Jersey, US) drug label and ref. 76.

[d] Refs. 78 and 80.

As is often the case with marketed drugs, pharmacokinetic data is not available in the dose range where nonlinear absorption is clearly observed for the four model drugs. Therefore, the MAD_{obs} obtained in this study tends to be underestimated, even when D is the highest dose administered as a solid dosage form. However, this value is a useful surrogate indicator because it is reasonable to assume that MAD_{obs} does not deviate far from the real maximum absorbable dose under highly solubility-limited conditions.

2.4.3 Effect of supersaturation-nucleation behavior on oral absorption

Table 2.6 shows the calculated absorption-related parameters for the four model drugs developed in high-energy forms. As expected, the rank order of MAD_{obs} was consistent with that of the log $C(t_{1000})$ value. In order to show the quantitative *in vitro-in vivo* relationship, the logarithm of MAD_{obs} corrected by P_{eff} was plotted against log $C(t_{1000})$, as shown in Figure 2.5. The positive linear relationship demonstrated that the log $C(t_{1000})$ value, which is controlled by nucleation kinetics, was the determinant factor of MAD. A slope close to unity means that the MAD of drugs in high-energy forms is proportional to $C(t_{1000})$, probably because $C(t_{1000})$ is also proportional to the mean effective concentration for absorption in the intestine.

Studies focused on predicting human oral absorption have shown that the intestinal drug concentration is a determinant factor for the extent and rate of absorption, especially for Biopharmaceutical Classification System class II drugs (low solubility and high permeability).[6,76] For drugs in the stable form, the intestinal drug concentration can be predicted from the dissolution profile and thermodynamic solubility in FaSSIF. Under solubility-limited conditions, a simplified relationship between oral absorption and intestinal drug concentration is obtained by Eq. (2.3). On the other hand, we can predict the concentration of a drug in a high-energy form under the restricted condition where a thermodynamically stable form never precipitates within the intestinal transit time.[24]

Table 2.6. Absorption-Related Parameters

Compound	Dose mg	$F_{a,\ stable}$	$F_{a,\ obs}$	MAD_{stable} mg	MAD_{obs} mg	$F_{a,\ obs}/F_{a,\ stable}$
Itraconazole	200	1.1%	14%	2.2	28	13
Erlotinib	200	33%	27%	66	54	0.8
Troglitazone	600	6.4%	63%	38	378	9.8
Vemurafenib	1120	3.4%	48%	39	540	14

$F_{a,\ stable}$, fraction absorbed of stable forms; $F_{a,\ obs}$, fraction absorbed of high-energy forms; MAD_{stable}, maximum absorbable dose of stable forms; MAD_{obs}, maximum absorbable dose of high-energy forms; $F_{a,\ obs}/F_{a,\ stable}$, relative bioavailability of high-energy forms against stable forms.

Therefore, the prediction of oral absorption generally has not been applicable to a drug in a high-energy form.[81,82] Now, however, a good correlation represented in Figure 2.5 will provide us with a better prediction for the absorption of these drugs. Although further verification might be needed for the analytical time period, t_{ind} = 1000, the results presented above demonstrate that this time period is acceptable for understanding the relationship between supersaturation and absorption in the intestine. The crystal growth kinetics of a stable form is not discussed in this study, but it would not impact on the relationship in Figure 2.5, because it is mainly controlled by the diffusion process and is thought to be less compound-specific than nucleation kinetics.

MAD_{stable} obtained by Eq. (2.3) is useful for the discovery stage of drug development, but it often underestimates absorbability as shown in Table 2.6 because the drug concentration in Eq. (2.3) represents the worst case for the drug examined. On the other hand, our method is advantageous for assessing the potential absorbability of poorly soluble drugs and permits consideration of the additional effect of supersaturation. At an earlier drug discovery stage where manufacturing processes are not fully controlled, we will have

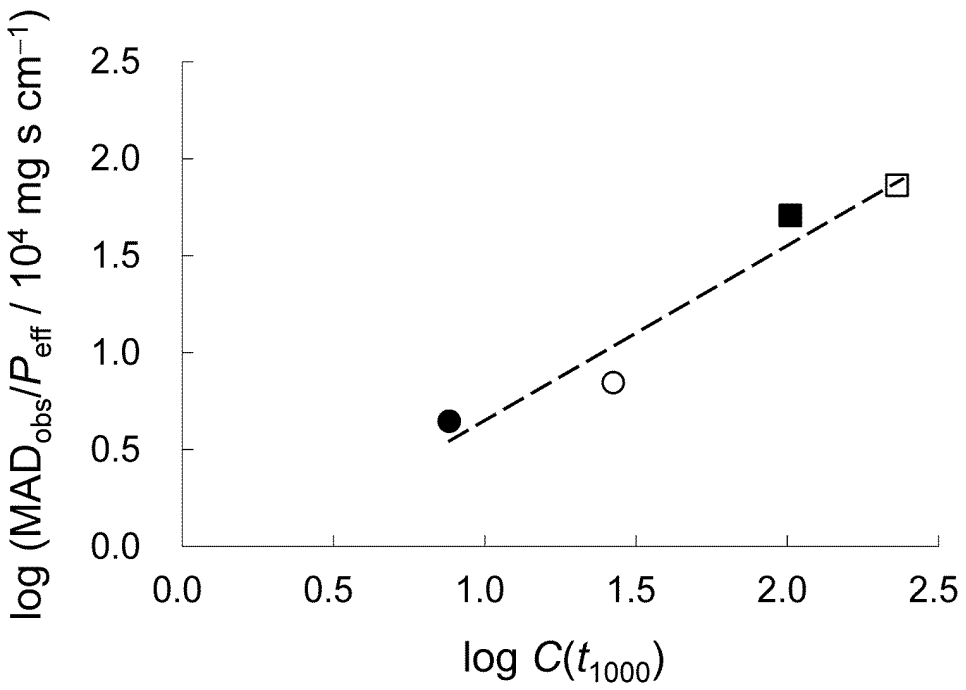

Figure 2.5. Plots of log (MAD_{obs}/P_{eff}) versus log $C(t_{1000})$ for itraconazole (●), erlotinib (○), troglitazone (■), vemurafenib (□). The broken line represents the regression line.

to pay attention to impurity amounts of tested compounds, which may affect nucleation kinetics. However, our method that needs only a small amount of drug substance (less than 10 mg) is still invaluable to evaluating its oral absorbability at the discovery phase. Although it has previously been reported that *in vitro* dissolution testing in biorelevant media is a powerful tool for assessing absorbability, to date this method has been costly, both because of the large amount of drug substance required and because suitable excipients or counter ions for the high-energy drug forms had to be explored before the dissolution tests could be conducted.

The log $C(t_{1000})$ value of a drug is a composite parameter composed of thermodynamic solubility and supersaturation stability. In order to separately evaluate the effect of supersaturation stability on oral absorption, the ratio of $F_{a,\,obs}$ to $F_{a,\,stable}$ ($F_{a,\,obs}/F_{a,\,stable}$ = MAD_{obs}/MAD_{stable}) was calculated (Table 2.6). This parameter indicates how successfully the high-energy forms of a poorly soluble drug can improve its oral

absorption. Our data clearly showed that improved oral absorption was observed only for vemurafenib, troglitazone and itraconazole, which showed higher log $S(t_{1000})$ values (= high supersaturation stability), whereas no improvement was observed for erlotinib, which had the smallest log $S(t_{1000})$ value. This result demonstrates that the effect of high-energy forms is dependent on drug properties, as well as on kinds of precipitation inhibitors or counter ions. Pharmaceutical researchers empirically understand that high-energy forms do not always improve solubility and oral absorbability. It is reasonable to assume that vemurafenib, troglitazone and itraconazole owe their success to their high supersaturation stability, even though we admit the importance of optimized formulation, which will support supersaturation of drugs, as an additional factor. If drug candidates that have high supersaturation stability are appropriately prioritized and moved forward into further formulation development including extensive screening of precipitation inhibitors or counter ions, the success rate will be enhanced. Therefore, the evaluation of the supersaturation stability of a drug will enable us to evaluate the potential absorbability of a candidate and make an informed decision whether or not to pursue high-energy forms of the drug as a means of enhancing oral bioavailability.

Finally, the importance of thermodynamic solubility, which is the other component determining the log $C(t_{1000})$ value, should not be underestimated. Although the high supersaturation stability of a candidate compound assures the enhancement of solubility and MAD by using high-energy forms, an increase in thermodynamic solubility is also needed for higher MAD. The high log $C(t_{1000})$ value and MAD_{obs} of troglitazone and vemurafenib are attributable to both their high supersaturation stability and their acceptable thermodynamic solubility.

2.5 CONCLUSION

Detailed analysis of the induction time for nucleation has clearly demonstrated the relationship between supersaturation-nucleation behavior and oral absorbability of drugs in high-energy forms. The maximum absorbable dose limited by solubility increased with an increase in the effective drug concentration in the intestine, which was explained by supersaturation stability and thermodynamic solubility in FaSSIF. Supersaturation stability in FaSSIF is compound-specific and contributes to improved oral bioavailability if the drug is in a high-energy form. Although the set of drugs is limited in the present study, the *in vitro* supersaturation-nucleation evaluation using $\log C(t_{1000})$ value and supersaturation stability will predict the development potentiality of poorly soluble drug candidates efficiently and accurately. Additional studies for a wider range of drugs are in progress and will allow us to much better understand and estimate the complicated absorption behavior of poorly soluble drugs in intestine.

3. Evaluation of Drug Supersaturation by Thermodynamic and Kinetic Approaches for the Prediction of Oral Absorbability in Amorphous Pharmaceuticals

3.1 INTRODUCTION

Accurate understanding of the supersaturation characteristics is essential in order to satisfactorily improve oral drug absorption by using metastable solid forms. The relationship between the supersaturation levels and the improvement in oral bioavailability can be easily derived from Eq. (I) (p. 1). Because the solubility-limited maximum absorbable dose levels are proportional to the intestinal drug concentration, the relative oral bioavailability of a metastable form against a stable crystalline form will be proportional to the degree of drug supersaturation in the intestinal fluid.

In Chapter 2, it has been demonstrated that crystal nucleation is a key factor which kinetically determines the degree of supersaturation and oral absorbability of drugs in metastable solid forms. However, there are several thermodynamic factors which can limit the supersaturation levels. For salts and cocrystals, the theoretical upper limit of their supersaturation ratio is controlled by solubility product values.[5,20,21] The solubility product values of salts and cocrystals are generally very high in aqueous media since electrostatic interaction and hydrogen bonding play an important role in their formation.[5,20,21,34] Therefore, it is reasonable to expect that the thermodynamic factor would not be the limiting factor and nucleation of stable forms predominantly controls the degree of supersaturation for salts and cocrystals.

On the other hand, theoretical upper limit of supersaturation for amorphous solids is determined by the thermodynamic potential difference between crystalline and amorphous forms.[26,27,79,83] When the thermodynamic limit of supersaturation of an amorphous drug is lower than the supersaturation ratio at which crystal nucleation should occur,

supersaturation ratio of the drug will be thermodynamically controlled. However, actual impact of the thermodynamic factor on the supersaturation profile has not been revealed. Consideration of the thermodynamic aspects, in addition to that of crystal nucleation kinetics, will allow us to predict the supersaturation characteristics and oral absorbability of amorphous solids more precisely.

In the present work, amorphous solids of five model drugs, danazol, griseofulvin, itraconazole, vemurafenib and ER-34122, were prepared and their *in vitro* dissolution-supersaturation profiles in a biorelevant medium were investigated. The degree of *in vivo* drug supersaturation was estimated from oral absorption data in clinical and preclinical studies.[22,78,80,84–88] Theoretical limit of supersaturation for each drug was calculated by the thermodynamic analysis of its amorphous and crystalline solid. The supersaturation stability was also evaluated according to the method described in Chapter 2. Relationships between *in vitro*/*in vivo* supersaturation and the obtained thermodynamic/kinetic characteristics of model drugs are discussed in order to clarify the mechanism that controls the *in vivo* absorption of amorphous pharmaceuticals.

3.2 MATERIALS AND METHODS

3.2.1 Chemicals

Vemurafenib and ER-34122 were synthesized in Eisai Tsukuba Research Laboratories (Ibaraki, Japan). Danazol and griseofulvin were purchased from Sigma-Aldrich Co. (St. Louis, Missouri, US). Itraconazole and sodium taurocholate were purchased from Wako Pure Chemical Industries, Ltd. (Osaka, Japan). Lecithin (Coatsome-50) was purchased from Nippon Oil and Fat Co., Ltd. (Tokyo, Japan). All other reagents were of reagent grade and were used without further purification. The water used was filtered through a Milli-Q Water Purification System (Millipore, Bedford, Massachusetts, US) prior to use. Physicochemical properties of the five model drugs are listed in Table 3.1.

Table 3.1. Molecular Properties of Model Drugs

	Structure	clog P[a]	MW	pK_a	Solubility[d] (± SD) μg mL^{-1}
Danazol	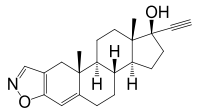	3.93	337.5	n/a (neutral)	5.7 ± 0.1
Griseofulvin	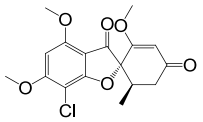	2.05	352.8	n/a (neutral)	12.6 ± 0.3
Itraconazole	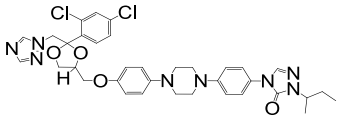	5.99	705.6	3.7 (basic)[b]	0.3 ± 0.0
Vemurafenib	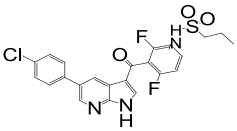	4.20	489.9	1.6 (basic)[c] 6.3 (acidic)[c]	4.4 ± 0.3
ER-34122	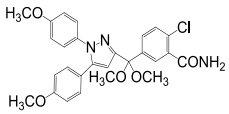	3.93	508.0	0.2 (basic)[c]	0.5 ± 0.0

[a] Calculated using CLOGP 5.1 in Daylight 4.94 (Daylight Chemical Information Systems Inc., Laguna Niguel, California, US).

[b] From the Sporanox® (Janssen Pharmaceuticals Inc., Titusville, New Jersey, US) drug label.

[c] Calculated using ACD/Physchem History 12.01 (Advanced Chemistry Development Inc., Toronto, Ontario, Canada).

[d] Thermodynamic solubility of crystalline materials in FaSSIF at 25 °C (see section 3.2.3).

3.2.2 Preparation of amorphous materials

Amorphous materials of the model drugs were prepared by a melt-quench method. A crystalline sample was heated on a platinum vessel at the temperature of melting. It was kept at the temperature until completion of melting was visually observed. The vessel was immediately placed on water to rapidly cool the molten material. Then, the obtained solid was ground using a mortar and pestle. The resulting samples were confirmed to be

amorphous by the absence of a distinct diffraction pattern characteristic of crystalline material in powder X-ray diffractometry (PXRD, model RINT-TTRIII, Rigaku Co., Tokyo, Japan), and the presence of a glass transition temperature (T_g) in temperature-modulated differential scanning calorimetry (MDSC, model Q2000, TA Instruments Inc., New Castle, Delaware, US). Amorphous samples were stored at –20 °C until use.

3.2.3 Dissolution test for amorphous drugs

The dissolution-supersaturation profiles of amorphous drugs were obtained by non-sink dissolution tests in fasted state simulated intestinal fluid (FaSSIF: 28.4 mM phosphate buffer (pH 6.5) containing 103.3 mM KCl, 3 mM sodium taurocholate and 0.75 mM lecithin) using a miniscale dissolution apparatus (model 708-DS, Agilent Technologies Inc., Santa Clara, California, US). An excess amount of the amorphous sample (ca. 20 mg) was added to 50 mL of FaSSIF at 25 °C. The test medium was stirred by a Teflon-coated minipaddle at 150 rpm to improve powder dispersion. Samples were withdrawn at determined times and filtered through 0.45 μm filters. The filtrate was immediately diluted twice by acetonitrile. The concentration of each drug was measured by HPLC analysis as shown in section 2.2.3. Dissolution tests were performed for 4 h, which was equivalent to the intestinal transit time in human.[6] The remaining solids were isolated by filtration and were analyzed by PXRD in order to investigate their crystallinity. The isolation and analysis of the sample were performed immediately after the dissolution experiments to avoid crystallization during sample manipulation. The thermodynamic solubility of crystalline drugs in FaSSIF at 25 °C was determined using a shake flask method. All experiments were performed in triplicate.

3.2.4 MDSC measurement

Thermodynamic properties including enthalpy of fusion, melting temperature, glass

transition temperature and differences in heat capacity between crystalline and amorphous materials were determined by MDSC.[26,79] For measurement of enthalpy of fusion, crystalline samples were heated at 1 °C min^{-1}. The heat capacity of crystalline and amorphous samples were measured by heating samples from −10 °C to melting point of the crystal at a heating rate of 5 °C min^{-1} with an oscillation period of 40 s and amplitude of ± 0.5 °C. All experiments were performed in triplicate and mean values of these were used for further investigation.

3.2.5 Measurement of water sorption isotherms

The water sorption isotherms of amorphous samples were determined at 25 °C using an automated dynamic vapor sorption (DVS) analyzer (model SGA-100, VTI, Hialeah, Florida, US). A suitable amount (~10 mg) of amorphous sample was placed in a sample cup installed in the DVS analyzer and was dried for 3 h under dry N_2 purged condition before analysis. The water sorption isotherm was measured by increasing relative humidity (RH) from 5% to 95% in steps of 5%. The weight stability criterion employed for the equilibrium was that the weight change was less than 0.01% in 5 min. Water sorption isotherms were generated on three separately weighed samples for each drug. At the end of the experiment, PXRD analysis was conducted for each sample tested in DVS to confirm that it still remained amorphous form. Calculation of theoretical supersaturation from thermodynamic properties

3.2.6 Calculation of theoretical supersaturation from thermodynamic properties

The theoretical limit of supersaturation ($R_{s,\ Therm}$), which is the ratio of thermodynamic solubility of an amorphous solid to that of its crystalline solid, is calculated based on their thermodynamic properties obtained by MDSC and DVS analysis.[26,79,83] The relationship between the change in Gibbs energy on transition from crystalline to amorphous states at a

given temperature ($\Delta G°_{ca}$) and $R_{s,\,Therm}$ is described as Eq. (3.1):

$$\Delta G^{\circ}_{ca} = RT \ln\left(\frac{a_c}{a_a} R_{s,\,Therm}\right) \quad (3.1)$$

where R is the gas constant, T is the temperature, a_c and a_a are the activities of a solute in crystalline and amorphous phases surrounded by an aqueous medium, respectively. The effect of micellar solubilization in FaSSIF is cancelled out based on the assumption that the bile partition coefficient is independent of drug concentrations.[71] $\Delta G°_{ca}$ is composed of enthalpy and entropy terms as shown in Eq. (3.2):

$$\Delta G^{\circ}_{ca} = \Delta H^{\circ}_{ca} - T\Delta S^{\circ}_{ca} \quad (3.2)$$

where $\Delta H°_{ca}$ and $\Delta S°_{ca}$ are the irreversible change in enthalpy and entropy on the transition from crystalline to amorphous states at T. $\Delta H°_{ca}$ and $\Delta S°_{ca}$ can be obtained as Eqs. (3.3) and (3.4) by considering reversible processes: heating a crystalline material from T to melting temperature (T_m), melting the crystal at T_m, cooling supercooled liquid from T_m to T_g, and cooling a glass material from T_g to T,[79,83]

$$\Delta H^{\circ}_{ca} = \Delta H_f - \Delta C_p^{c,l}(T_m - T_g) - \Delta C_p^{c,g}(T_g - T) \quad (3.3)$$

$$\Delta S^{\circ}_{ca} = \frac{\Delta H_f}{T_m} - \Delta C_p^{c,l} \ln\left(\frac{T_m}{T_g}\right) - \Delta C_p^{c,g} \ln\left(\frac{T_g}{T}\right) \quad (3.4)$$

where ΔH_f is the enthalpy of fusion, and $\Delta C_p{}^{c,l}$ and $\Delta C_p{}^{c,g}$ are the difference in heat capacity between a crystal and a supercooled liquid and that between a crystal and a glass material,

respectively. Both $\Delta C_p^{c,l}$ and $\Delta C_p^{c,g}$ are usually regarded as temperature-independent constants.[26,27]

The a_c value is regarded as unity because the activity of pure substance in the solid state is defined as 1. On the other hand, a_a is usually less than 1 because a number of water molecules adsorb to the amorphous solid and form a water-drug mixture in aqueous media.[26] The value of a_a can be obtained from a water sorption isotherm by applying the Gibbs-Duhem equation to the water-adsorbed amorphous solid.[89] Because the chemical potential of water in the solid phase is equal to that in the vapor phase at equilibrium, Eq. (3.5) can be obtained by integrating the Gibbs-Duhem equation:

$$\ln a_a = -\int_0^{P_w} \left(\frac{X_w}{X_a}\right)\frac{1}{P_w}\mathrm{d}P_w = -\int_0^{P_w} \left(\frac{n_w}{n_a}\right)\frac{1}{P_w}\mathrm{d}P_w \qquad (3.5)$$

where P_w is the partial vapor pressure of water, and X_w and X_a are the molar fraction of water and a drug in the water-amorphous solid mixture, respectively. X_w/X_a is equal to the ratio of moles of water (n_w) to moles of the drug (n_a), which is obtained from the water sorption isotherms. Because a_w is defined as a ratio of P_w to the vapor pressure of pure water (P^0_w) and is equal to RH, the relationship between a_a and a_w is expressed as:

$$\ln a_a = -\int_0^{a_w} \left(\frac{n_w}{n_a}\right)\frac{1}{a_w}\mathrm{d}a_w = -\left[\left(\frac{n_w}{n_a}\right)_{a_a=0.05} + \int_{0.05}^{a_w}\left(\frac{n_w}{n_a}\right)\frac{1}{a_w}\mathrm{d}a_w\right] \qquad (3.6)$$

where $(n_w/n_a)_{aw=0.05}$ is the n_w/n_a value at $a_w = 0.05$ (= 5% RH). In Eq. (3.6), the RH region no more than 5% is presumed to be the Henry's law region, where a_w is proportional to n_w/n_a, for the numerical calculation. The integral in the a_w region from 0.05 to 0.95 can be calculated from the area under the $n_w/n_a/a_w$ versus a_w curve by the trapezoidal rule. The value of a_a in the aqueous medium, where a_w is close to unity, is evaluated by plotting a_a

versus a_w and extrapolating to $a_w = 1$. The $R_{s,Therm}$ values at $T = 298$ K were calculated for each model drug by using Eqs. (3.1–3.4) and (3.6).

3.2.7 Kinetic analysis of crystal nucleation in FaSSIF

Supersaturation stability of model drugs was evaluated by measuring the induction time for nucleation (t_{ind}), which is defined as the time lag for the observable crystals to appear, as reported in Chapter 2. t_{ind} was measured by using solvent shift and UV detection techniques.[73,74] Experimentally, supersaturated solution was prepared by adding an aliquot of dimethyl sulfoxide (DMSO) stock solution of drugs to 2 mL of FaSSIF. The supersaturated solution was stirred in a quartz cuvette (10 mm × 10 mm × 45 mm) using a controller (CS-1, As One Co. Osaka, Japan) at 300 rpm. The solution UV absorptions were monitored by using a UV-Vis spectrophotometer (UV2400PC, Shimadzu Co., Kyoto, Japan) at 320 nm (danazol), 350 nm (griseofulvin), 275 nm (itraconazole), 340 nm (vemurafenib) and 295 nm (ER-34122) until a sharp change in the absorption-time curve due to the crystal nucleation was observed. A different wavelength for each drug was used in order to monitor the drug concentration and confirm the reproducibility in preparing supersaturated solution. The measurement of t_{ind} was performed in triplicate.

3.3 RESULTS

3.3.1 In vitro drug supersaturation during dissolution test

Figure 3.1 shows the concentration versus time profiles of the amorphous model drugs in the dissolution test using FaSSIF. The degree of supersaturation at each time point was calculated by dividing the drug concentration by the thermodynamic solubility of a crystalline form. The highest drug concentration was about 60 μg mL^{-1}, which was observed for vemurafenib and corresponded to ca. 15% of complete dissolution. Therefore, non-sink conditions were maintained for the five model drugs throughout the dissolution test. Each drug in amorphous forms quickly reached supersaturated concentrations which were higher than the thermodynamic solubility of their crystalline forms. A decrease in the concentration was observed at 20–40 min for danazol and griseofulvin, and at 120–180 min for itraconazole and ER-34122. No significant decrease in the concentration was observed for vemurafenib up to 240 min.

The PXRD patterns of resultant solids (Figure 3.2) demonstrated that crystallization occurred significantly in danazol and griseofulvin, and at least partially in itraconazole and ER-34122. It was reasonable to assume that the crystallization predominantly occurred during dissolution because immediate isolation and PXRD analysis of the samples would minimize the solid-state transformation during sample manipulation.

The degree of supersaturation achieved in the dissolution test was highly dependent on the drug species. The amorphous forms of griseofulvin and danazol showed only 1.5 ~ 3 times higher solubility than their crystalline forms and this result was consistent with the previous report.[27] On the other hand, the supersaturation ratio of ER-34122 (ca. 80-fold) was the highest level ever observed experimentally in aqueous solutions.[26,27,79,83] The apparent rank order of the degree of *in vitro* supersaturation was ER-34122 > vemurafenib ≥ itraconazole > danazol > griseofulvin.

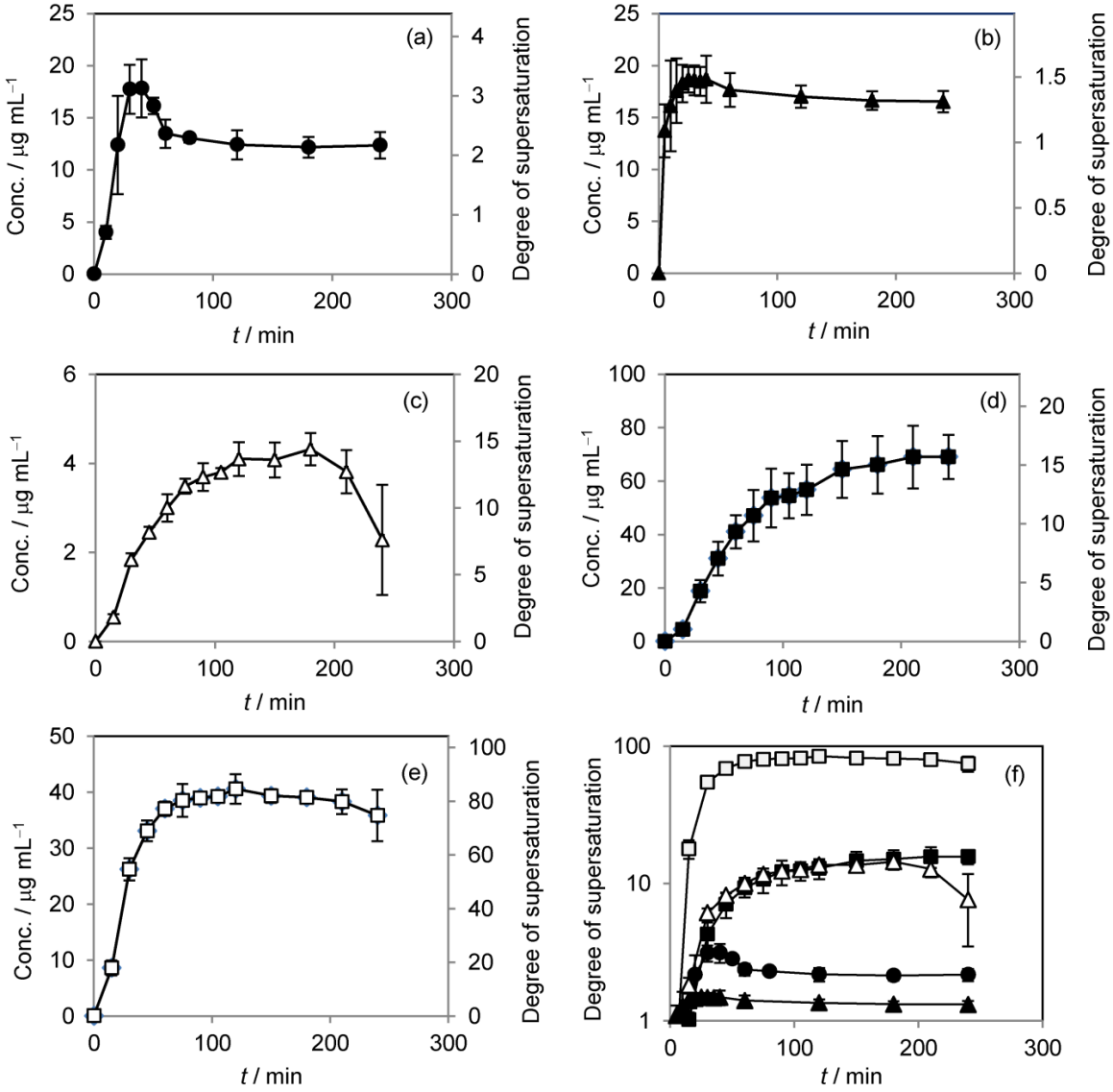

Figure 3.1. Concentration-time profiles of amorphous (a) danazol, (b) griseofulvin, (c) itraconazole, (d) vemurafenib and (e) ER-34122 in the dissolution test (left axis). The right axis shows the degree of supersaturation at each time point. The degree of supersaturation-time profiles for the five model drugs [danazol (●), griseofulvin (▲), itraconazole (Δ), vemurafenib (■) and ER-34122 (□)] are summarized in (f). Each value represents the mean ± SD (n = 3).

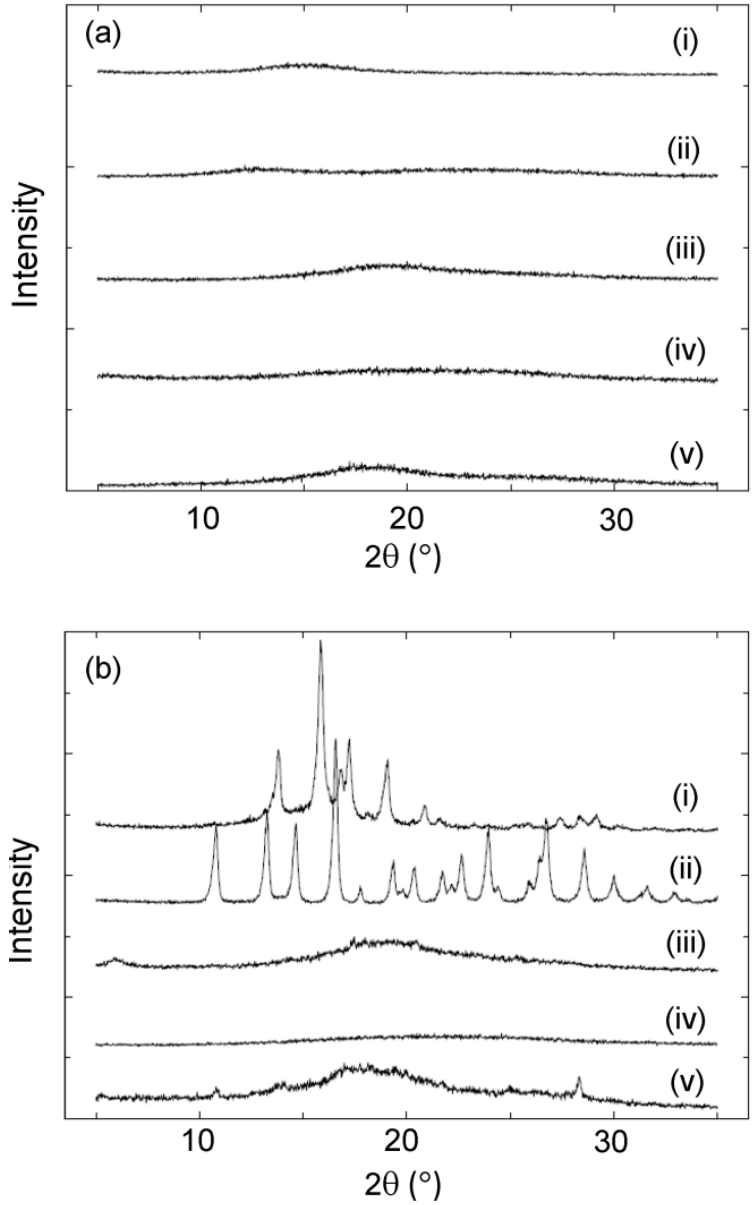

Figure 3.2. Powder X-ray diffraction patterns of danazol (i), griseofulvin (ii), itraconazole (iii), vemurafenib (iv) and ER-34122 (v) before (a) and after (b) their dissolution tests.

3.3.2 Thermodynamic analysis of crystalline and amorphous solids

Figure 3.3 shows the heat capacity versus temperature profiles of crystalline and amorphous danazol measured by MDSC. The heat capacity of the amorphous solid was greater than that of its crystalline solid at any temperature. The marked increase observed in the heat capacity of the amorphous solid reflects the rise in the molecular specific volume at T_g.[79] A small peak observed near T_g is attributable to the enthalpy relaxation of the amorphous solid.

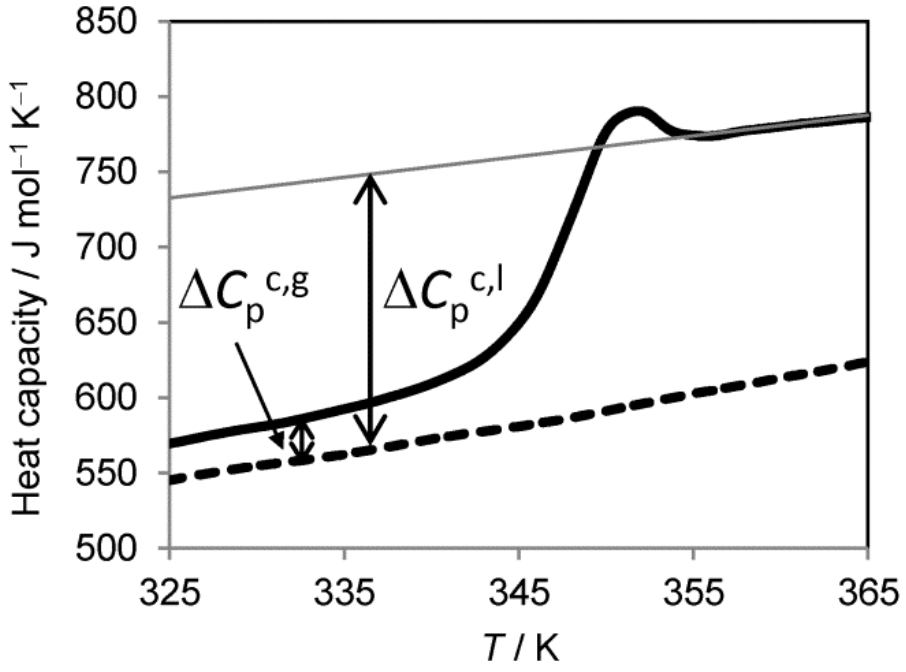

Figure 3.3. Heat capacity of danazol in the crystalline (broken line) and amorphous (solid line) forms.

Although it was difficult to measure absolute heat capacity accurately, the difference in heat capacity between crystalline and amorphous solids was reproducibly evaluated. Similar results were obtained for the other drugs. Thermal properties determined by MDSC represent a wide range of values as listed in Table 3.2. For the five model drugs, T_g (333.9 to 386.5 K) was relatively high and the amorphous solids existed in a glass state at room temperature (298 K).

Figure 3.4(a) shows water sorption isotherms of the model drugs in amorphous forms at 25 °C. No crystallization was observed during the course of experiments (confirmed by PXRD, data not shown). At the maximal RH of 95%, the amount of water uptake ranged from 1.5% to 3%, which was equivalent to ca. 0.3–0.6 moles of water per unit mole of a drug. The a_a values at each a_w (= RH) were calculated using Eq. (3.6) and plotted in Figure 3.4(b). The a_a value at a_w = 1 for the model drugs ranged from 0.570 to 0.769 (Table 3.2). The theoretical limit of supersaturation ($R_{s,\ Therm}$) calculated by using thermodynamic properties was compound-specific (Table 3.2) and ranged from 13.7 to 168.0. The rank order of $R_{s,\ Therm}$ was ER-34122 > itraconazole > griseofulvin >

vemurafenib ≥ danazol. This rank order was predominantly dependent on the thermal properties. Although the consideration of a_a significantly decreased the absolute value of $R_{s,\,Therm}$, it did not impact the rank order of $R_{s,\,Therm}$.

Table 3.2. Thermodynamic Properties of Model Drugs

	ΔH_f	$\Delta C_p^{g\text{-}c}$	$\Delta C_p^{l\text{-}c}$	T_g	T_m	$\Delta G°_{ca}$	a_a	$R_{s,\,Therm}$
	kJ mol^{-1}	J mol^{-1} K^{-1}	J mol^{-1} K^{-1}	K	K	kJ mol^{-1}		
Danazol	34.0	20.3	150.7	350.8	497.7	7.1	0.769	13.7
Griseofulvin	41.4	48.7	187.5	363.4	490.2	8.9	0.709	25.6
Itraconazole	61.3	74.6	323.2	333.9	439.5	11.9	0.618	75.6
Vemurafenib	39.9	15.8	190.9	386.5	531.7	7.8	0.687	15.9
ER-34122	60.7	50.5	248.1	353.9	472.6	14.1	0.570	168.0

ΔH_f, enthalpy of fusion; $\Delta C_p^{g\text{-}c}$, heat capacity difference (glass-crystal); $\Delta C_p^{l\text{-}c}$, heat capacity difference (liquid-crystal); T_g, glass transition temperature; T_m, melting temperature; $\Delta G°_{ca}$, change in Gibbs energy on transition from crystalline to amorphous states at 298 K; a_a, solute activity; $R_{s,\,Therm}$, theoretical limit of supersaturation.

3.3.3 Supersaturation stability of model drugs

Figure 3.5(a) shows typical UV absorbance versus time curves of 25, 30 and 40 μg mL^{-1} danazol in FaSSIF. These solutions were in supersaturated states (the solubility of crystalline danazol: 5.7 μg mL^{-1}, Table 3.1). After a given period of time, a steep increase in absorbance occurred due to the crystal nucleation from the supersaturated solution. The PXRD patterns of precipitated materials were the same as those of the intact crystalline forms (data not shown). The more concentrated the solution was, the sooner nucleation took place. The t_{ind} value was determined by drawing regression lines through the two distinct linear regions and taking the intersection of the two lines. As shown in Figure 3.5(b), the logarithm of t_{ind} was plotted against the logarithm of the degree of supersaturation, S (the

ratio of the initial drug concentration to the solubility of the crystalline form), to the minus second power, according to Eq. (2.2) (p. 34). The measured log t_{ind} of each drug followed a linear relationship with $(\log S)^{-2}$. The t_{ind} value of ER-34122 in the higher S [i.e., lower $(\log S)^{-2}$] region cannot be measured because the supersaturated solution was not available by the solvent-shift method. Since the compounds plotted in the left side in Figure 3.5(b) nucleate only under the highly supersaturated conditions, we can say that they have high supersaturation stability. The approximate rank order of supersaturation stability was ER-34122 > vemurafenib ≥ itraconazole > danazol ≥ griseofulvin.

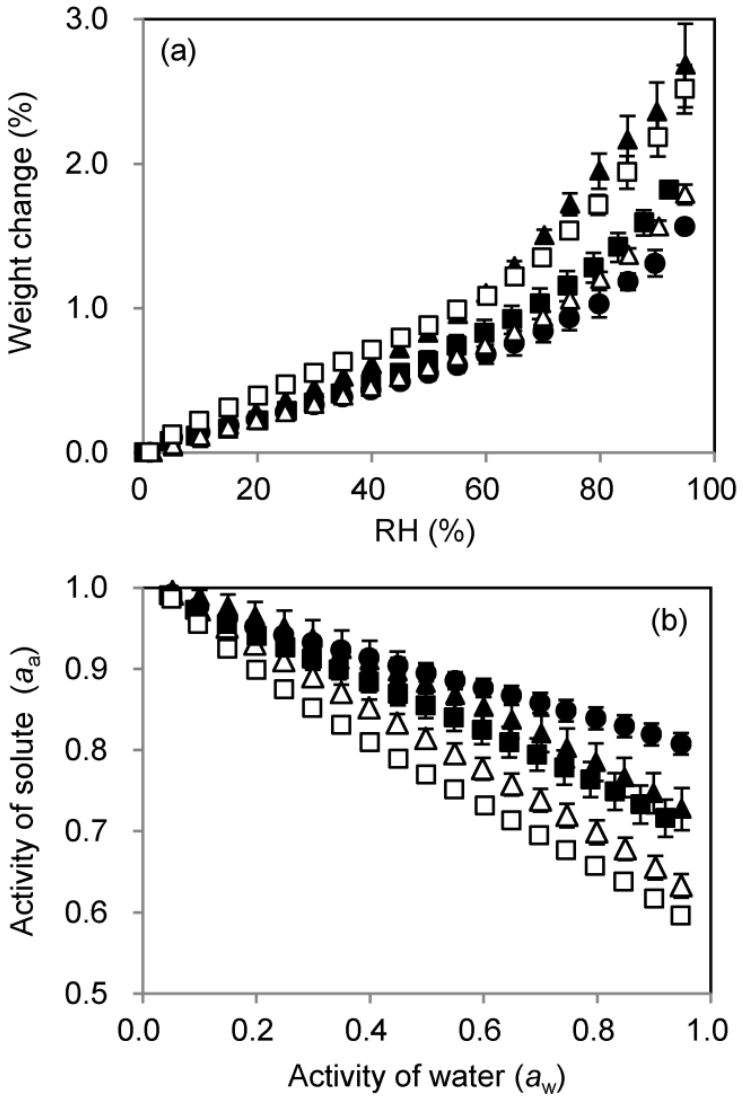

Figure 3.4. (a) Water absorption isotherms and (b) plots of solute activity in amorphous solids for danazol (●), griseofulvin (▲), itraconazole (Δ), vemurafenib (■) and ER-34122 (□).

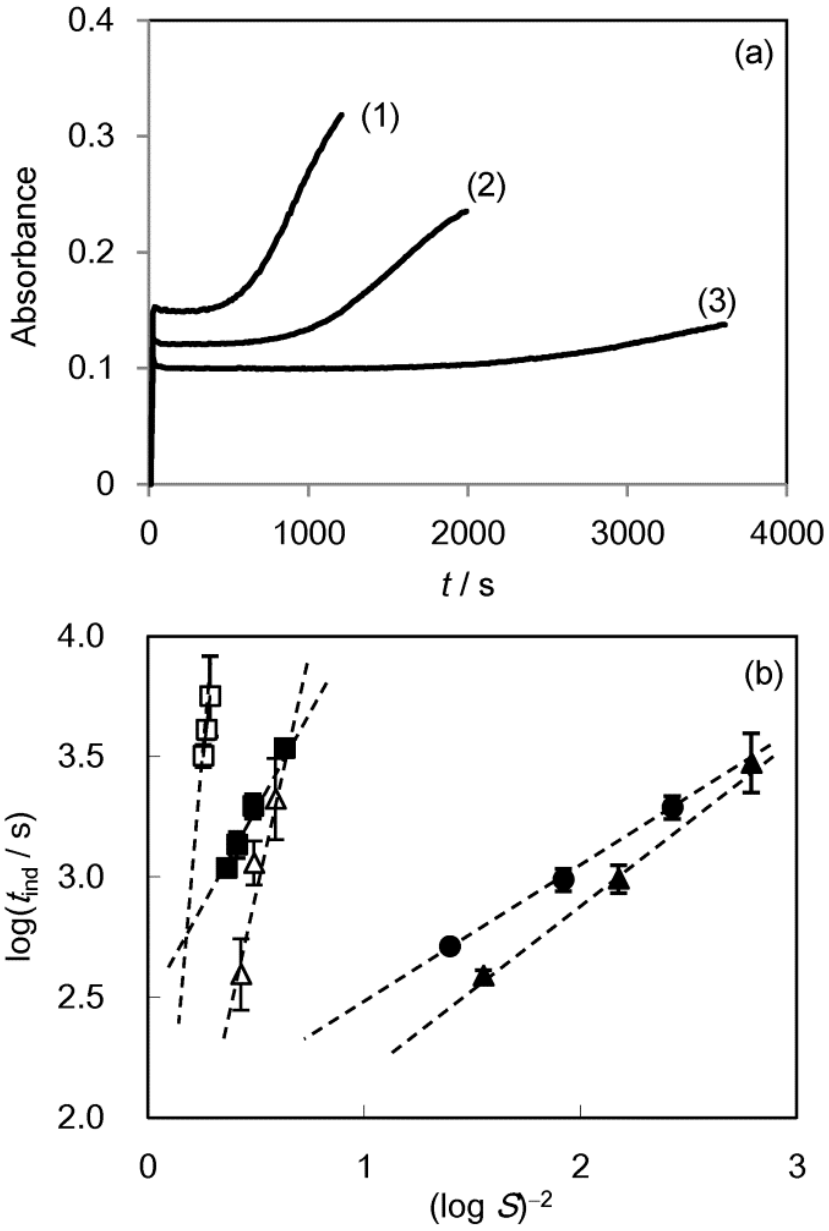

Figure 3.5. (a) Time-absorbance curves of supersaturated solution in the presence of (1) 40, (2) 30, and (3) 25 μg mL^{-1} of danazol and (b) plots of log t_{ind} versus $(\log S)^{-2}$ for danazol (●), griseofulvin (▲), itraconazole (Δ), vemurafenib (■) and ER-34122 (□). Each value represents the mean ± SD (n = 3). The broken lines are the regression lines.

3.4 DISCUSSION

3.4.1 Relationship between *in vitro* and *in vivo* supersaturation

The amorphous solids of the five model drugs produced compound-specific supersaturation during dissolution in FaSSIF (Figure 3.1). Oral absorption of their crystalline forms is limited by poor thermodynamic solubility, but is significantly improved by amorphization.[22,78,80,84–88] This means that the *in vivo* supersaturation of their amorphous forms impacts the oral absorption. In order to clarify the relationship between *in vitro* and *in vivo* drug supersaturation, relative bioavailability (relative BA) of amorphous formulations against crystalline formulations was investigated in literatures and drug labels for danazol, griseofulvin, itraconazole, vemurafenib and ER-34122.[22,78,80,84,86] The relative BA is equal to the degree of enhancement in fraction absorbed (F_a) when we assume that oral clearance is constant between formulations. According to the theory of physiologically-based drug absorption models,[5,24] F_a under the solubility-limited condition will be proportional to the drug concentration in the intestinal fluid. Therefore, the relative BA between amorphous and crystalline formulations should be consistent with the mean supersaturation ratio in the intestinal fluid.

The relative BA of itraconazole was estimated from the clinical data of an amorphous formulation and the imaginary drug exposure of a crystalline formulation which was calculated by using a simple absorption model, as described in section 2.4.2. In addition, relative BA in patients with elevated gastric pH was calculated in order to investigate the situation where both dissolution and precipitation of itraconazole occur predominantly in the intestine. The dissolution in the stomach of vemurafenib (Table 2.2) and ER-34122,[22] which also contain basic groups, is negligible due to their poor solubility in the absence of bile acids. For danazol and ER-34122, relative BA was evaluated for mice and dogs, respectively, as human data was not available. In spite of interspecies differences in the gastrointestinal physiology,[4,90,91] relative BA is often comparable between humans and preclinical animals. For example, similar relative BA has been observed between rats

(200%),[85] dogs (200%–270%)[87] and humans (230%)[86] for griseofulvin, and between rats (840%–2200%, a formulation containing hydroxypropyl methylcellulose acetate succinate is excluded from the analysis due to its poor disintegration property)[88] and humans (1300%, Table 2.6) for itraconazole, respectively. Therefore, it is reasonably expected that the relative BA of danazol and ER-34122 in preclinical animals is close to that in humans.

The calculated relative BA for the model drugs is listed in Table 3.3, where a good *in vitro-in vivo* correlation (IVIVC) is apparently observed. The rank order of relative BA was consistent with that of the degree of supersaturation observed in the dissolution test of amorphous solids (ER-34122 > vemurafenib ≥ itraconazole > danazol ≥ griseofulvin). This kind of IVIVC has been reported for some drugs in supersaturable forms such as salts and amorphous forms.[24,29,88] Furthermore, the relative BA value of each drug was close to the maximum degree of supersaturation achieved in the dissolution test, $R_{s,\,Diss}$ (Table 3.3). It might be more appropriate to consider a mean supersaturation ratio during dissolution, not the maximum value, when IVIVC is discussed for the extent of drug absorption. In further discussion, however, $R_{s,\,Diss}$ is used as a representative value of *in vitro* supersaturation level for simplicity because it was close to the average supersaturation value throughout the dissolution. A good agreement between $R_{s,\,Diss}$ and relative BA suggests that the obtained *in vitro* supersaturation levels of each model drug provide rough approximation of those *in vivo*. Therefore, it is reasonable to assume that the determinant factor for supersaturation behavior is common between them.

3.4.2 Difference between experimental and theoretical supersaturation

As shown in Table 3.3, $R_{s,\,Diss}$ was compared with the theoretical limit of supersaturation ($R_{s,\,Therm}$) predicted by the thermodynamic analysis. A good agreement between $R_{s,\,Diss}$ and $R_{s,\,Therm}$ for vemurafenib indicates that its supersaturation is thermodynamically controlled. On the other hand, $R_{s,\,Diss}$ values were significantly smaller than $R_{s,\,Therm}$ for the other drugs. We observed a 2- to 17-fold difference between $R_{s,\,Diss}$ and $R_{s,\,Therm}$, and the difference was

the largest for griseofulvin, which showed the smallest supersaturation during the dissolution (Table 3.3). Although the consideration of solute activity in the amorphous phase (a_a) improved the theoretical prediction as previously reported,[26] the significant discrepancy still remained.

Table 3.3. *In vitro* and *In vivo* Supersaturation Characteristics for Model Drugs

	Relative BA /100%	$R_{s,\,Diss}$	$R_{s,\,Therm}$	log $S(t_{1000})$
Danazol	2.3–3.7	3.1	13.7	0.72
Griseofulvin	2.3	1.5	25.6	0.69
Itraconazole	13	14	75.6	1.41
Vemurafenib	14	16	15.9	1.72
ER-34122	100	85	168.0	2.28

$R_{s,\,Diss}$, supersaturation ratio observed in dissolution tests; $R_{s,\,Therm}$, theoretical limit of supersaturation; log $S(t_{1000})$, index of supersaturation stability.

The disagreement between $R_{s,\,Diss}$ and $R_{s,\,Therm}$ may be partly attributable to several approximations in the thermodynamic analysis. For instance, the system is treated as an equilibrium state in the calculation of the change in Gibbs energy on transition from crystalline to amorphous states ($\Delta G°_{ca}$). In fact, an amorphous state is not an equilibrium state and its thermodynamic properties slowly change with time. Aging (annealing) of the amorphous phase, which is indicated by the enthalpy relaxation in MDSC, may have a negative effect on solubility. In addition, water sorption may cause a subtle structural change in the amorphous phase, which may stabilize the amorphous phase and is not considered in Eq. (3.6). However, the impact of these approximations on the thermodynamic analysis would be relatively small[26] and will not explain the compound-dependent deviation between $R_{s,\,Therm}$ and $R_{s,\,Diss}$. Therefore, it is reasonable to assume that the thermodynamic properties of solid phases are not the limiting factor of $R_{s,\,Diss}$, except for

vemurafenib.

The concentration-time profiles of danazol, griseofulvin, itraconazole and ER-34122 (Figure 3.1) indicate that their supersaturation is hampered by precipitation before reaching the theoretical limit. The precipitation is clearly attributable to the generation of a crystal phase (Figure 3.2). The crystal nucleation is a critical step of crystallization.[5,28] Once nucleation is initiated, the particle growth of the nuclei leads to a decrease in drug concentration. It has been reported that the generation of crystalline forms often frustrates the attempt to produce the supersaturation levels theoretically attainable by the amorphous form.[26–28,79,83] Thus, in many cases, the kinetics of crystal nucleation, rather than the thermodynamic properties of an amorphous solid, would be a predominant factor determining supersaturation behavior.

3.4.3 Mechanisms determining supersaturation behavior of amorphous drugs

In Chapter 2, it has been demonstrated that supersaturation stability is a useful kinetic parameter to describe the supersaturation-nucleation characteristics in the intestinal fluid. It is derived from the classical theory on nucleation kinetics and is easily evaluated by measuring induction time for crystal nucleation. High supersaturation stability means the ability to maintain a high degree of supersaturation without nucleation, which corresponds to the magnitude of the kinetic barrier to form nuclei. It has been shown that this parameter contributes to improved solubility and oral bioavailability of several drugs in supersaturable forms.

As expected, the apparent rank order of supersaturation stability, which is obtained from the relationship between t_{ind} and $(\log S)^{-2}$ in Figure 3.5(b), is consistent with that of $R_{s,\,Diss}$ (ER-34122 > itraconazole > danazol ≥ griseofulvin). We designated "$\log S(t_{1000})$," the logarithm of the S value at t_{ind} = 1000 s, as an index of supersaturation stability (Table 3.3). It has been suggested that this analysis time, t_{ind} = 1000 s, is appropriate to describe drug supersaturation behavior *in vivo*. A high $\log S(t_{1000})$ value corresponds to high

supersaturation stability. The $\log S(t_{1000})$ values for each drug were calculated by linear regression analysis in Figure 3.5(b) and were plotted against the logarithm of $R_{s,\,Diss}$ value as shown in Figure 3.6. The positive linear relationship demonstrates that the supersaturation stability is the determinant factor of the supersaturation behavior of amorphous danazol, griseofulvin, itraconazole and ER-34122 , and the $\log S(t_{1000})$ value is a good predictor variable of $R_{s,\,Diss}$ when it is controlled by nucleation kinetics. A slope close to unity means that $S(t_{1000})$ is proportional to the critical supersaturation ratio for crystal nucleation, which would be close to $R_{s,\,Diss.}$ Figure 3.1 and Figure 3.2 satisfactorily explain the relationship between the $\log S(t_{1000})$ value, $R_{s,\,Diss}$ and PXRD patterns after the dissolution test. The crystallization of danazol and griseofulvin, which have low $\log S(t_{1000})$ values, occurred quickly after the dissolution, and thus intense peaks appeared in their PXRD diffractograms. On the other hand, it took longer time for itraconazole and ER-34122 to reach the critical supersaturation ratio and the precipitation was initiated in a later stage of the dissolution test (120–180 min) due to their relatively high $\log S(t_{1000})$ values. As a result, their crystallization hardly proceeded as shown in Figure 3.2(b).

Vemurafenib was also plotted in Figure 3.6 although its supersaturation was thermodynamically controlled. The regression line drawn by the other four drugs can be considered as the imaginary limit of supersaturation controlled by nucleation for vemurafenib. The plot of vemurafenib which is located below the line means that the supersaturation stability of vemurafenib is high enough to allow its supersaturation ratio to reach the level of $R_{s,\,Therm}$ without nucleation. In other words, the relatively low $R_{s,\,Therm}$ level would prevent the drug concentration from reaching the critical supersaturation limited by nucleation. The relationships between $R_{s,\,Diss}$, $R_{s,\,Therm}$ and crystal nucleation in the supersaturation profiles of amorphous solids are shown in Figure 3.7. In the present study, supersaturation stability (= nucleation kinetics) controlled the degree of supersaturation [Figure 3.7(a)] for four out of the five model drugs and only one drug showed thermodynamically limited supersaturation [Figure 3.7(b)]. Therefore, the extent of

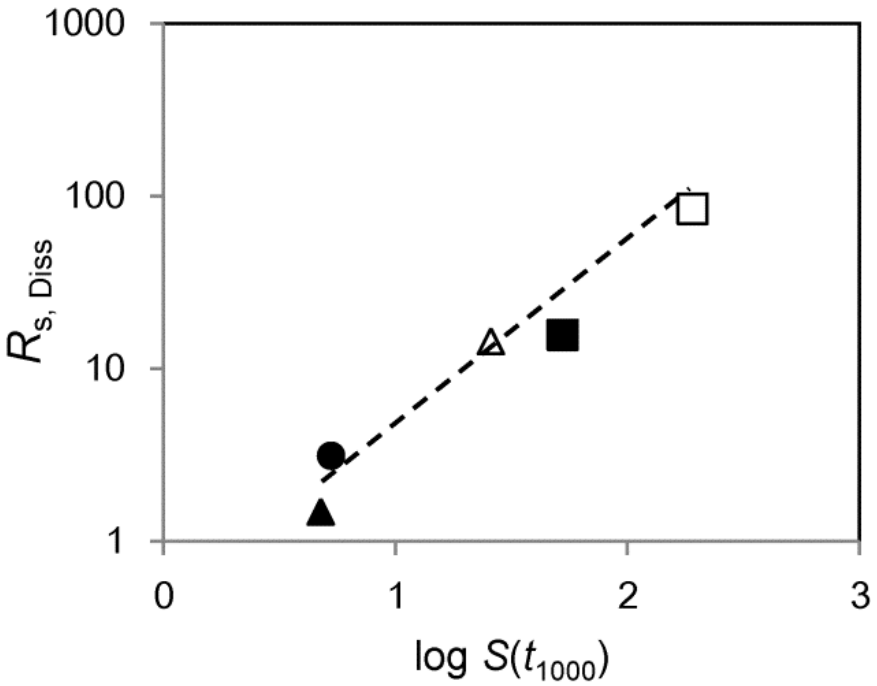

Figure 3.6. Plots of log $R_{s,\ Diss}$ versus log $S(t_{1000})$ for danazol (●), griseofulvin (▲), itraconazole (Δ) vemurafenib (■) and ER-34122 (□). The broken line represents the regression line. Vemurafenib is excluded from the regression analysis because its supersaturation is thermodynamically controlled.

supersaturation of amorphous drugs tends to be overestimated when the thermodynamic analysis is solely used for prediction. More accurate prediction will be available by concomitantly considering the kinetic limit of supersaturation, because the limit of supersaturation will be determined by the lower between the thermodynamic and kinetic limits. The extremely high supersaturation level of ER-34122 is attributable to both preferable thermodynamic properties of amorphous solid and high supersaturation stability. A better understanding of the supersaturation mechanism will lead to a precise estimation for limitations and possibilities of amorphous formulations in oral absorbability. Concomitant use of thermodynamic and kinetic approaches will allow us to make a science-based decision in the formulation development.

Finally, the results from the present study also suggest the mechanism of transformation from amorphous to crystalline states during *in vitro* and *in vivo* dissolution.

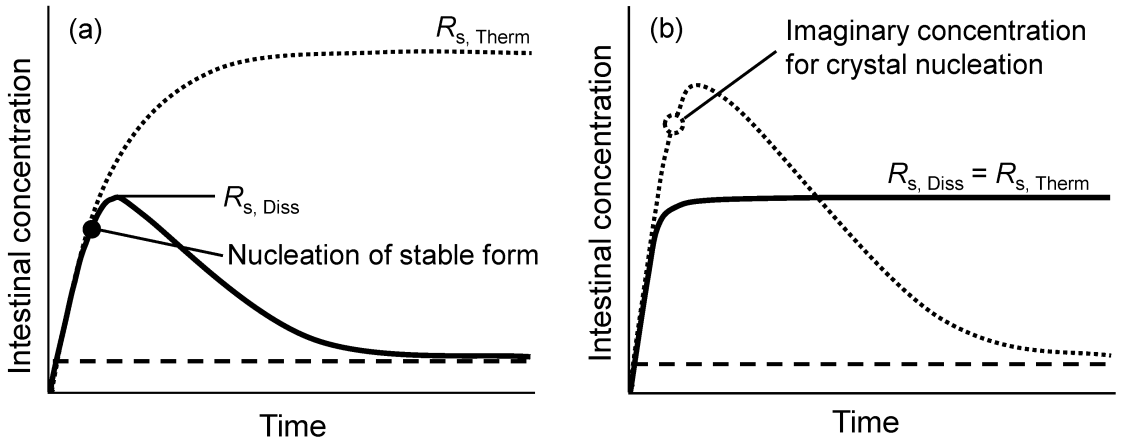

Figure 3.7. Schematic diagrams of (a) kinetically-controlled and (b) thermodynamically-controlled supersaturation of amorphous solids. Solid and dotted lines are actual and imaginary supersaturation profiles, respectively. Broken lines show the thermodynamic solubility of stable forms.

Although a crystal layer is likely to form on the amorphous surface, it is generally difficult to distinguish the solid-state transformation from the solution-mediated transformation that occurs near the surface of amorphous solids.[27,92] In some previous studies, solid state parameters such as a fragility index [$\gamma_{Cp} = (\Delta C_p^{c,l} - \Delta C_p^{c,g})/\Delta C_p^{c,l}$] and the difference between crystallization temperature and T_g in MDSC analysis have been used to predict the tendency of amorphous forms to crystallize during dissolution.[27,79] However, both of them have failed to provide quantitative explanation, probably because these parameters are related to the solid-state transformation mechanism. On the other hand, a good correlation between log $S(t_{1000})$ and $R_{s, Diss}$ indicates that the crystallization during dissolution probably proceeds through the solution-mediated transformation, since the evaluation of supersaturation stability is based on the theory of the homogenous nucleation mechanism in supersaturated solutions.[73–75] Crystal nuclei might be frequently generated near the surface of amorphous solids, where drug concentration is heterogeneously higher than that in the bulk medium.

3.5 CONCLUSION

Thermodynamic and kinetic approaches have clearly elucidated the mechanism controlling supersaturation behavior of drugs in amorphous form. For five amorphous drugs, the degree of supersaturation during *in vitro* dissolution was consistent with that *in vivo*, which was obtained from clinical and preclinical absorption data. The degree of supersaturation for vemurafenib was thermodynamically limited and was predictable from MDSC and DVS analysis of the amorphous and the crystalline solids. On the other hand, that of danazol, griseofulvin, itraconazole and ER-34122 was controlled by supersaturation stability, which was obtained by the kinetic analysis of crystal nucleation. A good correlation between the degree of *in vitro*/*in vivo* supersaturation and the supersaturation stability also suggests that crystallization of amorphous solids proceeds through the solution-mediated transformation mechanism. Concomitant use of the thermodynamic analysis and the evaluation of supersaturation stability will allow us to evaluate possibilities and limitations in supersaturation of amorphous pharmaceuticals. A better understanding of the supersaturation characteristics will lead to accurate estimation of potential oral absorbability and development possibility for poorly water-soluble drugs.

4. Inhibition of Crystal Nucleation and Growth by Water-Soluble Polymers and its Impact on the Supersaturation Profiles of Amorphous Drugs

4.1 INTRODUCTION

An amorphous form is a versatile high-energy form for poorly soluble non-ionizable drugs. Oral absorbability of an amorphous form is determined by the degree of supersaturation achieved in the intestinal fluid. The supersaturation levels are dependent on drug species and controlled by thermodynamic properties of an amorphous solid or nucleation kinetics of a stable form, as shown in Chapter 3. It is difficult to further enhance the supersaturation ratio when it is thermodynamically limited. On the other hand, the degree of supersaturation and oral absorbability of a drug in an amorphous form can be improved by inhibiting crystallization when its supersaturation behavior is kinetically controlled. For this purpose, several kinds of excipients including cyclodextrins, surfactants and water-soluble polymers are often used as crystallization inhibitors.

Cyclodextrins and surfactants cause a decrease in the degree of supersaturation, which is the driving force for crystallization, through complexation and micellar solubilization, and inhibit crystallization thermodynamically.[23] On the other hand, water-soluble polymers such as cellulose-based polymers and polyvinylpyrrolidones generally have little impact on apparent drug solubility.[22,23,28] This means that they kinetically inhibit the generation of crystalline forms. Crystallization of stable forms occurs in two steps: crystal nucleation and crystal growth. In several recent studies, the effect of polymers on each step was individually investigated for several drugs and polymers.[94,95] It has been demonstrated that some polymers inhibit crystal nucleation and/or growth of stable forms. However, the relationship between the crystallization inhibitory efficiency of polymers and the supersaturation behavior of drugs in amorphous forms has not been clarified

satisfactorily. A better understanding of the role of polymers will allow us to precisely predict the effect of polymers on drug supersaturation and thus make an informed decision on the selection of excipients during formulation development.

In this chapter, the ability of representative water-soluble polymers (hydroxypropyl methylcellulose, polyvinylpyrrolidone and Eudragit L-100) to inhibit the crystallization of two model drugs, danazol and griseofulvin, from supersaturated solutions was investigated. The supersaturation profiles of amorphous danazol and griseofulvin were obtained in biorelevant dissolution tests in the presence and absence of polymers. The impact of polymers on crystal growth kinetics was characterized by measuring the decrease in concentration of supersaturated drug solutions in the presence of seed crystals. a simple and practical method to evaluate crystal nucleation kinetics has been developed in Chapter 2. The inhibitory efficiency against nucleation was characterized using kinetic analysis based on classical nucleation theory. Relationships between the inhibition efficiency of polymers against crystallization and the supersaturation profiles of amorphous solids are discussed to clarify the effect of polymers on supersaturated drug solutions.

4.2 MATERIALS AND METHODS

4.2.1 Chemicals

Danazol, griseofulvin and PVP10 were purchased from Sigma-Aldrich Co. (St. Louis, Missouri, US). Sodium taurocholate was purchased from Wako Pure Chemical Industries, Ltd. (Osaka, Japan). Lecithin (Coatsome-50) was purchased from Nippon Oil and Fat Co., Ltd. (Tokyo, Japan). Hydroxypropyl methylcellulose Tc-5Ew (HPMC) was purchased from Shin-Etsu Chemical Co., Ltd. (Tokyo, Japan). Eudragit L-100 (Eudragit) was purchased from Evonik Röhm GmbH (Darmstadt, Germany). All other reagents were of reagent grade and were used without further purification. The water used was filtered through a Milli-Q Water Purification System (Millipore, Bedford, Massachusetts, US) prior to use.

4.2.2 Dissolution test for amorphous drugs

Amorphous forms of the model drugs were prepared by a melt-quench method as shown in section 3.2.2. The dissolution-supersaturation profiles of amorphous drugs were obtained by non-sink dissolution tests in fasted state simulated intestinal fluid (FaSSIF: 28.4 mM phosphate buffer (pH 6.5) containing 103.3 mM KCl, 3 mM sodium taurocholate and 0.75 mM lecithin) in the absence and presence of 0.1% (w/v) water-soluble polymers (HPMC, PVP10 and Eudragit) using a miniscale dissolution apparatus (model 708-DS, Agilent Technologies Inc., Santa Clara, California, US). An excess amount of the amorphous sample (ca. 20 mg) was added to 50 mL of FaSSIF at 25 °C. The test medium was stirred with a Teflon-coated minipaddle at 150 rpm to improve powder dispersion. Samples were withdrawn at determined times and filtered through 0.45 μm filters. The filtrate was immediately diluted twice with an acetonitrile/water (1/1, v/v) solution. The concentration of each drug was measured by HPLC analysis as described in section 2.2.3. Dissolution tests were performed for 4 h, which is equivalent to the intestinal transit time in human.[6] The remaining solids were isolated by filtration and were analyzed by powder X-ray diffractometry (PXRD, RINT TTR-III, Rigaku, Tokyo, Japan) in order to investigate their crystallinity. Dissolution tests were also performed for amorphous solids containing seed crystals. About 20 mg of amorphous griseofulvin and danazol were mixed with 5% (w/w, ca. 1 mg) of their crystalline solids and were added to FaSSIF containing 0.1% (w/v) HPMC. The other experimental conditions were the same as those for the unseeded experiment. The thermodynamic solubility of crystalline drugs in FaSSIF at 25 °C in the absence and presence of polymers was determined using a shake flask method. In this chapter, the degree of supersaturation is defined as the ratio of the drug concentration in a supersaturated solution to its thermodynamic solubility determined in exactly the same media in order to cancel out the solubilization effect of polymers. The dissolution test and the measurement of thermodynamic solubility were performed in triplicate.

4.2.3 Evaluation of crystal nucleation kinetics

The induction time for crystal nucleation (t_{ind}) was measured to evaluate the inhibitory effect of water-soluble polymers on nucleation kinetics. t_{ind} is defined as the time lag for the observable crystals to appear and was measured using a technique developed in Chapter 2. Experimentally, a supersaturated solution was prepared by adding an aliquot of dimethyl sulfoxide (DMSO) stock solution of drug to 2 mL of FaSSIF in the absence and presence of polymers (HPMC, PVP10 and Eudragit). The supersaturated solution was stirred in a quartz cuvette (10 mm × 10 mm × 45 mm) using a controller (CS-1, As One Co., Osaka, Japan) at 300 rpm. t_{ind} was measured by monitoring the solution UV absorption (UV-Vis spectrophotometer model UV2400PC, Shimadzu Co, Kyoto, Japan) at 320 nm (danazol) and 350 nm (griseofulvin) and detecting the sharp change in the absorption-time curve due to crystal nucleation. The t_{ind} value was determined by drawing regression lines through the two distinct linear regions in the absorption-time curve and taking the intersection of the two lines. The measurement of t_{ind} was performed in triplicate at various degrees of supersaturation.

4.2.4 Measurement of crystal growth rate

The inhibitory effect of polymers on crystal growth rate was characterized by monitoring the decrease in drug concentration of supersaturated solutions in the presence of crystalline solids. Supersaturated solution was prepared in a miniscale dissolution apparatus by adding 250 μL of DMSO stock solution to 50 mL FaSSIF in the absence and presence of 0.1% (w/v) polymers (HPMC, PVP10 and Eudragit) at 25 °C. Stock solutions of various concentrations were prepared to induce a degree of supersaturation equal to ca. 5 (30–33 ug mL^{-1}) for danazol and ca. 4 (50–60 ug mL^{-1}) for griseofulvin, corresponding to the thermodynamic solubility determined in the exact same media. The supersaturated solutions were reproducibly prepared without immediate precipitation. Crystal growth was initiated

by adding 2 mg of crystalline drug to the solution and stirring with a Teflon-coated minipaddle at 150 rpm. The same lots of the crystalline drugs were used as seed crystals under each condition to assure the constant surface area. Samples were withdrawn 2 min prior to the addition of the crystalline drug and at 0, 2, 5, 10, 15, 20, 30 and 60 min after addition of the crystalline drug. Each aliquot was filtered through a 0.45 μm filter and the filtrate was immediately diluted two-fold with acetonitrile. The concentration of each drug was measured by HPLC analysis (see section 2.2.3). The measurement of crystal growth rate was performed in triplicate.

4.3 RESULTS

4.3.1 Dissolution profiles of amorphous drugs

The thermodynamic solubility of crystalline danazol and griseofulvin is summarized in Table 4.1. Thermodynamic solubility was not affected by PVP or HPMC, but slightly increased in the presence of Eudragit. Figure 4.1 shows the degree of supersaturation versus time profiles of amorphous danazol and griseofulvin in the absence and presence of polymers. The degree of supersaturation at each time point was calculated using the thermodynamic solubility values in Table 4.1. Regardless of the dissolution media, danazol and griseofulvin showed higher apparent solubility than their thermodynamic solubility. Following a certain period of time, drug concentration decreased due to crystallization of the stable form (confirmed by PXDR, data not shown). In the absence of polymers (= control condition), griseofulvin and danazol achieved only a small degree of supersaturation (~1.5 for griseofulvin and ~3 for danazol), and a decrease in concentration was initiated within 10–15 min for griseofulvin and 30–40 min for danazol. The supersaturation ratio of these two amorphous drugs was improved in the presence of polymers, and the degree of enhancement was dependent on the polymer species. For griseofulvin, the degree of supersaturation peaked at around 8 and 3 in the presence of HPMC and PVP, respectively,

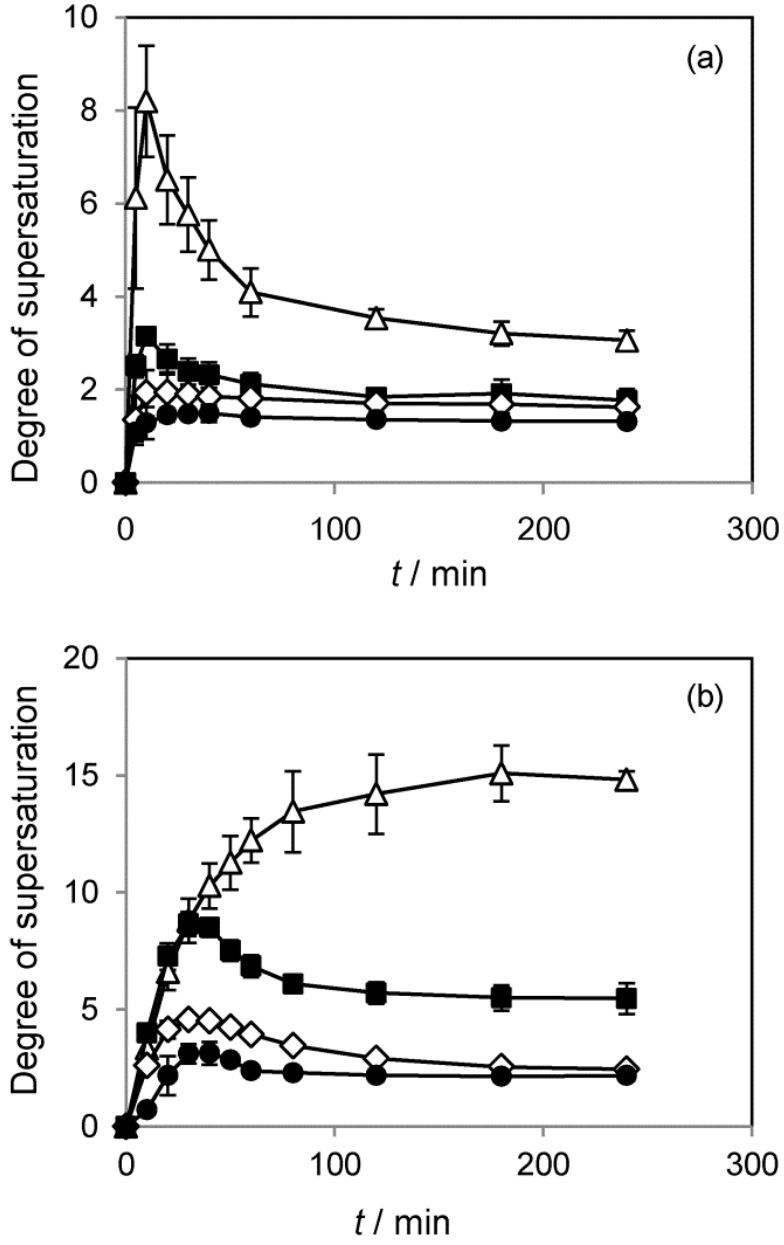

Figure 4.1. The degree of supersaturation versus time profiles of amorphous griseofulvin (a) and danazol (b) in dissolution tests in the absence of polymers (●) and in the presence of HPMC (Δ), PVP (■) and Eudragit (◊). Each value represents the mean ± SD (n = 3).

whereas the impact of Eudragit was relatively small. The contribution of Eudragit to supersaturation was also limited with danazol. In contrast, HPMC and PVP dramatically increased the degree of supersaturation of danazol up to ca. 15 and 9, respectively. The impact of HPMC on danazol supersaturation was especially large, and appearance of the

supersaturation peak was delayed to a later stage of the dissolution test (180–240 min). Although the effect of each polymer on supersaturation was dependent on the drug species, the apparent rank order of the polymers for supersaturation enhancement (HPMC > PVP > Eudragit) was identical for both griseofulvin and danazol.

Table 4.1. Solubility, Supersaturation Characteristics and Crystallization Kinetics of Model Drugs in the Absence and Presence of Polymers

	Polymers	Solubility[a] (±SD) μg mL^{-1}	R_s	log $S(t_{1000})$	G_0/G_p
Griseofulvin	Control	12.6 ± 0.3	1.5	0.69	1
	Eudragit	14.9 ± 0.1	1.9	0.68	1.02
	PVP	12.2 ± 0.1	3.1	0.76	1.22
	HPMC	12.9 ± 0.2	8.2	0.95	2.30
Danazol	Control	5.7 ± 0.1	3.1	0.72	1
	Eudragit	6.3 ± 0.1	4.5	0.75	1.07
	PVP	5.6 ± 0.1	8.6	1.04	1.56
	HPMC	5.4 ± 0.0	15.1	1.26	6.07

[a] Thermodynamic solubility of crystalline materials in FaSSIF at 25 °C; R_s, supersaturation ratio observed in dissolution tests; log $S(t_{1000})$, index of inhibition efficiency against crystal nucleation; G_0/G_p, index of inhibition efficiency against crystal growth.

4.3.2 Impact of polymers on crystal nucleation kinetics

The t_{ind} value of griseofulvin and danazol decreased with an increase in the degree of supersaturation, S (the ratio of the initial drug concentration to the solubility of the crystalline form), which is a driving force in crystal nucleation.[23] In order to relate t_{ind} to nucleation kinetics, the logarithm of t_{ind} was plotted against the logarithm of S to the minus second power (Figure 4.2), according to Eq. (2.2) (p. 34). Measured log t_{ind} followed a

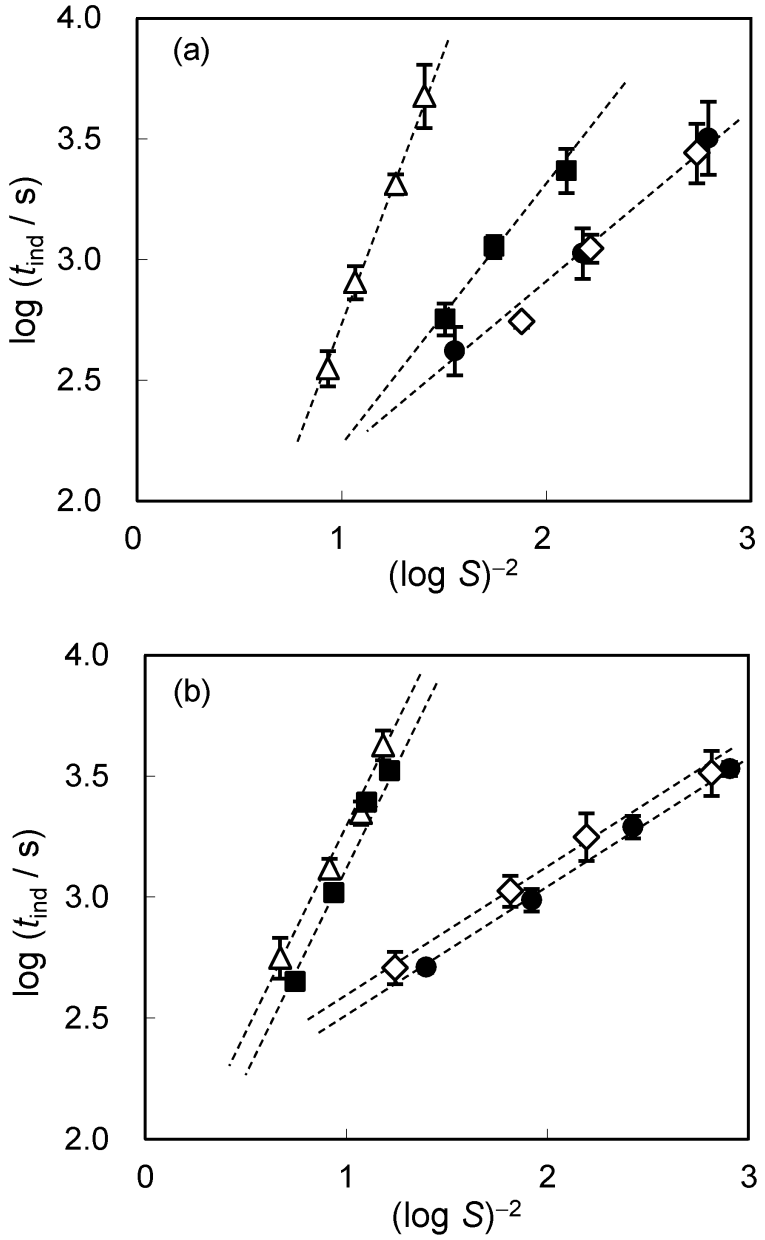

Figure 4.2. Plots of log t_{ind} versus (log S)$^{-2}$ for griseofulvin (a) and danazol (b) in the absence of polymers (●) and in the presence of HPMC (Δ), PVP (■) and Eudragit (◊). Each value represents the mean ± SD (n = 3).

linear relationship with (log S)$^{-2}$ for each drug-polymer system. Relative nucleation kinetics can be evaluated from the log t_{ind}–(log S)$^{-2}$ relationships. In the absence of polymers, nucleation of griseofulvin and danazol quickly occurred in the relatively low S [i.e., high (log S)$^{-2}$] region; their linear relationships are plotted on the extreme right in Figure 4.2. In

the presence of HPMC or PVP, the plot is shifted to the left. A left shift in the $\log t_{ind}$–$(\log S)^{-2}$ relationship means that higher S is required to induce crystal nucleation compared to the control condition. Therefore, these changes in nucleation kinetics indicate that HPMC and PVP clearly inhibit crystal nucleation of griseofulvin and danazol, whereas Eudragit had little impact on the crystallization kinetics of these two model drugs.

4.3.3 Impact of polymers on crystal growth kinetics

Figure 4.3 shows the desupersaturation curves of danazol and griseofulvin obtained by the addition of seed crystals to their supersaturated solutions. These profiles are considered to be directly proportional to the overall crystal growth rate in the absence and presence of polymers. No decrease in drug concentration was observed between –2 and 0 min, which demonstrated that no crystal nucleation occurred prior to the addition of seed crystals. Under all conditions, the growth rate decreased with a decrease in the degree of supersaturation, as previously reported.[95] In the absence of polymers, crystal growth rate was relatively high and the degree of supersaturation decreased by 2 to 3 units in 60 min. On the other hand, the crystal growth rate of the two model drugs significantly decreased in the presence of HPMC and PVP. This means that HPMC and PVP have an inhibitory efficiency against the crystal growth of danazol and griseofulvin. In particular, HPMC significantly inhibited the crystal growth of danazol, and thus only a slight decrease in the concentration of danazol was observed over 60 min. In contrast, Eudragit had little impact on the crystal growth rate of danazol and griseofulvin. From these results, the apparent rank order of the inhibitory efficiency of these polymers against crystal growth is HPMC > PVP >> Eudragit.

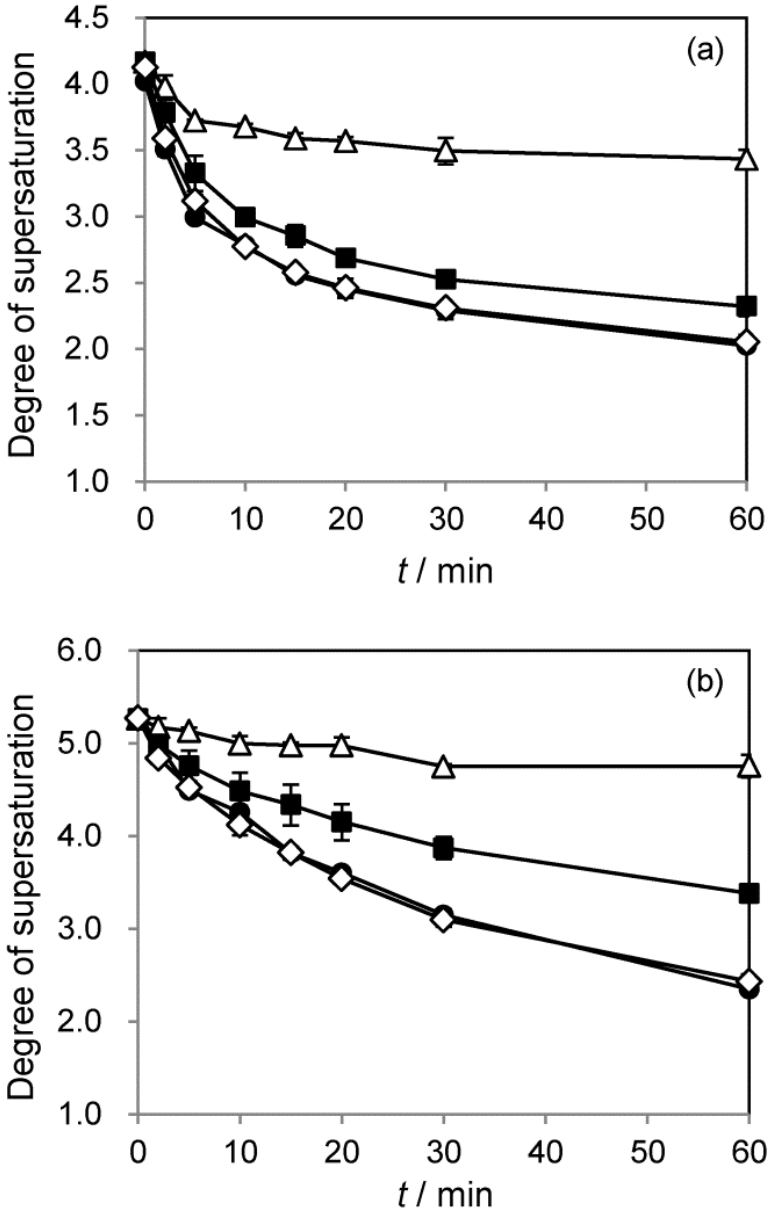

Figure 4.3. Desupersaturation curves of griseofulvin (a) and danazol (b) in the absence of polymers (●) and in the presence of HPMC (Δ), PVP (■) and Eudragit (◊). Each value represents the mean ± SD (n = 3).

4.3.4 Supersaturation profiles of amorphous drugs containing seed crystals

Figure 4.4 shows the dissolution-supersaturation profiles of amorphous griseofulvin and danazol containing 5% (w/w) crystalline solids in the presence of HPMC. For griseofulvin, the degree of supersaturation in this seeded condition was dramatically smaller than that in

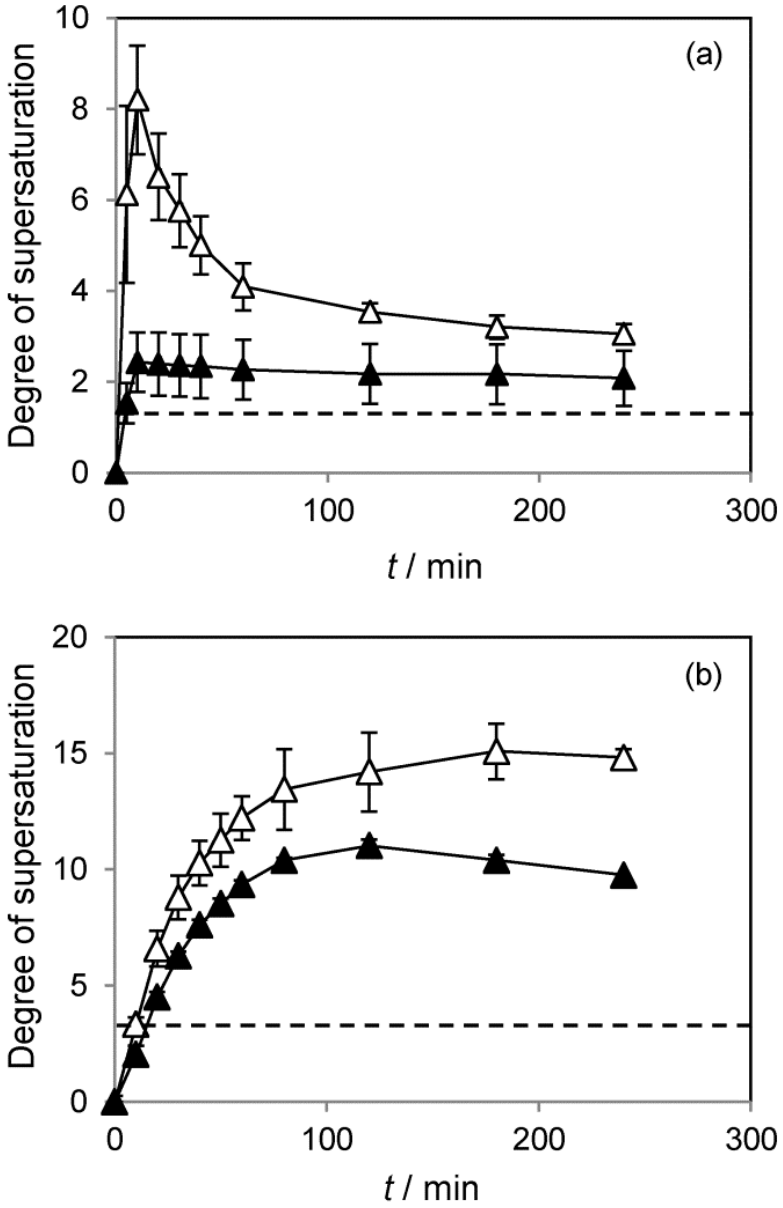

Figure 4.4. The degree of supersaturation versus time profiles of griseofulvin (a) and danazol (b) for pure (Δ) and crystal-contaminated (▲) amorphous solids in the presence of HPMC. Each value represents the mean ± SD (n = 3). The broken lines represent the R_s values in the absence of polymers and seed crystals.

the unseeded conditions. The supersaturation level of crystal-contaminated amorphous griseofulvin was close to that of the pure amorphous solid in the absence of polymers. The addition of crystalline solids also caused a decrease in the supersaturation ratio for danazol

in the presence of HPMC. However, amorphous danazol maintained a relatively high degree of supersaturation even in the presence of seed crystals, and the degree of decrease in supersaturation was much smaller than that of griseofulvin.

4.4 DISCUSSION

4.4.1 Polymer-dependent supersaturation profiles of amorphous drugs

Biorelevant dissolution tests in FaSSIF have often been used to evaluate and optimize amorphous formulations from the viewpoint of their bio-performance.[24,30,96] A higher degree of supersaturation *in vitro* will lead to higher oral bioavailability *in vivo*.[23,24] The polymers dissolved in FaSSIF had a significant impact on the dissolution-supersaturation profiles of amorphous griseofulvin and danazol (Figure 4.1). The polymer concentration used in the present study (0.1%) corresponds to 250 mg of polymer dissolved in 250 mL of medium (= the standardized volume of human intestinal fluid provided in the Biopharmaceutical Classification System), which is achievable using practical formulations. For the two model drugs, higher supersaturation levels were achieved in the presence of the polymers than in the control condition. In order to quantitatively compare the impact of the polymers on drug supersaturation, the maximum degree of supersaturation achieved during the dissolution test, R_s, was calculated for each condition (Table 4.1). It has been suggested that the R_s value is a good indicator for predicting the fraction absorbed of amorphous drugs *in vivo* (Table 3.3) and for selecting effective polymers for the development of amorphous formulations. The solubilization effect of the polymers is canceled out in the calculation of R_s (see section 4.2.2). Millar *et al*. have reported that the solubilized fraction is less important for oral absorption because a trade-off exists between solubilization and membrane permeability.[97] Thus, R_s is used as the representative value for characterizing supersaturation profiles in dissolution studies. For the two model drugs studied here, the rank order of the polymers for supersaturation enhancement was HPMC > PVP > Eudragit.

This polymer-dependent enhancement of drug supersaturation is attributable to the crystallization inhibitory effect of polymers.[23,28,30] Similar results have often been observed in studies on solid dispersion formulations.[22,29,84] In these studies, amorphous drugs are loaded on various solid polymers by amorphization techniques such as spray drying, freeze drying and hot-melt extrusion prior to the dissolution tests. Therefore, drug-polymer interactions probably exist in both the solid and solution phases. Drug-polymer interactions in the solid phase have extensively been studied using thermal analysis and various spectroscopic techniques including solid state nuclear magnetic resonance, infrared, and Raman spectroscopy.[22,98–100] It has been reported that polymers stabilize drugs in amorphous states by hydrogen bonding and thus inhibiting solid-state crystallization under long-term storage conditions.[31,101,102]

On the other hand, it is reasonable to assume that the crystallization of amorphous solids during dissolution proceeds predominantly through solution-mediated transformation, which is much faster than solid-state transformation. Dissolution studies of solid dispersion formulations may not be suitable for identifying the effect of polymers on drug supersaturation, since manufacturing processes often impact the quality and solid state properties of amorphous forms. Such influences would make it difficult to isolate the effect of polymers on the solution-mediated crystallization of amorphous drugs. In the present study, the polymers were dissolved in the medium prior to the dissolution test, and common amorphous solids were used for the dissolution test. Therefore, the polymer-dependent supersaturation of amorphous drugs described in Figure 4.1 is totally attributable to the drug-polymer interaction in the solution phase. However, clarification of the mechanism by which polymers enhance supersaturation will require detailed characterization of the inhibition efficiency against crystal nucleation and growth.

4.4.2 Relationships between crystal nucleation, growth and drug supersaturation

In Chapter 3, it has been demonstrated that the degree of supersaturation for amorphous griseofulvin and danazol is limited by crystal nucleation. Therefore, it is reasonable to expect that the nucleation inhibitory efficiency of polymers has a positive relationship with R_s. Figure 4.2 clearly shows that some water-soluble polymers have an impact on the crystal nucleation kinetics of griseofulvin and danazol. In the presence of HPMC and PVP, a significant left shift was observed in the $\log t_{ind}$–$(\log S)^{-2}$ relationships. The degree of the shift indicates the inhibitory efficiency of the polymers against crystal nucleation of griseofulvin and danazol; consequently, the apparent rank order of these three polymers is HPMC > PVP >> Eudragit for the two model drugs. Figure 4.2 also shows that each left shift is associated with the increase in slope in the $\log t_{ind}$–$(\log S)^{-2}$ relationship. According to classical nucleation theory, the slope (β in Eq. (2.2), p. 34) is determined by the molecular volume of the solute, the interfacial energy per unit area, the crystal shape, and the absolute temperature (see Eq. (2.1), p. 34). The steeper slopes and the nucleation inhibition in the presence of HPMC and PVP might be attributable to an increase in the interfacial energy and a change in the crystal habit[102] because the other parameters would be unchanged by the addition of polymer.

In order to quantitatively evaluate the inhibitory efficiency against nucleation, we designated "log $S(t_{1000})$," the logarithm of the S value at t_{ind} = 1000 s, as an index of nucleation kinetics (Table 4.1). A high log $S(t_{1000})$ value means that a high degree of supersaturation is maintained without nucleation occurring, due to a high kinetic barrier to the formation of nuclei. It has been demonstrated that this index is valuable for linking the nucleation kinetics to the supersaturation characteristics of amorphous drugs *in vitro* and *in vivo* (see Chapters 2 and 3). The log $S(t_{1000})$ values in the absence of polymers, 0.69 and 0.72, are the control values for griseofulvin and danazol, respectively. The higher log $S(t_{1000})$ values in the presence of HPMC and PVP demonstrate their inhibitory efficiency against nucleation. In contrast, it was concluded that Eudragit had little influence on the

log $S(t_{1000})$ values and the nucleation kinetics of the model drugs. As expected, the R_s value for each model drug increased with an increase in the log $S(t_{1000})$ value. Similar results were obtained in Chapter 3, in which the relationship between log $S(t_{1000})$ and R_s was examined for various model drugs in the absence of polymers. The good correlation between log $S(t_{1000})$ and R_s in Table 4.1 suggests that the inhibition of crystal nucleation contributes to the enhanced supersaturation ratio of amorphous griseofulvin and danazol.

On the other hand, the supersaturation level can also be enhanced by inhibiting crystal growth to mitigate a decrease in drug concentration. Several polymers adsorb onto crystal surfaces and prevent the incorporation of drug molecules into the crystal lattice.[94,95] As shown in Figure 4.3, the desupersaturation curves obtained using seeded conditions demonstrated that the crystal growth of griseofulvin and danazol was clearly inhibited by polymers. Since the surface area of the seed crystals is assumed to be constant, the growth inhibition efficiency can be compared to each other by evaluating the initial overall growth rate in the presence and absence of polymers. The relative inhibitory efficiency against crystal growth was evaluated by an effectiveness ratio, G_0/G_p, in accordance with a report by Ilevbare *et al.*[103] G_0/G_p is the ratio of the overall crystal growth rate in the absence of polymers (G_0) to that in the presence of the polymers investigated (G_p). G_0 and G_p were calculated from the slope of an initial straight segment (0–5 min) of each curve in Figure 4.3. The G_0/G_p values of griseofulvin and danazol in the absence and presence of the polymers are summarized in Table 4.1. A high G_0/G_p value corresponds to high inhibitory efficiency against crystal growth. HPMC and PVP effectively inhibited crystal growth of griseofulvin and danazol, whereas Eudragit was ineffective. It has been suggested that the G_0/G_p rank order of polymers is independent of the initial supersaturation ratio used for the experiments, although the absolute value of G_0/G_p for each polymer decreases with increased supersaturation ratio.[103] The rank order of G_0/G_p for the polymers (HPMC > PVP > Eudragit) is consistent with that of R_s for each model drug (Table 4.1). This result suggests that the inhibition of crystal growth by polymers also contributes to the enhanced

supersaturation of amorphous griseofulvin and danazol.

Kinetic analyses have shown that Eudragit only slightly inhibits griseofulvin and danazol crystal nucleation and growth. Therefore, the small enhancement of supersaturation in the presence of Eudragit might be caused by a nonspecific contribution such as an improvement in the wettability of amorphous solids.[22] On the other hand, the enhancement of supersaturation by HPMC and PVP is likely attributable to their inhibition activity against crystal nucleation and growth. The indexes of the inhibitory efficiency against nucleation and growth, log $S(t_{1000})$ and G_0/G_p, are valuable in predicting the improvement in the supersaturation ratio of amorphous solids by polymers. The evaluation of log $S(t_{1000})$ and G_0/G_p will allow us to select an optimal polymer in supersaturable formulations. However, the relative importance between nucleation and growth is still unclear because multicollinearity was observed between R_s, log $S(t_{1000})$ and G_0/G_p.

4.4.3 Contribution ratio of crystal nucleation and growth on drug supersaturation

Crystal nucleation and growth are separate phenomena. It would be reasonable to assume that the mechanisms inhibiting these two phenomena are different, although the molecular mechanism of nucleation inhibition is still unknown.[23,102] It has been reported that PVP inhibits only the crystal growth of bicalutamide[94] whereas HPMC inhibits both the crystal nucleation and growth of felodipine.[95] A polymer which has dual inhibitory activity would be preferable for improving the supersaturation ratio of amorphous drugs. In such a case, however, it is difficult to quantitatively evaluate the relative contribution of nucleation inhibition and crystal growth inhibition by polymers in enhancing drug supersaturation because nucleation and growth occur sequentially during a crystallization process.

In order to estimate the relative importance of nucleation inhibition and crystal growth inhibition in a semi-quantitative manner, supersaturation profiles of amorphous solids were obtained in the presence of seed crystals. In this experiment, we focused on HPMC, which was the most effective crystallization inhibitor for the two model drugs. As

shown in Figure 4.4, the supersaturation level of crystal-contaminated amorphous griseofulvin in the presence of HPMC (R_s = 2.4) was much lower than that of pure amorphous solid, and was close to that of the control level (in the absence of HPMC and seed crystals). This indicates that the effect of HPMC diminishes once crystal nuclei form in the supersaturated solution, and that HPMC enhances the supersaturation level of griseofulvin predominantly by inhibiting nucleation. In contrast, the supersaturation level of danazol was considerably improved by HPMC even in the presence of seed crystals. The R_s value in the seeded condition, 11, was about halfway between that of HPMC and the control conditions in the unseeded experiments (Figure 4.4). This result suggests that the inhibition of crystal nucleation and growth equally contributes to the improvement of supersaturation for danazol.

The magnitude of the inhibition efficiency against crystal nucleation is often larger than that against crystal growth.[95,104] In addition, the supersaturation behavior of griseofulvin and danazol is controlled by the nucleation kinetics. Therefore, it is reasonable to assume that inhibition of nucleation is the most important factor determining the supersaturation ratio of griseofulvin and danazol. Alonzo *et al*. also reported that the inhibition of crystal nucleation is much more efficient than the inhibition of crystal growth in stabilizing drug supersaturation,[95] although crystal growth inhibition may contributes to drug supersaturation when a polymer has enough inhibitory efficiency against crystal growth. The significant contribution of growth inhibition in improving danazol supersaturation would be attributable to the extremely high G_0/G_p value in the presence of HPMC.

The dual inhibition of nucleation and growth may have a positive impact on quality control strategies in formulation development since an insufficient supersaturation level in the intestinal fluid will cause variable and unsatisfactory absorption *in vivo*. Residual crystallinity is often a serious problem in amorphous formulations when nucleation kinetics predominantly controls supersaturation behavior, as is the case with griseofulvin (Figure

4.4). On the other hand, slight contamination with crystalline solids might be acceptable for amorphous formulations of danazol containing HPMC, where both nucleation and growth kinetics have an impact on supersaturation behavior. Adequate supersaturation and oral absorption will be achieved if an appropriate polymer, which has strong inhibitory efficiency against both crystal nucleation and growth, is used in the formulation. Thus, detailed characterization of crystallization inhibitors would be valuable in determining the design space in the development of amorphous formulations.

4.5 CONCLUSION

Kinetic analyses have demonstrated that HPMC and PVP have significant inhibitory efficiency against both crystal nucleation and crystal growth of griseofulvin and danazol. In contrast, Eudragit has little influence on the kinetics of crystal nucleation and growth, although it increased the solubility of both drugs. In biorelevant dissolution tests, the supersaturation levels of amorphous griseofulvin and danazol were dependent on the polymer species dissolved in FaSSIF. A good correlation between the supersaturation ratio and the inhibition efficiency against nucleation and growth in this study indicated that enhancement of supersaturation levels of the model drugs was attributable to the inhibition of both nucleation and growth by the polymers. HPMC was the most effective of the polymers tested for enhancing the supersaturation of griseofulvin and danazol. The improved supersaturation of griseofulvin by HPMC was predominantly caused by the inhibition of crystal nucleation. On the other hand, the inhibition of nucleation and growth by HPMC equally contributed to the enhancement of supersaturation of danazol. Water soluble polymers will enhance the supersaturation levels of other metastable forms such as salts and cocrystals as well as amorphous forms, since the polymers act on the nucleation and growth of stable forms. The detailed characterization of polymers will allow us to select the appropriate polymer for specific drugs and plan a quality control strategy in the development of supersaturable formulations.

Conclusions

In this study, thermodynamic solubility and supersaturation behavior of model drugs have been investigated from the viewpoint of physical chemistry in order to build a science-based development strategy for poorly soluble drug candidates.

In Chapter 1, thermodynamic analysis of the solubility of benzoylphenylurea derivatives was conducted to clarify the relative importance of crystal packing and hydration. The contribution of crystal packing to solubility was evaluated from the change in Gibbs energy on the transition from the crystalline to liquid state. Hydration Gibbs energy was estimated using a linear free-energy relationship between octanol-water partition coefficients and gas-water partition coefficients. The established solubility model satisfactorily explained the relative thermodynamic solubility of the model compounds and revealed that crystal packing and hydration equally controlled solubility of the structural analogs. All hydrophobic substituents were undesirable for solubility in terms of hydration, as expected. On the other hand, some of these hydrophobic substituents destabilized crystal packing and improved the solubility of the benzoylphenylurea derivatives when their impact on crystal packing exceeded their negative influence on hydration. The replacement of a single substituent could cause more than a 10-fold enhancement in thermodynamic solubility. These results have demonstrated the possibility of improving thermodynamic solubility with minor structural modification. In addition, the method presented may be useful for clarifying the structure-property relationships of drug candidates.

In Chapters 2 and 3, limitations and possibilities of supersaturable solid forms for improving solubility and oral absorbability have been clarified. The relationship between the oral absorbability and supersaturation-nucleation behavior of poorly water-soluble drugs was investigated in Chapter 2. The induction time for nucleation was measured for supersaturated solutions of model drugs, and the relationship between induction time and degree of supersaturation was analyzed in terms of classical nucleation theory. The defined supersaturation stability proved to be compound-specific. Clinical data on oral absorption

was investigated for drugs in thermodynamically high-energy forms such as amorphous forms and salts, and was compared with *in vitro* supersaturation-nucleation characteristics. The solubility-limited maximum absorbable dose was proportionate to intestinal effective drug concentrations, which are related to supersaturation stability and thermodynamic solubility. Supersaturation stability was shown to be an important factor determining the effect of high-energy forms.

In Chapter 3, supersaturation behavior of five model drugs was analyzed by a thermodynamic approach in addition to the kinetic approach explained in Chapter 2 to better understand the absorption characteristics of amorphous pharmaceuticals. For each amorphous drug, the extent of supersaturation during *in vitro* dissolution proved to be similar to that *in vivo*, which was estimated from relative bioavailability data. The theoretical limit of supersaturation was thermodynamically calculated from several thermal properties and water sorption isotherms of amorphous solids. *In vitro* and *in vivo* supersaturation of amorphous vemurafenib was thermodynamically controlled and was in good agreement with the theoretical limit. On the other hand, the supersaturation ratios of the other four drugs were highly overestimated by the thermodynamic calculation. However, the discrepancy can be satisfactorily explained by considering supersaturation stability, as elaborated in Chapter 2. Concomitant use of thermodynamic and kinetic approaches is therefore invaluable in evaluating supersaturation behavior of amorphous materials and assessing development potential of poorly water-soluble drugs.

In Chapter 4, the impact of water-soluble polymers on drug supersaturation behavior was investigated to elucidate the role of water-soluble polymers in further enhancing the supersaturation levels of amorphous pharmaceuticals. Hydroxypropyl methylcellulose (HPMC), polyvinylpyrrolidone (PVP) and Eudragit L-100 (Eudragit) were used as representative polymers, and griseofulvin and danazol were used as model drugs. Inhibitory efficiency of the polymers against crystal growth and nucleation was separately evaluated by kinetic analyses. In the presence of the polymers, the degree of *in vitro* supersaturation of

the amorphous model drugs increased with an increase in the inhibitory efficiency of polymers against crystal nucleation and growth (HPMC > PVP > Eudragit). The results demonstrated that the polymers contributed to drug supersaturation by inhibiting both nucleation and growth. The effect of the polymers was drug-dependent. The detailed characterization of polymers would allow selection of appropriate crystallization inhibitors and a planned quality control strategy for the development of supersaturable formulations.

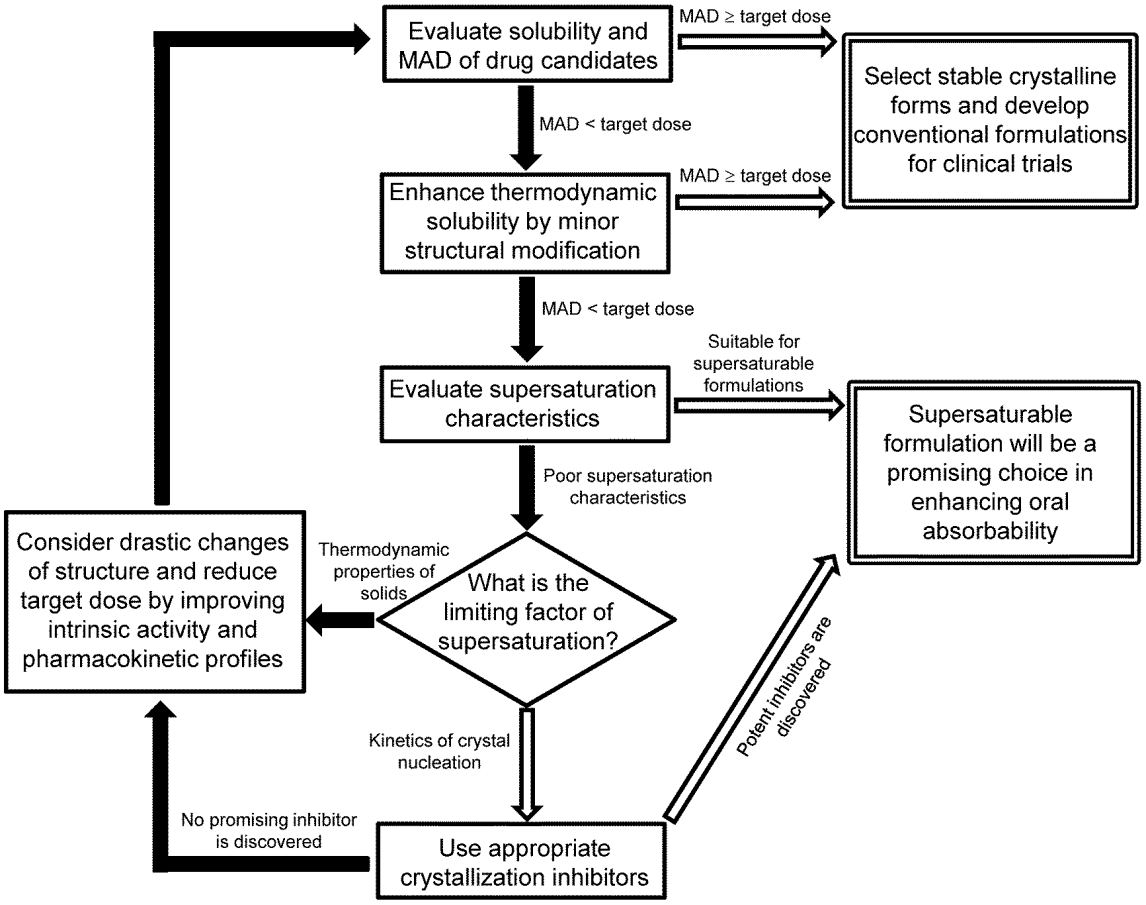

Figure IV. Decision tree for the strategic development of poorly soluble drug candidates; MAD, estimated maximum absorbable dose; target dose, clinical dose for the assessment of efficacy and safety profiles.

Based on in the findings described in Chapters 1–4, a development strategy of poorly soluble drug candidates is proposed (Figure IV). When the estimated maximum absorbable dose (MAD) of a drug candidate is smaller than its target dose, minor structural

modification is the first choice for the enhancement of solubility and MAD. The synthetic approach is very important since conventional formulations containing stable solid forms will pose fewer challenges to formulation developers. [33–35] Thermodynamic solubility will be efficiently improved by considering both crystal packing and hydration in structural optimization.

It is possible that the structural modifications made to improve solubility might be incompatible with other drug properties such as intrinsic activity, metabolic and pharmacokinetic properties and safety/toxicological profiles.[2,11,38] Metastable solid forms including salts, cocrystals and amorphous forms can improve solubility of promising candidates for whom solubility is the only problem. The development of a metastable solid form is usually time-consuming and requires extensive assessment of its potential for development since manufacturability, physical and chemical stability, and oral absorbability would be important factors that affect the development of supersaturable formulations.[33–35]

Oral absorbability of a drug candidate in metastable forms should be estimated by evaluating supersaturation characteristics in order to decide whether to pursue metastable forms of the drug candidate as a means of enhancing oral bioavailability. Discovery and utilization of crystallization inhibitors are important when the supersaturation ratio of a drug candidate is controlled by nucleation kinetics of stable forms. On the other hand, a crystallization inhibitor cannot further enhance thermodynamically-controlled supersaturation. Development of a supersaturable formulation can be considered when a drug candidate has preferable supersaturation characteristics and its estimated MAD is higher than the target dose.

In this research, we have presented several methods to characterize physicochemical properties of poorly soluble drug candidates and a strategy to efficiently solve solubility problems. The solubility and oral absorption problems for the majority of compounds can be addressed by a combination of the three approaches, minor structural modification, utilization of supersaturable forms, and selection of effective crystallization inhibitors.

However the physicochemical understanding of solubility and supersaturation has revealed limitations of each approach. When oral absorption is not improved by these approaches, we should recognize that development of these drug candidates is premature until they are improved in other respects. Specifically, drastic structural change might be necessary in order to not only enhance solubility but also reduce target dose by improving intrinsic activity and pharmacokinetic profiles.

To aid progress in drug development, it is critical to clarify the development potential of current drug candidates as early as possible according to the assessment flow in Figure IV. The evaluation methods developed in this study require only a small amount of the drug. and are invaluable for quantitative characterization of poorly soluble drug candidates. Early decisions about the solubility problems of these candidates will accelerate discovery and clinical introduction of promising drugs.

References

1. Benet LZ, Broccatelli F, Oprea TI. 2011. BDDCS Applied to Over 900 Drugs. AAPS J 13:519–547.
2. Kerns EH, Di L. 2008. Drug-like properties: concepts, structure design, and methods: from ADME to toxicity optimization. London, USA: Academic Press.
3. Yu LX 1999. An integrated model for determining causes of poor oral drug absorption. Pharm Res 16:1883–1887.
4. Sugano K, Okazaki A, Sugimoto S, Tavornvipas S, Omura A, Mano T 2010. Solubility and dissolution profile assessment in drug discovery. Drug Metab Pharmacokinet 22:225–254.
5. Sugano K 2009. Introduction to computational oral absorption simulation. Expert Opin Drug Metab Toxicol 5: 252–293.
6. Takano R, Sugano K, Higashida A, Hayashi Y, Machida M, Aso Y, Yamashita S 2006. Oral absorption of poorly water-soluble drugs: computer simulation of fraction absorbed in humans from a miniscale dissolution test. Pharm Res 23:1144–1156.
7. Lipinski CA, Lombardo F, Dominy BW, Feeney PJ 2001. Experimental and computational approaches to estimate solubility and permeability in drug discovery and development settings. Adv. Drug Deliv Rev 46:3–26.
8. Lipinski CA. 2004. Lead- and drug-like compounds: the rule-of-five revolution. Drug Discov Today 1:337–341.
9. Lipinski CA. 2000. Drug-like properties and the causes of poor solubility and poor permeability. J Pharmacol Toxicol Methods 44:235–249.
10. Paul D. Leeson, Brian Springthorpe. 2007. The influence of drug-like concepts on decision-making in medicinal chemistry. Nature Rev Drug Discov 6:881–890.
11. Ishikawa M, Hashimoto Y. 2011. Improvement in aqueous solubility in small molecule drug discovery programs by disruption of molecular planarity and symmetry. J Med Chem 54:1539–1554.

12. Williams HD, Trevaskis NL, Charman SA, Shanker RM, Charman WN, Pouton CW, Porter CJH. 2013. Strategies to address low drug solubility in discovery and development. Pharmcol Rev 65:315–499.
13. Takano R, Kataoka M Yamashita S. Strategies to address low drug solubility in discovery and development. Biopharm Drug Dispos 33:345–365.
14. Takano R, Furumoto K, Shiraki K, Takata N, Hayashi Y, Aso Y, Yamashita S 2008. Rate-limiting steps of oral absorption for poorly water-soluble drugs in dogs; prediction from a miniscale dissolution test and a physiologically-based computer simulation. Pharm Res 25:2334–2344.
15. Wu Y, Loper A, Landis E, Hettrick L, Novak L, Lynn K, Chen C, Thompson K, Higgins R, Batra U, Shelukar S, Kwei G, Storey D. 2004. The role of biopharmaceutics in the development of a clinical nanoparticle formulation of MK-0869: a beagle dog model predicts improved bioavailability and diminished food effect on absorption in human. Int J Pharm 285:135–146.
16. Sugano K. 2009. Estimation of effective intestinal membrane permeability considering bile micelle solubilisation. Int J Pharm 368:116–122.
17. C. R. Wilke, Pin Chang. 1955. Correlation of diffusion coefficients in dilute solutions. AIChE J 1:264–270.
18. Leuner C, Dressman JB 2000. Improving drug solubility for oral delivery using solid dispersions. Eur J Pharm Biopharm 50:47–60.
19. Yamashita K, Nakate T, Okimoto K, Ohike A, Tokunaga Y, Ibuki R, Higaki K, Kimura T 2003. Establishment of new preparation method for solid dispersion formulation of tacrolimus. Int J Pharm 267:79–91.
20. Serajuddin ATM 2007. Salt formation to improve drug solubility. Adv Drug Deliv Rev 59:603–616.
21. Schultheiss N, Newman A 2009. Pharmaceutical cocrystals and their physicochemical properties. Cryst Growth Des 9:2590–2967.

22. Kushida I, Ichikawa M, Asakawa N 2002. Improvement of dissolution and oral absorption of ER-34122, a poorly water-soluble dual 5-lipoxygenase/cyclooxygenase inhibitor with anti-inflammatory activity by preparing solid dispersion. J Pharm Sci 91:258–266.

23. Brouwers J, Brewster ME, Augustijns P 2009. Supersaturating drug delivery systems: the answer to solubility-limited oral bioavailability? J Pharm Sci. 98:2549–2572.

24. Takano R, Takata N, Saito R, Furumoto K, Higo S, Hayashi Y, Machida M, Aso Y, Yamashita S 2010. Quantitative analysis of the effect of supersaturation on in vivo drug absorption. Mol. Pharm 7:1431–1440.

25. Bevernage J, Brouwers J, Brewster ME, Augustijns P. 2013. Evaluation of gastrointestinal drug supersaturation and precipitation: Strategies and issues. Int J Pharm 453:25–35.

26. Murdande SB, Pikal MJ, Shanker RM, Bogner RH 2010. Solubility advantage of amorphous pharmaceuticals: I. A thermodynamic analysis. J Pharm Sci. 99:1254–1264.

27. Murdande SB, Pikal MJ, Shanker RM, Bogner RH 2010. Solubility advantage of amorphous pharmaceuticals: II. application of quantitative thermodynamic relationships for prediction of solubility enhancement in structurally diverse insoluble pharmaceuticals. Phram Res 27:2704–2714.

28. Murdande SB, Pikal MJ, Shanker RM, Bogner RH. 2011. Solubility advantage of amorphous pharmaceuticals: III. Is maximum solubility advantage experimentally attainable and sustainable? J Pharm Sci 100:4349–4356.

29. Guzman HR, Tawa M, Zhang Z, Ratanabanangkoon P, Shaw P, Gardner CR, Chen H, Moreau JP, Almarsson O, Remenar JF. 2007. Combined use of crystalline salt forms and precipitation inhibitors to improve oral absorption of celecoxib from solid oral formulations. J Pharm Sci 96:2686–2702.

30. Yamashita T, Shunsuke Ozaki, Ikuo Kushida. 2011. Solvent shift method for anti-

precipitant screening of poorly soluble drugs using biorelevant medium and dimethyl sulfoxide. Int J Pharm 419:170–174.

31. Konno H, Taylor LS. 2008. Ability of different polymers to inhibit the crystallization of amorphous felodipine in the presence of moisture. Pharm Res 25:969–978.
32. Tarsa PB, Towler CS, Woollam G, Berghausen J 1991. The influence of aqueous content in small scale salt screening-Improving hit rate for weakly basic, low solubility drugs. Eur J Pharm Sci 41:21–30.
33. Kushida I. 2011. Quantitative crystallinity determination for E1010, a novel carbapenem antibiotic, using differential scanning calorimetry. J Pharm Pharmacol 64:366–371
34. Eddleston MD, Thakuria R, Aldous BJ, Jones W. 2014. An investigation of the causes of cocrystal dissociation at high humidity. J Pharm Sci 103:2859–2864.
35. Kawakami K. 2009. Current status of amorphous formulation and other special dosage forms as formulations for early clinical phases. J Pharm Sci 98:2875–2885.
36. Hill AP, Young RJ. 2010. Getting physical properties in drug discovery: a contemporary perspective on solubility and hydrophobicity. Drug Dicov Today 15:648–655
37. Vistoli G, Pedretti A, Testa B. 2008. Assessing drug-likeness – what are we missing? Drug Dicov Today 13:285–294.
38. Dearden JC. 1985. Partitioning and lipophilicity in quantitative structure-activity relationships. Environ Health Perspect 61:203–228.
39. Stepan AF, Kauffman GW, Keefer CE, Verhoest PR, Edwards M. 2013. Evaluating the differences in cycloalkyl ether metabolism using the design parameter “lipophilic metabolism efficiency” (LipMetE) and a matched molecular pairs analysis J Med Chem 56:6985–6990.
40. Nakao K, Fujikawa M, Shimizu R, Akamatsu M. 2009. QSAR application for the prediction of compound permeability with in silico descriptors in practical use. J

Comput Aided Mol Des 23:309–319.

41. Fujita Y, Yonehara M, Tetsuhashi M, Noguchi-Yachide T, Hashimoto Y, Ishikawa M. 2010. *β*-Naphthoflavone analogs as potent and soluble aryl hydrocarbon receptor agonists: Improvement of solubility by disruption of molecular planarity. Bioorg Med Chem 18:1194–1203

42. Scott JS, Birch AM, Brocklehurst KJ, Broo A, Brown HS, Butlin RJ, Clarke DS, Davidsson O, Ertan A, Goldberg K, Groombridge SD, Hudson JA, Laber D, Leach AG, MacFaul PA, McKerrecher D, Pickup A, Schofield P, Svensson PH, Sörme P, Teague J. 2012. Use of small-molecule crystal structures to address solubility in a novel series of g protein coupled receptor 119 agonists: optimization of a lead and in vivo evaluation. J Med Chem 55:5361–5379.

43. Wenglowsky S, Moreno D, Rudolph J, Ran Y, Ahrendt KA, Arrigo A, Colson B, Gloor SL, Hastings G. 2012. Pyrazolopyridine inhibitors of B-RafV600E. Part 3: An increase in aqueous solubility via the disruption of crystal packing. Bioorg Med Chem Lett 22:912–915.

44. Lamanna C, Bellini M, Padova A, Westerberg G, Maccari L 2008. Straightforward recursive partitioning model for discarding insoluble compounds in the drug discovery process. J Med Chem 51:2891–2897.

45. Ritchiea TJ, Macdonald SJF. 2009. The impact of aromatic ring count on compound Developability- are too many aromatic rings a liability in drug design? Drug Discov Today 14:1011–1020.

46. Fray MJ, Bull DJ, Carr CL, Gautier ECL, Mowbray CE, Stobie A. 2001. Structure-activity relationships of 1,4-dihydro-(1H,4H)-quinoxaline-2,3-diones as *N*-methyl-d-aspartate (glycine site) receptor antagonists. 1. Heterocyclic substituted 5-alkyl derivatives. J Med Chem 44:1951–1962.

47. Yalkowsky SH, Valvani SC. 1985. Solubility and partitioning I: Solubility of nonelectrolytes in water. J Pharm Sci 69:912–922.

48. Jain N, Yalkowsky SH. 2001. Estimation of the aqueous solubility I: Application to organic nonelectrolytes. J Pharm Sci 90:234–252.

49. Campeta AM, Chekal BP, Abramov YA, Meenan PA, Henson MJ, Shi B, Singer RA, Horspool KR. 2010. Development of a targeted polymorph screening approach for a complex polymorphic and highly solvating API. J Pharm Sci 99:3874–3886.

50. Solinas A, Faure H, Roudaut H, Traiffort E, Schoenfelder A, Mann A, Manetti F, Taddei M, Ruat M. 2012. Acylthiourea, acylurea, and acylguanidine derivatives with potent hedgehog inhibiting activity. J Med Chem 55:1559–1571.

51. Klabunde T, Wendt KU, Kadereit D, Brachvogel V, Burger HJ, Herling AW, Oikonomakos NG, Kosmopoulou MN, Schmoll D, Sarubbi E, Roedern E, Schonafinger K, Defossa E. 2005. Acyl ureas as human liver glycogen phosphorylase inhibitors for the treatment of type 2 diabetes. J Med Chem 48:6187–6193.

52. Yang L, Zhou C, Guo L, Morriello G, Butora G, Pasternak A, Parsons WH, Mills SG, MacCoss M, Vicario PP, Zweerink H, Ayala JM, Goyal S, Hanlon WA, Cascieri MA, Springer MS. 2006. Discovery of 3,5-bis(trifluoromethyl)benzyl l-arylglycinamide based potent CCR2 antagonists. Bioorg Med Chem Lett 16:3735–3739.

53. Nakagawa Y, Akagi T, Iwamura H, Fujita T. 1989. Quantitativestructure-activity studies of benzoylphenylurea larvicides. VI. Comparison of substituent effects among activities against different insect species. Pestic Biochem Physiol 33:144-157.

54. Marsella AM, Jaskolka M, Mabury SA. 2000. Aqueous solubilities, photolysis rates and partition coefficients of benzoylphenylurea insecticides. Pest Manag Sci 56:789–794.

55. Hansch C, Leo A, Hoekman D. 1995. Exploring QSAR: Hydrophobic, electronic, and steric constants. Washington, DC: American Chemical Society.

56. Perlovich GL. 2014. Thermodynamic approaches to the challenges of solubility in drug discovery and development. Mol Pharm 11:1–11.

57. Goss KU, Schwarzenbach RP. 2001. Linear free energy relationships used to evaluate

equilibrium partitioning of organic compounds. Environ Sci Technol 35:1–9

58. Fujita T, Nishioka T, Nakajima M. 1977. Hydrogen-bonding parameter and its significance in quantitative structure-activity studies. J Med Chem 20:1071–1081.
59. Yamagami C, Fujita T. 2000. Hydrophobicity parameter of diazines IV: a new hydrogen-accepting parameter of monosubstituted (di)azines for the relationship of partition coefficients in different solvent systems. J Pharm Sci 89:1505–1517.
60. Hansch C, Quinlan JE, Lawrence GL. 1968. Linear free-energy relationship between partition coefficients and the aqueous solubility of organic liquids. J Org Chem 33:347–350.
61. Brazier DW, Freeman GR. 1969. The effects of pressure on the density, dielectric constant, and viscosity of several hydrocarbons and other organic liquids. Can J Chem 47:893–899.
62. Pudipeddi M, Serajuddin ATM. 2005. Trends in solubility of polymorphs. J Pharm Sci 94:929–939.
63. Sotomatsu T, Nakagawa Y, Fujita T. 1987. Quantitative structure-activity studies of benzoylphenylurea larvicides: IV. Benzoyl ortho substituent effects and molecular conformation. Pestic Biochem Physiol 27:156–164.
64. Janssens S, Nagels S, Armas HN, D'Autry W, Schepdael AV, Mooter GV 2008. Formulation and characterization of ternary solid dispersions made up of Itraconazole and two excipients, TPGS 1000 and PVPVA 64, that were selected based on a supersaturation screening study. Eur J Pharm Biopharm 69:158–166.
65. Kojima T, Tsutsumi S, Yamamoto K, Ikeda Y, Moriwaki T 2010. High-throughput cocrystal slurry screening by use of in situ Raman microscopy and multi-well plate. Int J Pharm 399:52–59.
66. Dalvi SV, Dave RN 2010. Analysis of nucleation kinetics of poorly water-soluble drugs in presence of ultrasound and hydroxypropyl methyl cellulose during antisolvent precipitation. Int J Pharm 387:172–179.

67. Bevernage J, Brouwers J, Clarysse S, Vertzoni M, Tack J, Annaert P, Augustijns P 2010. Drug supersaturation in simulated and human intestinal fluids representing different nutritional states. J Pharm Sci 99:4523–4534.

68. Furukawa S, Zhao C, Ohki Y 2010. Methodology for phase selection of a weak basic drug candidate, utilizing kinetic solubility profiles in bio-relevant media. Eur J Pharm Biopharm 74:298–303.

69. Gu CH, Rao D, Gandhi RB, Hilden J, Raghavan K 2005. Using a novel multicompartment dissolution system to predict the effect of gastric pH on the oral absorption of weak bases with poor intrinsic solubility. J Pharm Sci 94:199–208.

70. Kostewicz ES, Wunderlich M, Brauns U, Becker R, Bock T, Dressman JB 2004. Predicting the precipitation of poorly soluble weak bases upon entry in the small intestine. J Pharm Pharmacol 56:43–51.

71. Sugano K 2009. A simulation of oral absorption using classical nucleation theory. Int J Pharm 378:142–145.

72. Gu CH, Young Jr V, Grant DJW 2001. Polymorph screening: Influence of solvents on the rate of solvent-mediated polymorphic transformation. J Pharm Sci 90:1878–1890.

73. Bernardo A, Calmanovici CE, Miranda EA 2003. Induction time as an instrument to enhance comprehension of protein crystallization. Cryst Growth Des. 4:799–805.

74. Kuldipkumar A, Kwon GS, Zhang GGZ 2007. Determining the growth mechanism of tolazamide by induction time measurement. Cryst Growth Des. 7:234–242.

75. Cao S, Zhang Y, Zhang Y 2010. Nucleation and morphology of monosodium aluminate hydrate from concentrated sodium aluminate solutions. Cryst Growth Des 10:1605–1610.

76. Nicolaides E, Symillides M, Dressman JB, Reppas C 2001. Biorelevant Dissolution testing to predict the plasma profile of lipophilic drugs after oral administration. Pharm Res 18:380–388.

77. Hasegawa S, Furuyama N, Yada S, Hamaura T, Kusai A, Yonemochi E, Terada K

2007. Effect of physical properties of troglitazone crystal on the molecular interaction with PVP during heating. Int J Pharm 336:82–89.

78. Bollag G, Hirth P, Tsai J, Zhang J, Ibrahim PN, Cho H, Spevak W, Zhang C, Zhang Y, Habets G, Burton EA, Wong B, Tsang G, West BL, Powell B, Shellooe R, Marimuthu A, Nguyen H, Zhang KYJ, Artis DR, Schlessinger J, Su F, Higgins B, Iyer R, D'Andrea K, Koehler A, Stumm M, Lin PS, Lee RJ, Grippo J, Puzanov I, Kim KB, Ribas A, McArthur GA, Sosman JA, Chapman PB, Flaherty KT, Xu X, Nathanson KL, Nolop K 2010. Clinical efficacy of a RAF inhibitor needs broad target blockade in BRAF-mutant melanoma. Nature 467:596–599.
79. Matteucci ME, Miller MA, Williams III RO, Johnston KP 2008. Highly supersaturated solutions of amorphous drugs approaching predictions from configurational thermodynamic properties. J Phys Chem B 112: 16675−16681
80. Flaherty KT, Puzanov I, Kim KB, Ribas A, McArthur GA, Sosman JA, O'Dwyer PJ, Lee RJ, Grippo JF, Nolop K, Chapman PB 2010. Inhibition of mutated, activated BRAF in metastatic melanoma. N Engl J Med 363:809–819.
81. Sugano K 2010. Computational oral absorption simulation of free base drugs. Int J Pharm 398:73–82.
82. Sugano K 2011. Fraction of a dose absorbed estimation for structurally diverse low solubility compounds. Int J Pharm 405:79–89.
83. Hancock BC, Parks M 2000. What is the True solubility advantage for amorphous pharmaceuticals? Pharm Res 17:397–404.
84. Vaughn JM, McConville JT, Crisp MT, Johnston KP, Williams III RO 2006. Supersaturation produces high bioavailability of amorphous danazol particles formed by evaporative precipitation into aqueous solution and spray freezing into liquid technologies. Drug Dev Ind Pharm 32:559–567.
85. Zhang S, Kawakami K, Yamamoto M, Masaoka Y, Kataoka M, Yamashita S, Sakuma S 2011. Coaxial electrospray formulations for improving oral absorption of a poorly

water-soluble drug. Mol Pharmaceut 8:807–813.

86. Chiou WL, Riegelman S 1971. Absorption characteristics of solid dispersed and micronized griseofulvin in man. J Pharm Sci 60:1376–1380.

87. Chiou WL, Riegelman S 1970. Oral absorption of griseofulvin in dogs: Increased absorption via solid dispersion in polyethylene glycol 6000. J Pharm Sci 59:937–942.

88. Speybroeck MV, Mols R, Mellaerts R, Thi TD, Martens JA, Humbeeck JV, Annaert P, Mooter GV, Augustijns P 2010. Combined use of ordered mesoporous silica and precipitation inhibitors for improved oral absorption of the poorly soluble weak base itraconazole. Eur J Pharm Biopharm 75:354–365.

89. Sacchetti M 1998. Thermodynamic analysis of moisture sorption isotherms. J Pharm Sci 87:982–986.

90. DeSesso JM, Jacobson CF 2001. Anatomical and physiological parameters affecting gastrointestinal absorption in humans and rats. Food Chem Toxicol 39:209–228.

91. Kararli TT 1995. Comparison of the gastrointestinal anatomy, physiology, and biochemistry of humans and commonly used laboratory animals. Biopharm Drug Dispos 16:351–380.

92. Wu T, Yu L 2006. Surface crystallization of indomethacin below T_g. Phram Res 23:2350–2355.

93. Carlert S, Pålsson A, Hanisch G, Corswant C, Nilsson C, Lindfors L, Lennernäs H, Abrahamsson B. 2010. Predicting intestinal precipitation—A case example for a basic BCS class II drug. Phram Res 27:2119-2130.

94. Lindfors L, Forssén S, Westergren J, Olsson U. 2008. Nucleation and crystal growth in supersaturated solutions of a model drug. J Colloid Interface Sci 325:404–413.

95. Alonzo DE, Raina S, Zhou D, Gao Y, Zhang GG.Z, Taylor LS. 2012. Characterizing the impact of hydroxypropylmethyl cellulose on the growth and nucleation kinetics of felodipine from supersaturated solutions. Cryst Growth Des 12:1538–1547.

96. Dressman JB, Reppas C. 2000. In vitro-in vivo correlations for lipophilic, poorly

water-soluble drugs. Eur J Pharm 11:S73–S80.

97. Miller JM, Beig A, Carr RA, Webster GK, Dahan A. 2012. The solubility–permeability interplay when using cosolvents for solubilization: Revising the way we use solubility-enabling formulations. Mol Pharm 9:581–590.

98. DiNunzio JC, Miller DA, Yang W, McGinity JW, Williams RO III. 2008. Amorphous compositions using concentration enhancing polymers for improved bioavailability of itraconazole. Mol Pham 5:968–960.

99. Taylor LS, Zografi G. 1997. Spectroscopic characterization of interactions between PVP and indomethacin in amorphous molecular dispersions. Pharm Res 14:1691–1698.

100. Kushida I, Gotoda M. 2013. Investigation for the amorphous state of ER-34122, a dual 5-lipoxygenase/cyclooxygenase inhibitor with poor aqueous solubility, in HPMC solid dispersion prepared by the solvent evaporation method. Drug Dev Ind Pharm 39:1582–1588.

101. Konno H, Taylor LS. 2006. Influence of different polymers on the crystallization tendency of molecularly dispersed amorphous felodipine. J Pharm Sci 95:2692–2705.

102. Raghavan SL, Trividic A, Davis AF, Hadgraft J. 2001. Crystallization of hydrocortisone acetate: influence of polymers. Int J Pharm 212:213–221.

103. Ilevbare GA, Liu H, Edgar KJ. Taylor LS. 2012. Inhibition of solution crystal growth of ritonavir by cellulose polymers–factors influencing polymer effectiveness. Cryst Eng Comm 14:6503–6514.

104. Ilevbare GA, Liu H, Edgar KJ. Taylor LS. 2013. Maintaining supersaturation in aqueous drug solutions: impact of different polymers on induction times. Cryst Growth Des 13:740–751.

Acknowledgements

I wish to acknowledge valuable guidance and strong encouragement from Dr. Kenji Kano, professor of Kyoto University. I am very grateful to Dr. Osamu Shirai, associate professor of Kyoto University, and Dr. Yuki Kitazumi, assistant professor of Kyoto University, for their kind support and a number of critical comments. I would like to express my gratitude to Ms. Toshie Koyama and all students in Kano Laboratory for their warm hospitality. Discussions with Mr. Jun Fukuda, my contemporary at Kyoto University, have been insightful. I deeply appreciate Dr. Hisashi Miyagawa, professor of Kyoto University, and Dr. Yoshiaki Nakagawa, associate professor of Kyoto University, for their kind gift of benzoylphenylurea derivatives. Advice and comments given by Dr. Ikuo Kushida, Dr. Taro Yamashita, Dr. Takuma Minamisono, Mr. Takashi Kato and Dr. Takashi Hasebe, co-researchers in Eisai Co., Ltd., are invaluable. Special thanks to Dr. John Orr and Dr. Arani Chanda in Eisai Inc. Andover Site for their helpful review of the original articles. I offer my sincere thanks to Mr. Tomohiro Watanabe, Mr. Ken-ichi Tagami, Mr. Hideki Kumobayashi, Dr. Makoto Yokoyama, Dr. Katsuya Tagami, Mr. Takao Omae, Dr. Itaru Sakai and Dr. Naoki Asakawa for their understanding and cooperation in Eisai Co., Ltd. Finally, my heartfelt appreciation goes to support and encouragement from my parents, Kaoru and Kiyomi, and my wife, Sayuri.

Shunsuke Ozaki

2015

List of Publications

S. Ozaki, Y. Nakagawa, O. Shirai, K. Kano. 2014. Substituent effect on the thermodynamic solubility of structural analogs: relative contribution of crystal packing and hydration. J Pharm Sci 103:3524–3531. (Chapter 1)

S. Ozaki, T. Minamisono, T. Yamashita, T. Kato, I. Kushida. 2012. Supersaturation–nucleation behavior of poorly soluble drugs and its impact on the oral absorption of drugs in thermodynamically high-energy forms. J Pharm Sci 101:214–222. (Chapter 2)

S. Ozaki, I. Kushida, T. Yamashita, T. Hasebe, O. Shirai, K. Kano. 2012. Evaluation of drug supersaturation by thermodynamic and kinetic approaches for the prediction of oral absorbability in amorphous pharmaceuticals. J Pharm Sci 101:4220–4230. (Chapter 3)

S. Ozaki, I. Kushida, T. Yamashita, T. Hasebe, O. Shirai, K. Kano. 2013 .Inhibition of crystal nucleation and growth by water-soluble polymers and its impact on the supersaturation profiles of amorphous drugs. J Pharm Sci 102:2273–2281. (Chapter 4)